EFFECTIVE MEDIUM APPROXIMATION
AND DEPOSITION OF COLLOIDAL PARTICLES
IN FIBROUS AND GRANULAR MEDIA

By

YONGCHENG LI

A DISSERTATION PRESENTED TO THE GRADUATE SCHOOL
OF THE UNIVERSITY OF FLORIDA IN PARTIAL FULFILLMENT
OF THE REQUIREMENTS FOR THE DEGREE OF
DOCTOR OF PHILOSOPHY

UNIVERSITY OF FLORIDA

1998

To my parents, my wife and my son.

ACKNOWLEDGMENTS

TABLE OF CONTENTS

CHAPTERS

LIST OF TABLES

LIST OF FIGURES

A	integral constant, dimensionless
A_c	flow field parameter for fibrous media, defined by equation (1-36), dimensionless
A_s	flow field parameter for granular media, defined by equation (1-37), dimensionless
A_{sp}	specific surface area of media, m^2/m^3
a	packing element radius, m
a_{avg}	number average packing element radius, m
a_p	radius of colloidal particles, m
B	integral constant, dimensionless
$B(\varepsilon)$	model parameter defined in equation (1-25)
c	colloidal particle concentration, $mole/m^3$
c	speed of light, m/s
C	integral constant, dimensionless
D	integral constant, dimensionless
e	electron charge, 1.602×10^{-9} C
$\mathcal{D}$	particle diffusion coefficient, m^2/s
Da	Damkohler number, $= K_s a/\mathcal{D}$, dimensionless
$\mathcal{D}e$	effective diffusion coefficient, m^2/s
F_D	hydrodynamic drag on a unit length of fiber, N/m, or per sphere, N or $F_D / (U\mu)$ for cylinders and $F_D/U\mu a$ for spheres, dimensionless
g(h)	hydrodynamic retardation function, dimensionless
H	Hamaker constant, J
h	surface-to-surface separation distance, m
I_0	modified Bessel function of the first kind of the 0th order

I_1	modified Bessel function of the first kind of the 1st order
J	mass transfer flux, mole/m²s
K	dimensionless permeability, $= k/a^2$, dimensionless
K_0	Bessel function of the second kind of the 0th order
K_1	Bessel function of the second kind of the 1st order
Kn	Knudsen number, mean free path/2a, dimensionless
K_Φ	surface reaction constant, m/s
k	Darcy's permeability, $-\dfrac{dp}{dl} = \dfrac{1}{k}\mu U$, m²
k_B	Boltzmann constant, 1.3805×10^{-23} J/K
k_m	mass transfer coefficient, m/s
l	packing depth coordinate, m
L	packing depth, m
M_3	third order moment of size distribution, m³
	or M_3/a^3, dimensionless
	or M_3/a^3_{avg}, dimensionless
m	particle mobility, m/(Ns)
m_1, m_2, m_3	parameters defined in equations (1-20, 1-21 and 1-22)
n	electrolyte concentration, mole/m³
p	pressure, N/m²
	or $p/(U\mu/a)$, dimensionless
$P_a(a)$	size distribution probability density, dimensionless
$P_A(a)$	area availability density of size a, dimensionless
Pe	Peclet number, $= Ua/\mathcal{D}$, dimensionless
Q	function defined by equations (3-34) or (4-19), dimensionless
R	relative fluid envelope radius, dimensionless
Re	Reynolds number, $2aU\rho/\mu$, dimensionless
r	radial coordinate, m
	or r/a, dimensionless

S(0)	structure factor, dimensionless
Sh	Sherwood number, =mass or heat transfer coefficient $\times a / \mathcal{D}$, dimensionless
U	superficial velocity, m/s
u	velocity vector, m/s
	or **u**/U, dimensionless
V	volume, m^3
	or V/a^3, dimensionless
X	$\equiv Y(2/9z)^{1/3}$, dimensionless
Y	$\equiv \tau_w y / 2$, dimensionless
y	$\equiv r - 1$ dimensionless
Z	Total length of fibers, m
	or Z/a, dimensionless
z	fiber length coordinate, m
	or z/a, dimensionless
z	valence, dimensionless

<u>Greek letters</u>

α	$= a / \sqrt{k}$
β	function, defined in equation (1-39) and (1-40), dimensionless
χ	packing structure correction factor for mass transfer coefficient for fibrous media, defined in equations (5-16) and (5-17)
ε	dielectric constant, dimensionless
ε	packing porosity, dimensionless
γ(β)	integral function, tabulated in Table 1-3
η	filtration efficiency, dimensionless
Φ	surface interaction potential, J
ϑ	circumferential coordinate with packing column axis as axis of a cylindrical coordinate, radian
φ	surface potential, V

κ	Debye reciprocal length, 1/m
Λ	model parameter defined in equations (1-5, 1-6 and 1-7)
λ	filter coefficient, 1/m
λ_w	characteristic wavelength, m
μ	liquid viscosity, N/m²s
σ	stress, N/m²
	or $\sigma/(\mu U/a)$, dimensionless
τ	Shear stress, N/m²
	or $\tau/(\mu U/a)$, dimensionless
θ	circumferential coordinate with fiber axis as axis of a cylindrical
	coordinate or with sphere center as origin of a spherical coordinate, radian
ω	solid angle, steridian
ω_v	dispersion frequency, 1/s
Ω	dimension parameter, 2 for cylinders, and 3 for spheres, dimensionless
ψ	stream function, m²/s for cylinders and m³/s for spheres
$\hat{\psi}$	$= \psi/Ua$ for cylinders, $= \psi/Ua^2$ for spheres, dimensionless

Subscript

$_0$	initial property
$_{//}$	parallel
$_\perp$	normal or perpendicular
$_\infty$	bulk property
$_c$	cylinder
$_{DL}$	double layer
$_e$	effective or equivalent
$_{eff}$	effluent
$_H$	hydration
$_{HP}$	hydrophobic
$_{in}$	influent

PB	polymer bridging
r	radial direction
s	sphere or solid
	or steric
surf	surface
vdW	van der Waals
w	at the collector surface
z	fiber length direction
θ	circumferential direction

EFFECTIVE MEDIUM APPROXIMATION AND DEPOSITION OF COLLOIDAL
PARTICLES IN FIBROUS AND GRANULAR MEDIA

By

Yongcheng Li

April 1998

Chairman: Dr. Chang-Won Park
Cochairman: Dr. Tim Anderson
Major Department: Chemical Engineering

Laminar flow of fluid through fibrous and granular media and deposition of colloidal particles from a liquid suspension are two fundamental phenomena encountered in many industrial applications. Finite Element Method (FEM) and Effective Medium Approximation (EMA) are used to determine the fluid flow permeability and particle capture efficiency of regular array and random arrays of cylindrical and spherical collectors. The FEM takes into account of the detailed layout of the packing but it can not handle randomly packed collectors yet at the current stage, while the EMA gives an averaged estimation of all the flow parameters but is not able to provide a resolution to distinguish the detailed structure differences and orientations.

The EMA assumes a model system in which a packing element (a single fiber in the fibrous medium and a single sphere in the granular medium) is surrounded by a fluid

envelope and an effective-medium beyond the envelope. It integrates the important features of both the cell models and Brinkman's model. The Stokes equation and Brinkman's equation are solved for the fluid envelope and effective medium regions, respectively, to obtain the permeability and close-to-surface velocity field around the collectors. The convective diffusion equation is then solved to determine the particle deposition rate. The analytical expressions for the permeability and particle deposition rate are derived for all possible cases of random packing of uniform and non-uniform cylinders and spheres.

Effects of various system properties and operating conditions on deposition of colloidal particles are investigated. The physical or chemical conditions include the properties which affect the magnitude of double layer interaction, the electrolyte concentration and surface potentials, and the property which affects the van der Waals interaction, the Hamaker constant. It was found that the effects of the above properties are much more significant when the surface interactions play more important roles in the particle deposition, i.e., when the height of the total interaction energy barrier is higher than 5 k_BT. Particle deposition becomes virtually impossible when the height of the repulsive energy barrier increases beyond 20 k_BT.

CHAPTER 1
GENERAL INTRODUCTION

1-1 Fibrous and Granular Porous Medium Models

Theory of fluid flow through fibrous and granular media is a branch of the physics of fluid flow through porous media. In the current study, our major interest is the slow flow with applications to particle deposition in filter media, although the developed results can have much broader uses. In this instance, the concept of laminar, incompressible and Newtonian flow though porous media governed macroscopically by Darcy's law can be applied. The Darcy's law simply states that the pressure gradient across a porous medium is proportional to the superficial velocity and the fluid viscosity:

$$\frac{dp}{dl} = -\frac{1}{k}\mu U \tag{1-1}$$

the reciprocal of the proportionality constant, k, is called the permeability of the medium. On the other hand, the Stokes law applies in the clear fluid regions locally:

$$\nabla p = \mu \nabla^2 \mathbf{u} \tag{1-2}$$

The solution of the Stokes equation (1-2) gives the fluid velocity field needed for many mass and heat transfer applications. The difficulty in applying equation (1-2) in the fibrous and granular media is with the boundary conditions. Because of the complex geometric nature of the fluid-solid boundaries in the media, some simplified models have to be introduced. There have been a few good reviews on the porous medium models,

1

such as Rajagopalan and Tien (1979), Tien (1989) and Pich (1986). Summarized below are the key concepts and the major conclusions of the models which have applications in mass and heat transfer processes and which will be referred to frequently in the context of the current work for comparison.

The early porous medium models, such as the well known Kozeny-Carman's model based on the equivalent capillary idea, concerned only the pressure gradient predictions. The models developed later on, like the Happel's and Kuwabara's, can not only give reasonable good predictions of pressure gradient but also a representative flow field in the vicinity of the individual elements. It is this second class of models that is of interest to the current study.

The widely used cell models portray a porous medium as a collection of unit cells of a finite size which consist of a spherical or cylindrical solid element surrounded by a fluid envelope. The size of the solid element is assumed to be identical to the characteristic size of the packing elements, and the size of the fluid envelope is determined based on the porosity of the porous medium (Happel 1958). For the description of the flow characteristics in a porous medium, the momentum equation is solved for the simplified flow geometry with appropriate boundary conditions. Since the characteristic pore size of packed beds are usually small, the Reynolds number based on the pore size is small. Consequently, the creeping flow equation is typically solved in these models with the no-slip condition at the solid surface (i.e., at the inside wall of capillary models or at the surface of the solid element of cell models). Another boundary condition needs to be specified at the outer surface of the fluid envelope. In Happel's model (1958), a stress-free condition is applied whereas a vorticity-free condition is

applied in Kuwabara's model (1959). Although either conditions may appear to be plausible considering the symmetry at the surface of the fluid envelope, some ambiguity exists regarding the boundary conditions and these cell models may not account for the influence of the neighboring elements.

The physical picture underlying the Brinkman's model (Brinkman 1947) is that of a packing element embedded in a macroscopic porous medium. The flow field is described by the Darcy's law at distances remote from the element, but by the Stokes equation near the element; in other words, the Brinkman's equation:

$$\nabla p = -\frac{1}{k}\mu\mathbf{u} + \mu\nabla^2\mathbf{u} \tag{1-3}$$

is solved. The essence of the Brinkman equation is that, on the average, the fluid in the proximity to an obstacle embedded in a porous medium experiences a body damping force proportional to the velocity in addition to the viscous and the pressure forces, which accounts for the influence of neighboring solid elements on the flow. The Brinkman's model applied to fibrous media was worked out by Spielman and Goren (1968), to Granular media by Payatakes et al. (1974b).

The velocity fields in the vicinity of the fiber surfaces for all these models in the case of flow perpendicular to all the fiber axes in fibrous media can be summarized by the following equation:

$$\psi(r,\theta) = \frac{aU\sin\theta}{2\Lambda}\left[\frac{a}{r} - \frac{r}{a} + 2\frac{r}{a}\ln\frac{r}{a}\right] \tag{1-4}$$

where r and θ are the polar coordinates and ψ(r,θ) is the stream function related to velocity components by $u_r = (1/r)(\partial\psi/\partial\theta)$ and $u_\theta = -\partial\psi/\partial r$, a is the radius of the packing elements, Λ is the model parameter given by

$$\Lambda = -\frac{3}{4} - \frac{1}{2}\ln(1-\varepsilon) + (1-\varepsilon) - \frac{1}{4}(1-\varepsilon)^2 \quad \text{(Kuwabara's model)} \quad (1\text{-}5)$$

$$\Lambda = -\frac{1}{2} - \frac{1}{2}\ln(1-\varepsilon) + \frac{(1-\varepsilon)^2}{1+(1-\varepsilon)^2} \quad \text{(Happel's model)} \quad (1\text{-}6)$$

$$\Lambda = \frac{K_0(a/\sqrt{k})}{(a/\sqrt{k})K_1(a/\sqrt{k})} \quad \text{(Brinkman's model)} \quad (1\text{-}7)$$

For some applications it is adequate to approximate the velocity field of equation (1-4) by using only the first term in a power series expansion by powers (r-a)/a. The result is

$$\psi(r,\theta) = \frac{aU\sin\theta}{\Lambda}\left[\frac{r}{a} - 1\right]^2 \quad (1\text{-}8)$$

When the flow is parallel to the fibers, Happel's model gives the following flow field

$$u(r) = \frac{2U\left[a^2 - r^2 + \frac{2a^2}{1-\varepsilon}\ln\frac{r}{a}\right]}{a^2(1-\varepsilon)\left[2\ln\frac{1}{1-\varepsilon} - 3 + 4(1-\varepsilon) - (1-\varepsilon)^2\right]} \quad . \quad (1\text{-}9)$$

The flow field predicted by the Brinkman's model for the current flow pattern has not been reported, but the result will be given in Chapter 3 considering the fact that it is a special case of the effective medium approximation model studied in the current research.

The permeability predictions by these models are summarized in Table 3-1 and Table 3-2.

The general velocity field around the spheres in granular media for the cell models can be written as:

$$\psi = \left[C_1 \frac{a}{r} + C_2 \frac{r}{a} + C_3 \left(\frac{r}{a}\right)^2 + C_4 \left(\frac{r}{a}\right)^4 \right] \sin^2 \theta \tag{1-10}$$

where the stream function ψ is defined by $u_r = [-1/(r^2 \sin\theta)](\partial\psi/\partial\theta)$ and $u_\theta = [1/(r\sin\theta)](\partial\psi/\partial r)$, and C_1, C_2, C_3 and C_4 are the model parameters. For Happel's model,

$$C_1 = \frac{Ua^2}{2}\left[2 - 3(1-\varepsilon)^{1/3} + 3(1-\varepsilon)^{5/3} - 2(1-\varepsilon)^2\right]^{-1} \tag{1-11}$$

$$C_2 = -\frac{Ua^2}{2}\left[3 + 2(1-\varepsilon)^{5/3}\right]\left[2 - 3(1-\varepsilon)^{1/3} + 3(1-\varepsilon)^{5/3} - 2(1-\varepsilon)^2\right]^{-1} \tag{1-12}$$

$$C_3 = \frac{Ua^2}{2}\left[2 + 3(1-\varepsilon)^{5/3}\right]\left[2 - 3(1-\varepsilon)^{1/3} + 3(1-\varepsilon)^{5/3} - 2(1-\varepsilon)^2\right]^{-1} \tag{1-13}$$

$$C_4 = -\frac{Ua^2}{2}(1-\varepsilon)^{5/3}\left[2 - 3(1-\varepsilon)^{1/3} + 3(1-\varepsilon)^{5/3} - 2(1-\varepsilon)^2\right]^{-1} \tag{1-14}$$

and for Kuwabara's model,

$$C_1 = \frac{Ua^2[3 + 2\varepsilon]}{20\left[2 - 3(1-\varepsilon)^{1/3} + 3(1-\varepsilon)^{5/3} - 2(1-\varepsilon)^2\right]\left[1 - (1-\varepsilon)^{1/3}\right]^3} \tag{1-15}$$

$$C_2 = \frac{-3Ua^2}{4\left[2 - 3(1-\varepsilon)^{1/3} + 3(1-\varepsilon)^{5/3} - 2(1-\varepsilon)^2\right]\left[1 - (1-\varepsilon)^{1/3}\right]^3} \tag{1-16}$$

$$C_3 = \frac{Ua^2[1 + \varepsilon]}{4\left[2 - 3(1-\varepsilon)^{1/3} + 3(1-\varepsilon)^{5/3} - 2(1-\varepsilon)^2\right]\left[1 - (1-\varepsilon)^{1/3}\right]^3} \tag{1-17}$$

$$C_4 = \frac{-3Ua^2(1-\varepsilon)}{20\left[2 - 3(1-\varepsilon)^{1/3} + 3(1-\varepsilon)^{5/3} - 2(1-\varepsilon)^2\right]\left[1 - (1-\varepsilon)^{1/3}\right]^3} \qquad (1-18)$$

The stream function for the Brinkman's model in granular media is (Payatakes et al. 1974b):

$$\psi = -\frac{U}{2}\left[r^2 + \frac{2m_2}{m_1^2 r}\left(1 + \frac{m_3}{m_2}m_1^2 - e^{-m_1 r}(1 + m_1 r)\right)\right]\sin^2\theta \qquad (1-19)$$

where

$$m_1 = \frac{a}{\sqrt{k}} \qquad (1-20)$$

$$m_2 = -\frac{3}{2}e^{m_1} \qquad (1-21)$$

$$m_3 = \frac{1}{2}\left[-1 + \frac{3}{m_1^2}\left(e^{m_1} - 1 - m_1\right)\right] \qquad (1-22)$$

The permeability predictions of flow through granular media are:

$$k = \frac{2a^2\left[1 - 3(1-\varepsilon)^{1/3} + 3(1-\varepsilon)^{5/3} + 2(1-\varepsilon)^2\right]}{3\left[3 + 2(1-\varepsilon)^{5/3}\right]} \qquad \text{(Happel's Model)} \qquad (1-23)$$

$$k = \frac{2}{9}\frac{a^2}{1-\varepsilon}B(\varepsilon) \qquad \text{(Kuwabara's Model)} \qquad (1-24)$$

where

$$B(\varepsilon) = \left[1 - (1-\varepsilon)^{1/3}\right]^3\left[1 + \frac{6}{5}(1-\varepsilon)^{1/3} + \frac{3}{5}(1-\varepsilon)^{2/3} + \frac{1}{5}(1-\varepsilon)\right]^2 \cdot$$
$$\left\{\begin{array}{l} 1 + \frac{51}{50}(1-\varepsilon)^{1/3} + \frac{3}{50}(1-\varepsilon)^{2/3} - \frac{7}{25}(1-\varepsilon) + \frac{2}{5}(1-\varepsilon)^{4/3} \\ + \frac{12}{25}(1-\varepsilon)^2 + \frac{6}{25}(1-\varepsilon)^{7/3} + \frac{2}{25}(1-\varepsilon)^{8/3} \end{array}\right\} \qquad (1-25)$$

Theoretically speaking, the cell models and the Brinkman's model can be employed only in cases where the packing porosity is relatively high (e.g., $\varepsilon > 0.6$, Happel and Brenner 1965, Spielman and Goren 1968, Pich 1986) although all of them have been used in the study of granular beds where the porosity is usually in the range of 0.35-0.45, simply because no other good model is available for low porosity packings where the effect of the neighboring elements plays a very important role. The theoretical models for packings of non-uniform fibers and spheres have not been found in the literature.

1-2 Particle-Collector Interactions

Dispersion of particles in liquids is commonly encountered in a wide range of process industries. Dispersed particles can have sizes ranging from fractions of a millimeter to macromolecular dimensions (a few nanometers). Particles bigger than about 1µm in size are usually called suspended particles, smaller than about 1nm are molecules or atoms while the sizes in between are usually defined as colloidal particles.

Compared with suspended particles, colloidal particles may have the following properties. They are difficult to be seen under the usual optical microscopes because their sizes are mostly smaller than the wavelength of the ordinary light (about 0.5µm). Sedimentation can not be used to separate them from the suspending liquids because of the unacceptable long time required. It can be shown that the important types of inter-particle (or particle-surface) forces, known collectively as *colloidal interactions*, vary roughly in proportion to the particle size, whereas external forces, such as gravity and hydrodynamic drag have a stronger dependence on particle size. For instance, the gravity

force is proportional to the mass of particle and hence to the cube of the particle size. The hydrodynamic forces, as a result of fluid flow, depend roughly on the square of particle size. This means that for large particles, gravitational and drag forces will predominate over colloidal forces, but the later may be much more significant for colloidal particles. Colloidal interactions play a crucial role in determining the particle deposition efficiency, stability and rheological behavior of colloidal dispersions.

There are several types of colloidal interactions which are known to be important, the best known of which are the van der Waals attraction and double layer interactions. These two contributions form the basis of the classical DLVO theory of colloidal stability, independently proposed by Derjaguin and Landau (1941) and Verwey and Overbeek (1948). Other effects are now known to be important in certain cases and may play a large part in determining whether or not particles will adhere to each other or to other surfaces. In aqueous systems, the effect of hydration can be important. This is often associated with hydration of ions at particle surfaces and usually gives an extra repulsion. It is now known that hydrophobic effects can also be important, giving an extra attraction between particles or between particle and other surfaces. Other significant effects arise from the presence of adsorbed polymers, giving either a repulsion (steric interaction) or an attraction (polymer bridging). There have been a few very good reviews on this subjects (Isrealachvili 1992, Russel et al. 1989). Presented here is a recapitulation of the major colloidal forces and a summary of the well known equations, which serves as a reference for colloidal interaction calculations used in particle deposition modeling.

1-2-1 Van der Waals Interactions

The universal attractive forces between atoms and molecules, known as van der Waals forces, also operate between macroscopic objects. Van der Waals attraction originates from the instantaneous dipole moments generated by the temporary asymmetrical distribution of electrons around atomic nuclei.

Essentially there are two theoretical approaches to the evaluation of the van der Waals attraction. The microscopic approach, due largely to Hamaker(1937), calculates the interaction between macroscopic bodies by the pairwise summation of all the relevant intermolecular interactions. The expressions obtained in this manner may be split into a purely geometric part and a constant H, the Hamaker constant, which is related only to the properties of the interacting bodies and the medium. The assumption of pairwise additivity is a serious deficiency and always results an overestimation of the van der Waals force. This deficiency can be overcome in the macroscopic approach suggested by Liftshitz (1956), in which the interaction is calculated entirely from considerations of the macroscopic electromagnetic properties of the medium, but its application is limited to cases where detailed knowledge of the dielectric responses of the interacting media over a wide frequency range is available. Certain simplifications are possible, very clearly described by Hough and White (1980) and Prieve and Russel (1988), but considerable computation is needed. It is also worth noticing that the difference between the results obtained from the two approaches is not too great (usually less than 60%, Elimelech et al. 1995). Hence, the practical way to calculate the van der Waals interaction is to rely on

the simple Hamaker-type expressions with corrections to account for the difference between the two approaches (retardation effect). Listed in Table 1-1 are a few expressions for the retarded van der Waals interaction potential between a sphere and a plate, which is the geometry encountered in particle deposition modeling.

1-2-2 Double layer Interaction

Practically all solid surfaces in an aqueous medium carry a surface charge, which can arise from mechanisms such as ionization of surface groups and specific adsorption of ions. In an electrolyte solution, the distribution of ions in the vicinity of the solid surface is determined by electrical interaction with the surface and the thermal motions of the ions (diffusion). Counter-ions are attracted toward the surface and can be either closely associated with the surface or distributed exponentially into the solution. Solid surfaces of the same charge approaching each other begin to experience repulsion when their diffusion layers overlap. On the other hand, solid surfaces with different charges undergo an attraction when they come close to each other.

In considering the double layer interaction, an important quantity is the electric potential at the inner boundary of the diffusion layer, i.e., close to the surface but just outside a layer of closely associated counter-ions, usually called Stern layer. This potential is not measurable directly, but is close to another quantity, the zeta-potential, which can be obtained from a number of electrokinetic experiments such as the streaming potential and electro-osmosis measurements. Some of the widely used expressions for

calculating the double layer interaction potential for the sphere-plate geometry are listed in Table 1-2.

Table 1-1 Retarded van der Waals interactions for sphere-plate geometry

Author	Expression	Validity
Schenkel & Kitchener (1960)	$-\dfrac{Ha}{6h}\left[\dfrac{1}{1+11.12h/\lambda_w}\right]$	$h<\lambda_w/\pi$ $h<<a$
Ho and Higuchi (1968)	$-\dfrac{Ha}{6h}\left[\dfrac{2.45}{10\pi}\left(\dfrac{\lambda_w}{h}\right)-\dfrac{2.17}{60\pi^2}\left(\dfrac{\lambda_w}{h}\right)^2+\dfrac{0.59}{280\pi^3}\left(\dfrac{\lambda_w}{h}\right)^3\right]$	$h>\lambda_w/\pi$ $h<<a$
Gregory (1981)	$-\dfrac{Ha}{6h}\left[1-\dfrac{5.32h}{\lambda_w}\ln\left(1+\dfrac{\lambda_w}{5.32h}\right)\right]$	$h<<a$
Czarnecki (1979)	$-H\left[\dfrac{2.45\lambda_w}{60\pi}\left(\dfrac{h-a}{h^2}-\dfrac{h+3a}{(h+2a)^2}\right)-\dfrac{2.17\lambda_w^2}{720\pi^2}\left(\dfrac{h-2a}{h^3}-\dfrac{h+4a}{(h+2a)^3}\right)+\dfrac{0.59\lambda_w^3}{5040\pi^3}\left(\dfrac{h-3a}{h^4}-\dfrac{h+5a}{(h+2a)^4}\right)\right]$	$h>\lambda_w/\pi$

Note: $\lambda_w = 2\pi c/\omega_v$, where c is the velocity of light and ω_v is the dispersion frequency.

$\quad\lambda_w$ is a characteristic wavelength with a value around 100nm for most materials.

Table 1-2 Double layer interaction potential for sphere-plate geometry

Author	Expression	Validity
Hogg et al. (1966) Wiese & Healy (1970) Usui (1973)	$\pi a\varepsilon(\varphi_1^2+\varphi_2^2)\left[\dfrac{2\varphi_1\varphi_2}{\varphi_1^2+\varphi_2^2}\ln\left(\dfrac{1+e^{-\kappa h}}{1-e^{-\kappa h}}\right)\pm\ln(1-e^{-2\kappa h})\right]$ $+$ for constant potential approximation $-$ for constant charge approximation	Small φ_i $h<<a$ $\kappa a_i>>1$
Gregory (1975)	$128\pi an_\infty k_B T\dfrac{e^{-\kappa h}}{\kappa^2}\tanh\dfrac{ze\varphi_1}{4k_B T}\tanh\dfrac{ze\varphi_2}{4k_B T}$	$h<<a_i$ $\kappa a_i>5$ Symmetric electrolyte

Note: $\kappa=\sqrt{\dfrac{e^2\sum n_{i\infty}z_i^2}{\varepsilon k_B T}}$, the reciprocal Debye length.

$\quad z_i$ is the valence of ion i.

1-2-3 Non-DLVO Interactions

Since the development of the DLVO theory, many investigators reported experimental results which can not be explained by the consideration of the two principle forces. In such cases, additional interactions have been proposed. Among them the most widely accepted ones are the hydration, hydrophobic, steric and polymer bridging interactions, which will be discussed briefly. It should also be noted that the quantitative expressions for these non-DLVO forces are still not available, therefore they can not be incorporated into the modeling work.

Hydration force

The nature of water close to a particle surface can be very different from bulk water, for these portion of water tend to be bounded more tightly to the surface by ionic groups or hydrophilic sites on the surface. The approach of a particle toward a collector with one or both of the surfaces hydrated will generally be hindered by an extra repulsive interaction. This hydration repulsion arises essentially from the need for the surfaces to become dehydrated if true contact between the particle and the collector surface is to occur.

Hydrophobic force

When a surface has no polar or ionic groups or hydrogen-bonding sites, there is no affinity for water and the surface is said to be hydrophobic. The nature of water in

contact with such a surface will be different from that of the bulk water, which is significantly structured because of the hydrogen bonding between the molecules. Water confined in the gap between two such surfaces will not be as structured as the bulk water when the two hydrophobic surfaces come close to each other. For a narrow gap, this would result in an increased free energy of the water relative to the bulk water. Hence, the water in the gap has the tendency to leave the gap. In other words, there would be an attraction between hydrophobic surfaces when they are close enough.

Steric and Polymer bridging force

Polymer adsorption onto solid surfaces can greatly change the interactions. With a very small adsorption amount, the individual polymer chains can be attached to two or more surfaces, providing an extra attraction between them. This effect is called polymer bridging. On the other hand, if a big amount is adsorbed onto the surfaces, the polymer layer can cause a strong repulsive force between them, usually termed as steric repulsion. As the surfaces approach sufficiently close, the adsorbed layers come into contact and any closer approach would involve some penetration of the hydrophilic chains. Since these chains are hydrated, overlapping of the layers would cause some degree of dehydration and hence a repulsion between the surfaces.

1-2-4 Combined Interaction

The total interaction energy between two surfaces is the summation of all the contributions.

$$\Phi = \Phi_{vdW} + \Phi_{DL} + \Phi_H + \Phi_{HP} + \Phi_S + \Phi_{PB} + \cdots \qquad (1\text{-}26)$$

Here, Φ_{vdW}, Φ_{DL}, Φ_H, Φ_{HP}, Φ_S and Φ_{PB} represent the van der Waals, double layer, hydration, hydrophobic, steric and polymer bridging interaction energies, respectively. Up to now, only the van der Waals and double layer interactions can be predicted reliably through theoretical models as discussed above. However, with the development of surface interaction force measurement instrumentation, such as the atomic force microscopy (AFM) and the total internal reflection microscopy (TIRM), the total interaction energy can be measured accurately. This information instead of the theoretical predictions can be more reliably used as the input data in the particle deposition modeling.

A typical curve for the combined interaction energy as a function of the separation distance with consideration of only the van der Waals and double layer interactions is shown in Figure 1-1. The most important features of this curve include a deep primary minimum and an energy barrier. The existence of the deep primary minimum means that once a particle comes into this region it will be dragged toward the surface and permanently attached to it. On the other hand particles must overcome the energy barrier in order to come into the primary minimum. Because of the different distance dependence of the van der Waals and the double layer potentials, the former is always greater than the latter at sufficiently large separation distances. This gives a secondary minimum in the potential curve, which can be responsible for particle deposition too. Since the interaction potentials are directly proportional to particle size, secondary minimum effects are more significant with larger particles (greater than about 1µm in

diameter, Elimelech et al. 1995). The possible particle deposition in the secondary minimum will be neglected in the current research because only the colloidal particles will be treated.
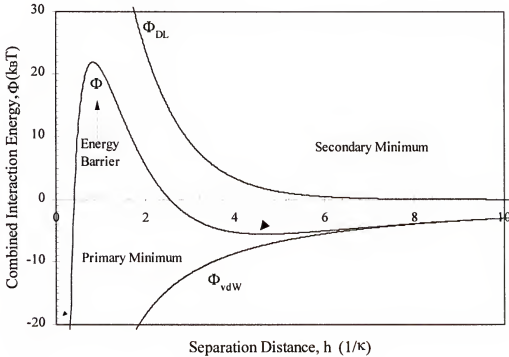
Figure 1-1 Van der Waals, double layer and the combined interaction potentials between a 0.5 μm (diameter) particle and a plate. (The surface potentials are assumed to be 16.8mV, the solution is a 20mM 1-1 electrolyte, the Hamaker constant is 8.5×10^{-21} J, the reciprocal Debye length is 2.17nm)

1-2-5 Effect of Surface Heterogeneity on Surface Interactions

Most of the work on surface interactions have been focused on ideal surfaces: molecularly smooth and uniform distribution of properties. In the recent years, it becomes clearer that the surface heterogeneity, such as non-uniform distribution of surface charge and the surface roughness, may play an important role in altering the particle deposition

behavior. Most solid surfaces in aqueous media are heterogeneously charged at both the microscopic (molecular) and macroscopic levels (Elimelech et al. 1995). Surface charge heterogeneity is attributed to the complexity of the crystaline structure of solids and to their complex chemical composition (Spoito 1984, Jaroniec and Madey 1988). Surface-bound impurities may be an additional source of charge heterogeneity.

Due to the charge heterogeneity on the surfaces, especially that on the collector surface, some sites may be favorable while others may be unfavorable to particle deposition and this can greatly affect the overall particle deposition (Hull and Kitchener 1969, Bowen and Epstein 1979, Gregory and Wishart 1980, Adamczyk et al. 1983, Dabros and van de Ven 1983, Vaidyanathan and Tien 1991, Kihira et al. 1992, Song et al. 1994).

The effect of surface roughness on colloidal interactions has also been investigated in the recent years through modeling (Elimelech and O'Melia, 1990a, Suresh and Waltz 1996). Rough surfaces may decrease the total energy barrier.

1-3 Deposition of Colloidal Particles onto Solid Surfaces

Deposition of small solid particles from a liquid dispersion are encountered in a variety of situations in manufacturing and process technologies and in natural aquatic environments. In some cases, deposition is desirable, as in filtration and various processes in which a coating of deposited particles needs to be formed. In many other instances, deposition needs to be prevented. These include detergency, mineral processing, where slime coating of colloidal particles onto larger grains can be a serious

problem, and the fouling of heat exchanger surfaces. A number of biological examples could also be mentioned, such as the deposition of bacteria on the tooth surface and thrombus formation associated with artificial organs. There is considerable interest in the transport of colloidal contaminants including bacteria and viruses in the ground water and this depends greatly on the deposition behavior of such particles in soils and aquifers. Fundamental studies of particle deposition have been undertaken with different perspectives and with various objectives (Tien 1989, Elimelech et al. 1995). The current section presents the key outlines of the two general approaches, Lagrangian and Eulerian, used in the particle deposition modeling, followed by a detailed description of the Eulerian method which will be applied in the current study.

1-3-1 Filtration Efficiency, Penetration, Mass Transfer Coefficient and Filter Coefficient

A filter's ability to collect particles is usually expressed in one of the following four qualities: filtration efficiency, penetration, filter coefficient and mass transfer coefficient. The filtration efficiency η for a certain depth L of filter is defined as

$$\eta = \frac{c_{in} - c_{eff}}{c_{in}} \tag{1-27}$$

where c_{in} and c_{eff} denote the influent and effluent particle concentrations, respectively. The penetration, most often used in aerosol science, is defined as the effluent and influent concentration ratio c_{eff}/c_{in}, or $1-\eta$. These two qualities are the overall measurement of the collection ability. The filter coefficient λ and the mass transfer coefficient k_m are, on the other hand, local variables, which may change with position. But in most cases these two

qualities were given as averaged values in the whole filter medium. The definition of the mass transfer coefficient is

$$k_m = \frac{J}{c - c_{surf}} \tag{1-28}$$

where J is the particle deposition flux, c the bulk particle concentration and c_{surf} is the particle concentration on the collector surface. In most of the particle deposition studies, a perfect sink of particles is assumed on the collector surface, i.e., c_{surf}=0. That is because the particles themselves become part of the collector once they are attached to the collector surface. Balancing the movement of particles in a differential depth of filter gives

$$-U \frac{dc}{dl} = J A_{sp} \tag{1-29}$$

where U is the superficial velocity of the suspension, A_{sp} the specific surface area of the filter, l is the coordinate of the filter depth. If k_m is assumed to be constant along the depth of the filter, substituting equation (1-28) into (1-29) and carrying out the integration yields

$$c = c_0 e^{-\frac{A_{sp} k_m}{U} l} \tag{1-30}$$

which shows that the particle concentration decays exponentially in the direction of the flow. The exponential constant is called filter coefficient, λ, i.e.,

$$\lambda = \frac{A_{sp} k_m}{U} \tag{1-31}$$

The relationship between the filtration efficiency and the filter coefficient is

$$\eta = 1 - e^{-\lambda L} \tag{1-32}$$

It is obvious that the mass transfer coefficient is the most intrinsic property of the particle deposition process, therefore k_m will be used throughout the current work.

(a) Lagrangian Approach

(b) Eulerian Approach
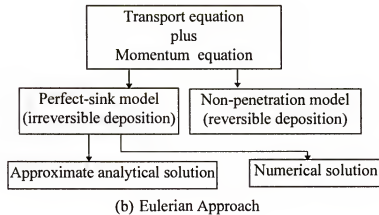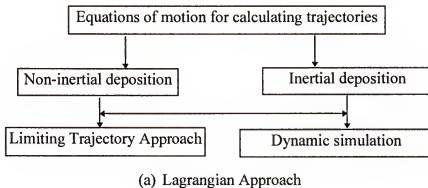
Figure 1-2 Two approaches for particle deposition modeling

1-3-2 Two Approaches in Particle Deposition Modeling

Due to its practical importance, numerous studies have been conducted to model the particle deposition process during the past several decades (Rajagopalan and Tien 1979, Tien 1989, Elimelech et al. 1995). Two principal approaches are available for

modeling purposes. The *Lagarangian* approach considers the behavior of individual particles, or their trajectories, at the microscopic level, whereas the *Eulerian* approach describes the particles collectively in terms of their distribution, or probability density, in time and space, thus it is a typical macroscopic approach. The general procedures of these two basic methodologies are summarized in Figure 1-2. In the current research, we will take the Eulerian approach, because all the equations derived by using this method can be directly applied to other heat and mass transfer processes in the same medium due to the similarity between them.

1-3-3 General Procedure for the Eulerian Approach

Figure 1-3 is an exploded detail of the Eulerian method. Also shown in the same figure are the two major tasks of the current research: an improved porous medium model and the particle deposition modeling based on it.

Removal of small colloidal particles in a porous filter is not achieved by straining since the pore size of the porous filter is usually a few order of magnitude larger than the colloidal particles being removed. Thus the only way for the particles to be removed is by deposition on the collector surfaces through colloidal interactions between particles and collectors. Deposition of particles from an aqueous fluid medium flowing through a porous medium may be viewed as a two-step process: the transport of the particles from liquid bulk to the proximity of the fiber surfaces by the combination of convection and Brownian diffusion (which we may call "bulk transport") and the subsequent adhesion of
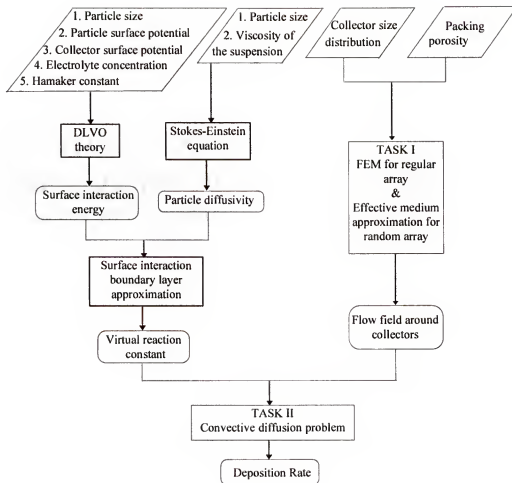
Figure 1-3 General procedure for modeling of particle deposition rate in fibrous or granular media used in the current research

particles to the collector surface by colloidal forces ("surface deposition"). The interaction forces of non-hydrodynamic origin include van der Waals attraction and electrostatic (or double layer) interactions for most particulate systems. In some cases, hydrophobic, steric, and hydration forces also play an important role especially for biological particles or the particles with absorbed polymers or surfactants. Since all these surface forces are very short ranged, they usually take effect only when the particles come

very close to the collector surface (< 0.1 μm). Since the colloidal particles are much smaller than the collector, the interactions between particles and the collectors may be considered as interactions between particles and a flat surface.

The concentration distribution of particles convected with a fluid passing through the porous medium can be described by the following steady state convective diffusion equation. It includes the contribution of an external force field (Bird et al. 1959; Spielman and Friedlander 1974) :

$$\mathbf{u} \cdot \nabla c = \nabla \cdot \left[\mathcal{D} \nabla c + \frac{\mathcal{D}}{k_B T} \nabla \Phi c \right] \tag{1-33}$$

Here $\mathbf{u}$ is the fluid velocity, c the particle concentration, $\mathcal{D}$ the particle diffusion coefficient, Φ the total interaction potential, k_B the Boltzmann constant and T the absolute temperature. Since the colloidal particles are so small, their size is neglected and the particle laid fluid is viewed as a continuum. When the particles are very close to the collector surface, however, the size effect may become significant as the diffusivity is influenced significantly. This hydrodynamic interaction at close range is usually taken care of by lumping its contribution into a position-dependent diffusion coefficient: $\mathcal{D}(h) = \mathcal{D}_\infty / g(h)$. Here $\mathcal{D}_\infty$ is the particle diffusion coefficient in the bulk, which may be estimated by the Stokes-Einstein equation (Bird et al. 1960). g(h) is the hydrodynamic retardation function g(h) given by Brenner (1961).

Although colloidal particles are small, their diffusivity is still very small compared to those of molecular species. Therefore, convective transport is usually dominant over diffusion (i.e., Peclet number Pe>> 1) even when the Reynolds number is small. Consequently, a diffusion boundary layer exists. In addition, in many cases of

practical interest, the thickness of the electrical double layer (which characterizes the range of electrostatic interaction) is even smaller than the diffusion boundary layer thickness. In this case, the prescribed problem can be simplified in which the external force term in equation (1-33) can be dropped while the contribution of the colloidal interactions are represented by a modified boundary condition on the collector surface:

$$\mathcal{D}_\infty \left(\frac{\partial c}{\partial n} \right) = K_\Phi c \tag{1-34}$$

Here n is the coordinate in the outward normal direction from the collector surface, and K_Φ is a constant which depends on the particle-surface interaction potential as follows:

$$K_\Phi = \mathcal{D}_\infty \left\{ \int_0^\infty \left[g(h) e^{\Phi/k_B T} - 1 \right] dy \right\}^{-1} \tag{1-35}$$

where h is the separation distance between a particle and the surface and h=y-a. This simplification is often called the Interaction Force Boundary Layer (IFBL) approximation which was first described independently by Ruckenstein & Prieve (1973) and Spielman & Friedlander (1974). Later, this IFBL approximation was rigorously justified by the method of matched asymptotic expansions (Shapiro et al. 1990).

As we may note from equation (1-33), the flow field **u** needs to be specified in order to determine the particle deposition rate on to the collector surface. As it was pointed out, the diffusive transport and subsequent deposition of particles occurs within the diffusion boundary layer. Thus, the flow field description is required only in the immediate vicinity of the collector surface in solving equation(1-33). Therefore, the linearized velocity field as in typical boundary layer equations will suffice the need. For

the cylindrical and spherical geometries, the linearized velocity fields are represented by the following stream functions, respectively:

$$\psi = -2A_c(r-1)^2 \sin\theta \tag{1-36}$$

$$\psi = \frac{3}{4}A_s(r-1)^2 \sin^2\theta \tag{1-37}$$

Here A_c and A_s are the flow field parameters which are unique to each of the porous medium models.

Using the IFBL approximation, Spielman and Friedlander (1974) obtained the following particle deposition rates on a cylindrical collector and a spherical collector using the linearized flow fields:

$$Sh_c = 0.731A_c^{1/3}Pe^{1/3}\gamma_c(\beta_c) \tag{1-38}$$

$$Sh_s = 0.635A_s^{1/3}Pe^{1/3}\gamma_s(\beta_s) \tag{1-39}$$

where

$$\beta_c = 1.022A_c^{-1/3}Pe^{-1/3}Da \tag{1-40}$$

$$\beta_s = 1.125A_s^{1/3}Pe^{-1/3}Da \tag{1-41}$$

Here $Sh = k_m a/\mathcal{D}$, $Pe = Ua/\mathcal{D}$ and $Da = K_\Phi a/\mathcal{D}$. $\mathcal{D}$ is the particle diffusivity, a the collector radius, K_Φ the virtual reaction constant. $\gamma_c(\beta_c)$ and $\gamma_s(\beta_s)$ are the functions tabulated in Table 1-3. If the virtual surface reaction is instantaneous, $\gamma(\beta)=1$ in equations (1-38) and (1-39), the equations are then reduced to the ones without reaction on the surface, which were first derived by Levich (1962). For an isolated sphere, the flow field is given by the Stokes equation, $A_s=1$. So, the flow field parameter A_s in equation (1-38) represents the influence of neighboring spheres in a granular packing.

Table 1-3 Numerical values of the functions γ_c and γ_s
(converted from Spielman and Friedlander, 1974)

β_c or β_s	$\gamma_c(\beta_c)$	$\gamma_s(\beta_s)$
0	0	0
0.01	0.014044	0.013198
0.02	0.02772	0.026078
0.05	0.066686	0.062857
0.1	0.125445	0.118709
0.2	0.2241	0.213217
0.5	0.423033	0.407133
1	0.5984	0.5822
2	0.7518	0.738867
5	0.885083	0.877833
10	0.939455	0.935364
20	0.968952	0.966667
50	0.987353	0.986373
100	0.993663	0.993069
∞	1	1

1-4 Interaction Force Boundary Layer Approximation

As shown above, the particle deposition rate can be found by solving the convective diffusion equation (1-33) under the surface interaction force field if the flow field is known. But this equation is difficult to solve analytically. An approximate analytical solution for calculating the particle deposition rate when electrical double layer repulsive forces are significant may be useful. The most widely used one is the so called

Interaction Force Boundary Layer (IFBL) approximation. The IFBL approximation was developed by Ruckenstein and Prieve (1973) and Spielman and Friedlander (1974) independently. The basic ideas behind the approximation are presented here.

Colloidal interaction forces take effect only over very short distances from the surface of the collector, usually less than 0.1 μm. It is possible to identify two regions adjacent to the collector surface, characterized by the relative magnitude of the colloidal interaction forces. In the vicinity of the collector surface, the colloidal interaction forces predominate while the convective transport may be neglected. It is this region that is referred to as the interaction force boundary layer. The thickness of this region is characterized by the operating distance of the double layer, on the order of the Debye length κ^{-1}. In the region away from the IFBL, the colloidal interaction forces vanish while convective transport becomes important. The thickness of this region is on the order of the diffusion boundary layer, δ_D, of the order $aPe^{-1/3}$(Levich 1962).

The IFBL approximation is based on the assumption that the diffusion boundary layer is very thick compared to the IFBL, i.e.,

$$\kappa aPe^{-1/3} \gg 1 \tag{1-42}$$

In the IFBL region, where the fluid velocity is negligible, the transport of particles is controlled by diffusion and colloidal forces. The convective diffusion equation (1-32) can be simplified to:

$$\nabla \cdot \left(\mathcal{D} \nabla c + \frac{c \mathcal{D}}{k_B T} \nabla \Phi \right) = 0 \tag{1-43}$$

With the assumptions that the total interaction potential Φ is only a function of the boundary layer coordinate y, which is perpendicular to the collector surface, and that the

tangential diffusion is negligible compared to the diffusion perpendicular to the surface, equation (1-43) can be easily solved to get:

$$c = -\frac{J(x)}{\mathcal{D}_\infty} e^{-\frac{\Phi}{k_B T}} \left[\int_0^y \left(g(h)e^{\frac{\Phi}{k_B T}} - 1 \right) dy + y \right] \tag{1-44}$$

This equation describes the particle concentration profile in the IFBL as a function of the distance away from the surface, which is shown schematically in Figure 1-4.
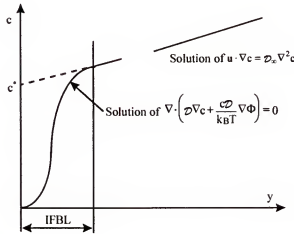
Figure 1-4 Concentration profile in the vicinity of the collector surface

At distances much larger than the thickness of the double layer ($y \gg \kappa^{-1}$) but still close enough to the collector surface, both the convection and the surface interaction forces may be neglected. In this instance, equation (1-43) can be simplified to:

$$c = -\frac{J(x)}{\mathcal{D}_\infty} \left[\int_0^\infty \left(g(h)e^{\frac{\Phi}{k_B T}} - 1 \right) dy + y \right] \tag{1-45}$$

which is linear in y as shown in Figure 1-4. In this equation, the upper limit of the integral has been arbitrarily chosen to be ∞, because $\int_b^\infty \left(g(h)e^{\Phi/k_B T} - 1 \right) dy = 0$ for any value b>>k^{-1}, and $\int_0^\infty \left(g(h)e^{\Phi/k_B T} - 1 \right) dy$ becomes a constant.

At distances further away from the collector surface, equation (1-33) is reduced to:

$$\mathbf{u} \cdot \nabla c = \mathcal{D}_\infty \nabla^2 c \tag{1-46}$$

It is obvious that the linear portion of the solution (1-44), i.e., equation (1-45) is the solution of (1-46). Taking any point along this linear part as one of the boundary conditions to (1-46), we can then solve it to obtain the concentration profile outside of the IFBL. The solution we get would be the same if we use the extrapolated point at y=0,

$$c^* = -\frac{J(x)}{\mathcal{D}_\infty} \int_0^\infty \left(g(h)e^{\frac{\Phi}{k_B T}} - 1 \right) dy \tag{1-47}$$

as the boundary condition instead of an arbitrary point as described above.

Equation (1-47) shows that the problem of deposition of colloidal particles with a potential barrier confined to a narrow region close to the collector surface can be found by solving the usual convective diffusion equation (without the external force field) subject to the following boundary condition:

$$J(x) = -K_\Phi c^*(x) \tag{1-48}$$

where

$$K_\Phi = \frac{D_\infty}{\int_0^\infty \left(g(h)e^{\Phi/k_B T} \right) dy} \tag{1-49}$$

The boundary condition (1-48) is equivalent to a first order reaction on the surface.

1-5 Dissertation Organization

As stated in Section 1-3, the major tasks of the current research are two folds: an improved porous medium model, the effective medium approximation, which will be applied to both fibrous and granular media and will also be extended to packings of polydisperse cylinders and spheres; and the particle deposition modeling based on the improved porous medium model.

Chapter 1 provides the necessary fundamentals for understanding the topic and also the major research developments in this field which will be frequently referred to in the dissertation. This includes a brief summary of the porous medium models and the corresponding flow field and permeability predictions, the surface interaction forces and the corresponding equations to calculate their potentials, and an outline of the procedures for particle deposition modeling, followed by a brief derivation of the interaction force boundary layer approximation which is the key simplification toward solving the complicated convective diffusion problem.

For simple regular array of cylindrical cylinders, the numerical simulation can provide accurate predictions of the detailed flow and concentration fields by solving the Stokes and convective diffusion equations. This is done in Chapter 2.

The analyses of the effective medium approximation applied to randomly packed fibrous and granular media are elaborated in Chapter 3 and Chapter 4, respectively. The Stokes and Brinkman's equations are solved to get the representative velocity fields. The

packing permeabilities are then obtained through force balances in the media. The results are compared with the predictions by other models and experimental data.

Chapter 5 treats the particle deposition in fibrous and granular media based on the flow fields obtained in the preceding chapters. Chapter 6 is an investigation of the influencing parameters such as electrolyte concentration, surface potentials and hydrodynamic interaction on the particle deposition rate.

It should also be noted that although the current research is focused on the deposition of colloidal particles in fibrous and granular media, the concluding equations can be applied to other mass and heat transfer processes in the same media.

CHAPTER 2
DEPOSITION OF COLLOIDAL PARTICLES IN PERIODIC ARRAYS OF CYLINDERS

2-1 Periodic Array of Cylindrical Collectors

As discussed in Chapter 1, the velocity field around each of the collectors has to be obtained in order to determine the deposition rate in a porous medium by solving the convective diffusion equation. For simpler geometries, like periodic arrays of cylindrical collectors which will be treated in this Chapter, some numerical algorithms can be used to solve the Stokes equation and the convective diffusion equation simultaneously. The Finite Element Method (FEM) will be used in the current study.

Figure 2-1 describes a square array of collectors which consists of two different size cylinders of r_1 and r_2 alternating with the minimum surface-to-surface distance of s. While all three collector parameters can be varied, there remain two degrees of freedom if the volume fraction of collectors (or porosity) is to be fixed. Thus for a fixed value of porosity, the ratio of r_1/r_2 can be varied and its influence on the filtration efficiency can be investigated. In the conventional modeling where the cell models of Happel or Kuwabara are used, the effect of distribution of collector size on filtration efficiency cannot be investigated as they take into account only the representative size and the volume fraction of collectors (Speilman 1977, Russel et al. 1989, Tien 1989).

Throughout the calculation, r_2 was fixed at 0.5 mm while r_1 was varied between 0.05 and 0.5 mm. s was also varied so that the porosity would be in the range of 50% to 70%. All other parameters were specified to simulate the filtration of silica or styrene latex particles which are smaller than 1.5 μm in diameter and dispersed in an aqueous solution. Thus, the Hamaker constant was set between 10^{-21} and 10^{-19} J. Assuming a spherical shape, the diffusivity of the particles was calculated using the Stokes-Einstein equation. The surface potential may vary depending on the hydronium ion concentration in the solution, and a broad range of values was used up to ±60 mV for the calculation. While the surface potentials of collectors and particles may vary independently, the same value was assigned to both collectors and particles for simplicity. This, however, does not restrict any conclusions drawn in the present study.

Also described in Figure 2-1 is the flow domain for the present numerical calculation which consists of four unit cells in series. The flow direction is from left to right, and the equations (1-2, 1-46) subject to the boundary condition (1-34) are solved by a finite element method to determine the velocity and the concentration fields. The particle concentration at the inlet of the flow domain is specified as 1.0 uniformly across the array as the concentration is scaled by the inlet concentration. The velocity profile at the inlet is also assumed to be uniform since it is not known *a priori*. This flat velocity profile relaxes very quickly to a new steady value within the first unit cell, and the velocity field in the subsequent three cells of the down stream matches one another exactly.
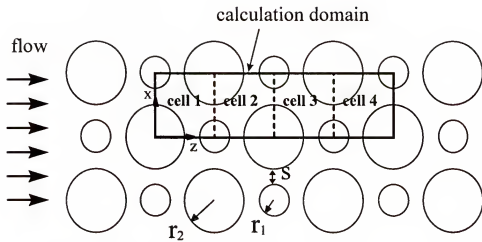
Figure 2-1 Periodic array of cylindrical collectors and the flow domain for numerical calculation
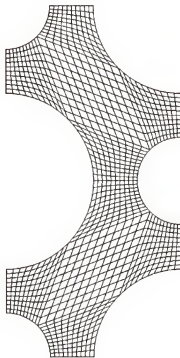
Figure 2-2 Finite element mesh used in the current investigation
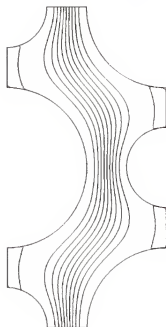
Figure 2-3 The velocity field calculated by FEM—stream line

Figure 2-4 The particle concentration distribution calculated by FEM—concentration contour lines (U=0.0001mm/s, K_a=1x10^{-9} m/s, the concentration from the middle toward outer boundary c/c_0=0.769,0.8,0.83,0.86,0.89,0.92,0.95,0.98)

Shown in Figure 2-2 2-3 and 2-4 are the finite element mesh, the velocity field and the particle concentration distribution calculated by the Finite Element Method. The unit cell described in Figure 2-2 contains 500 quadrilateral elements with their sizes decreasing gradually toward the collector surface. Thus, the flow domain of calculation contains a total of 2,000 elements. The accuracy of the present calculation has been checked by comparing the drag force imposed on a collector in the square array with the results of Sangani & Acrivos (1982). They have determined the drag on a cylinder in a square array by a boundary collocation method using an infinite series solution for vorticity and stream function for a low Reynolds number flow. The dimensionless drag force on a unit length cylinder ($F/\mu U$) was calculated to be 102.90 and 532.55 when the porosity was 70% and 50%, respectively. These values are exactly same as those of Sangani & Acrivos to the second decimal points. Although there are no data available for comparison, the calculated concentration field is expected to be as accurate as the velocity field. It should be noted that the superficial velocity was set to an extremely low value in order to show the particle concentration change pattern in the flow path.

In all calculations the superficial velocity of the fluid has been limited up to 0.1 mm/s. This value is rather small compared to those in actual filtration processes. Nevertheless, this limit was necessary in order to obtain a detectable concentration change over the calculation domain (i.e., four unit cells). If the superficial velocity is higher, the concentration change over a unit cell is very small requiring a longer calculation domain which is numerically too intensive. Even at a velocity as low as 0.001 mm/s, however, the Peclet number (Pe = $Ua/\mathcal{D}$) is still as large as 10^3, and consequently

the convection is still dominant in accordance with the assumptions described in Section 1-4. Thus, all physical phenomena occurring at a fluid velocity of order 1 mm/s should be preserved even at a fluid velocity as low as 0.001 mm/s. Unless the fluid velocity is unrealistically large (e.g., 1 m/s), the Reynolds number is always smaller than about 10^{-3} justifying the use of Stokes equation for the velocity field.

2-2 Effect of Surface Potentials

In Figure 2-5, the mass transfer coefficient is plotted against the surface potentials under the conditions specified in the figure caption. When the product of particle and collector surface potentials is higher than about 130 $(mV)^2$, the mass transfer coefficient is very small no matter whether the fluid velocity is high or low. It is due to the strong repulsion (or a high repulsive barrier) between the particles and the collectors which prevents the particle capture. As the surface potential is decreased, the repulsive barrier is lowered and the number of particles carried over the barrier increases resulting in a gradual increase in mass transfer coefficient. When the product of the surface potentials is lower than about 100 $(mV)^2$, the rate of particle capture does not increase any more since it is now limited by the diffusion which brings the particles to the proximity of collector surfaces. It may be interesting to note that the critical value of the product of the surface potentials at which the particle capture is diffusion limited is positive. It implies that collectors with opposite charge to the particles may not improve the filtration efficiency any further since the particle capture is still diffusion limited.
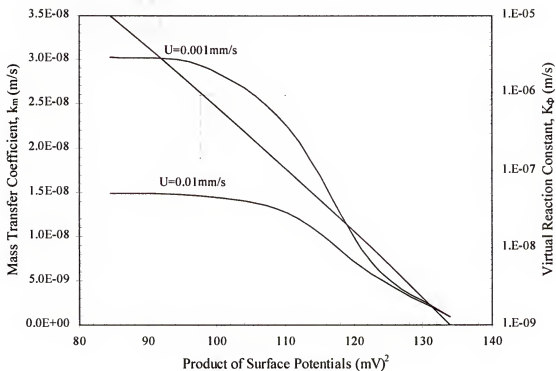
Figure 2-5 Dependence of mass transfer coefficient on surface potentials. (0.5 μm particles in diameter; temperature = 298K; Hamaker constant = 8.5 x 10^{-21}J; ionic concentration = 2mM, 1-1 electrolyte; r_1=0.25mm, r_2=0.5 mm, s=0.25mm).

The existence of a small region of the critical surface potential product below which the particle deposition is limited by diffusion and beyond which it is essentially impossible was, in fact, predicted by previous investigators (Ruckenstein and Prieve 1973) and also observed experimentally (Spielman and FitzPatrick, 1973). This will be explored in detail later in Chapter 6.
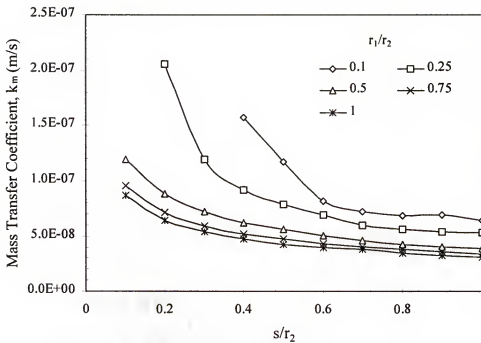
Figure 2-6 Influence of collector size ratio and porosity (U = 0.01 mm/s; K_ϕ=0.001m/s; D=8.73x10-13m^2/s)

2-3 Effect of Collector Size Ratio and Porosity

In Figure 2-6, the influence of porosity and the r_1/r_2 ratio on the mass transfer coefficient is shown. As we may anticipate, the mass transfer coefficient decreases with increasing porosity. It is due to the more favorable flow (or streamline) pattern for particle capture created at a smaller r_1/r_2 ratio. When $r_1/r_2 = 1$ (see Figure 2-1), the collector assemblage is simply a square array of same size cylinders. When r_1 is negligibly small compared to r_2, on the other hand, the assemblage is virtually a staggered array which should increase the capture efficiency as the flow pattern in this array

decreases the thickness of the mass transfer boundary layer. We may anticipate that this dependence of mass transfer coefficient on r_1/r_2 ratio becomes more significant with decreasing porosity as predicted by the present calculation.
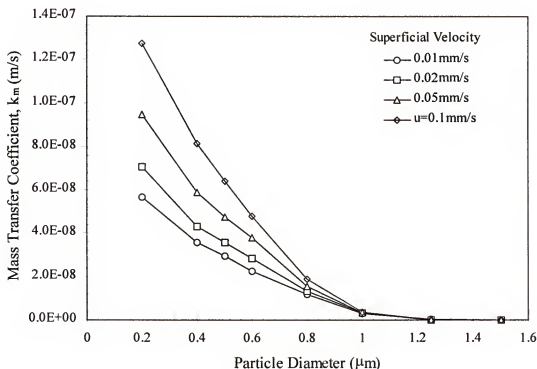
Figure 2-7 Dependence of mass transfer coefficient on particle size (Temperature = 298K; Hamaker constant =8.5 x10^{-21} J; ionic concentration = 2mM of 1-1 electrolyte; r_1=0.25mm, r_2=0.5mm, s=0.25mm; φ_1=φ_2=-10mV).

The dependence of mass transfer coefficient on the array (or packing) structure of collectors is rather significant as shown in Figure 2-6. Such dependence, however, cannot be predicted by the conventional isolated-collector models utilizing the cell models of either Happel or Kuwabara since only a representative collector size and the porosity are taken into account in these models (Spielman 1977).

2-4 Effect of Particle Size

The particle size has significant influence on the mass transfer coefficient since the filtration process is typically diffusion limited.   In Figure 2-7 the mass transfer coefficient is plotted as a function of particle size for which the diffusion coefficient has been calculated using the Stokes-Einstein equation for spherical particles.   With increasing particle size the mass transfer coefficient decreases due to smaller diffusivity. When the particle size is about 1.2 μm, the mass transfer coefficient is virtually zero since the particle diffusivity is very small.   As the particle size is further increased, the mass transfer coefficient is expected to increase gradually since the inertia effect, which has not been considered in the present study, will start to play a role.   Consequently, particles within the size range of about 1 to 5 μm are likely to be most difficult to capture since neither Brownian nor the inertia effect is significant.

2-5 Summary

We have studied the influence of the packing structure, surface potentials of the filter and particles, and particle size on the capture efficiency of colloidal particles in an idealized square array of cylindrical collectors using a finite element method.   The collector array which consists of cylinders of two different sizes has been considered for various values of porosity.   For fibrous media which are composed of simple regular array of fibers, the numerical solution of the Stokes equation and the convective diffusion

equation gives very accurate predictions of the flow field and concentration distributions. The numerical calculation is a very important technique for heat and mass transfer processes in porous media because the model approach as the one discussed in the next two chapters can not distinguish the detailed structures (different regular arrays) and the orientations of the structure relative to the superficial velocity. The calculated results can not only be used for predictions of deposition of colloidal particles in ideal fibrous media but, more importantly, can be extended to predict the heat and mass transfer in laminar flow though fibrous and granular media due to the analogy between these processes. With the development of computer technology and the software for numerical analysis, more and more complicated structures will be able to be attacked efficiently.

CHAPTER 3
EFFECTIVE MEDIUM APPROXIMATION FOR FIBROUS MEDIA

3-1 Concept of Effective Medium Approximation

For many applications, such as in modeling of particle removal (or filtration) and heat transfer in porous media, a good model should describe well not only the macroscopic behavior of the medium but also the flow characteristics around the individual element (or collector in case of particle removal process) in a smaller length scale because the flow field around the collector surface affects these processes significantly. Both the cell models and the Brinkman's model provide a flow field around a representative packing element, and have been used to predict the particle removal rate in the fibrous and granular media (Tien 1989). While the cell models appear to provide good predictions for permeability, the Brinkman's model tends to underestimate the permeability when the porosity is low. However it should be pointed out that a good prediction of the permeability of a medium is a prerequisite, and doesn't necessarily results in a good prediction of filtration rate or heat transfer rate. In fact, it was realized recently (Wang and Sangani, 1997) that very different flow fields, which result in different heat and mass transfer rate in a fibrous medium, may yield the same permeability. So the validity of the flow fields given by these models is still an open question.
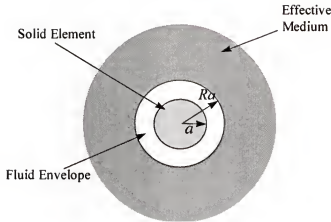
Figure 3-1 Schematic of a model unit for the Effective Medium Approximation (EMA)

In the present work, another model for porous media is presented in which the effective medium approximation (EMA) is applied. This model is, in a sense, a combination of the cell model and Brinkman's model as it assumes a representative packing element surrounded by a fluid envelope up to a certain radius and by an effective medium beyond it (Figure3-1). While this model, like the Brinkman's model, may account for the influence of neighboring elements on the flow better than cell models, the tendency of Brinkman's model to underestimate the permeability is apparently corrected by the presence of a fluid envelope in this model. In addition, as it will be shown, this model provides more accurate prediction of particle removal rate (or heat transfer rate) compared to other models.

The effective medium approximation was successfully used recently by Dodd et al. (1995) in the study of hydrodynamic interactions on diffusivities of integral membrane

proteins. It has been also applied in estimating the permeability of flow through an parallel array of randomly packed cylinders (Wang and Sangani 1997).

The effective medium approximation is essentially a combination of the Brinkman's model and the cell model. In this model, a representative packing element (which we will also call collector in particle removal process) is assumed to be surrounded by a liquid envelope up to a certain radius and by an effective medium beyond it (see Figure 3-1). The liquid envelope is intended to represent the environment around the collector in a length scale equivalent to collector size, whereas the effective medium away from the collector represents the environment in a macroscopic scale, thereby accounting for influence of the neighboring collectors on the flow field. In this model, the flow field is described by Stokes equation within the fluid envelope and by the Brinkman equation in the region of effective medium:

$$\nabla p = \mu \nabla^2 \mathbf{u} \qquad a < r < aR \qquad (3\text{-}1)$$

$$\nabla p = \mu \nabla^2 \mathbf{u} - \frac{1}{k}\mu \mathbf{u} \qquad r > aR \qquad (3\text{-}2)$$

Here, k is the Darcy's permeability, μ fluid viscosity, r the radial coordinate with its center at the origin of the representative collector, and a and aR are the radii of the packing element and the fluid envelope, respectively. One of the most important parameters in the EMA model may be the size of the fluid envelope, aR. While it may depend on the detailed structure of the cylindrical collector layout around the representative collector, the simplest choice may be R=1/(1-ε)$^{1/\Omega}$, where ε is the porosity of the porous medium and Ω the dimension parameter of the flow field, Ω=2 for a flow through fibrous media and Ω=3 for a flow through granular media. This choice of R is

equivalent to matching the void fraction of the model system with the porosity of the macroscopic medium. We may note that the Brinkman's model (Brinkman, 1947) can be considered as a special case of the EMA, with R=1, which is equivalent to assuming that the representative particle is surrounded by an effective medium without the presence of the fluid envelope. If the porosity is relatively high, the prescribed choice of R may be plausible. If the porosity is rather low, on the other hand, the influence of neighboring elements may not be represented by the porosity only. In this case, the detailed structure of the neighboring elements layout should have strong influence. Recently, Dodd et al. (1995) recognized this aspect and adopted $R = a_c [1 - S(0)]^{1/2} / (1 - \varepsilon)^{1/2}$ for two dimensional flow through fibrous media, where $S(0)$ is the zero-wave-number structure factor of the cylindrical element layout. The theoretical reason for this choice of R can be found in Dodd et al. (1995). For a random layout of cylinders, the expression for $S(0)$ has been given by Chae, Ree and Ree (1969) as follows:

$$S(0) = \frac{[(1 - 1.9682(1 - \varepsilon) + 0.9716(1 - \varepsilon)^2]^2}{1 + 0.0636(1 - \varepsilon) - 0.5446(1 - \varepsilon)^2 - 0.4632(1 - \varepsilon)^3 - 0.1060(1 - \varepsilon)^4 + 0.0087(1 - \varepsilon)^5}$$

$$(3-3)$$

We have found that the three dimensional analogue of this choice of R is not as good as the one determined by porosity matching. So the R calculated from the structure factor will only be applied to two-dimensional flow. For the purpose of presenting the results, we will denote the cases of R=1, R calculated by porosity matching, R determined from $S(0)$ as EMA-I, EMA-II and EMA-III, respectively.

The boundary conditions for equations (3-1) and (3-2) are: no-slip condition at r=a, continuity of velocity and stress at r=aR and the prescribed velocity field u=U far away from the collector (i.e., at r→∞).

The dimensionless form of the momentum equations are:

$$\hat{\nabla}\hat{p} = \hat{\nabla}^2\hat{u} \qquad\qquad 1 < \hat{r} < R \qquad\qquad (3\text{-}4)$$

$$\hat{\nabla}\hat{p} = \hat{\nabla}^2\hat{u} - \alpha^2\hat{u} \qquad\qquad \hat{r} > R \qquad\qquad (3\text{-}5)$$

where $\hat{p} = p/[\mu U/a]$, $\hat{u} = u/U$, $\alpha = a/\sqrt{k}$, and $\hat{r} = r/a$. For brevity, the carets indicating dimensionless variables are dropped in the following.

The solutions to equations (3-3) and (3-4) for the different hydrodynamic cases of flow through fibrous media are presented in the following sections of this Chapter and for flow through granular media will be given in Chapter 4.

3-2 Classification of Random Packings of Cylinders

According to their hydrodynamic behaviors, flow through fibrous media may be classified into the following categories: Flow-I, *All fiber (circular cylinder) axes are perpendicular to the superficial velocity*. Fiber axes all lay in planes which are parallel to each other but perpendicular to the superficial fluid velocity while the fibers can have random angles in the planes, as shown in Figure 3.2(a). This case is of great practical importance since many fibrous media are prepared by depositing fibers onto a flat surface with their axes almost completely parallel to the surface. A good example is filter paper prepared by passing a slurry of fibers through a screen on which the fibers are deposited.

Another case in which the fibers are in a bundle across which the fluid flows is a special case of this category, as seen in Figure 3-2 (b). Flow-II *Flow through completely randomly packed fibers*. Fiber axes are completely randomly orientated in all possible directions, Figure 3-2 (c). Flow-III, *Planar packing of fibers with mean flow parallel to the packing planes*. Fiber axes all lay in planes parallel to each other and to the superficial fluid velocity but have completely random angles in the planes, as seen in Figure 3-2(d). This category is encountered with media prepared as in the first case of Flow-I, but the flow is now in the direction parallel to the planes on which the fibers fall. Flow-IV, *All fibers are parallel to the mean flow*. Fibers are in a bundle and the fluid flows parallel to their axes, as shown in Figure 3-2(e).

(a) Flow-I   (b) Flow-I   (c) Flow-II

(d) Flow-III   (e) Flow-IV
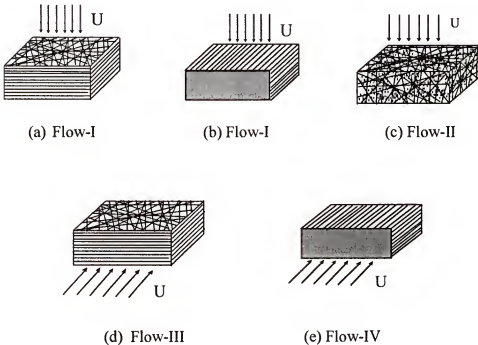
Figure 3-2 Hydrodynamic classification of random packings of cylinders

3-3 Packing of Uniform Circular Cylinders Parallel to Mean Flow

This is corresponding to the case of Flow-IV shown in Figure 3-2 (e). The schematic of the EMA model for this case is shown in Figure 3-3. The dimensionless form of the momentum equations (3-4) and (3-5) for the current case are reduced to:

$$\frac{dp}{dz} = \frac{1}{r}\frac{d}{dr}\left(r\frac{du_z}{dr}\right), \quad 1 < r < R \tag{3-6}$$

$$\frac{dp}{dz} = \frac{1}{r}\frac{d}{dr}\left(r\frac{du_z}{dr}\right) - \alpha_{//}^2 u_z, \quad r > R \tag{3-7}$$
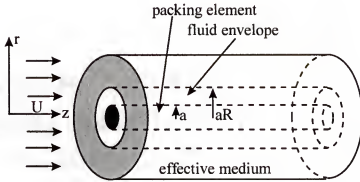
Figure 3-3 Schematic of the EMA model for flow parallel to circular cylinders

The boundary conditions include: (a) no-slip condition at cylinder surface ($r=1$); (b) fluid velocity tends to the superficial velocity far away from the cylinder; (c) flow field continues at $r = R$; (d) stress continues at $r = R$. For constant $-dp/dz(= \alpha_{//}^2)$, the solutions to equations (3-6) and (3-7) are readily obtained as:

$$u_z = \frac{r^2}{4}\frac{dp}{dz} + A\ln r + B, \quad 1 < r < R \tag{3-8}$$

$$u_z = CI_0(\alpha_{//}^2 r) + DK_0(\alpha_{//}^2 r) - \frac{dp}{dz}\frac{1}{\alpha_{//}^2}, \quad r > R \tag{3-9}$$

where A, B, C, D are integral constants, I_0 and K_0 are Modified Bessel functions of the 0th

order. The integral constants are determined by using the four boundary conditions as

$$A = -\frac{dp}{dz}\frac{R\alpha_{//}K_1(\alpha_{//}R)}{K_0(\alpha_{//}R) + \alpha_{//}RK_1(\alpha_{//}R)\ln R}\left(\frac{1}{\alpha_{//}^2} - \frac{1}{4} + \frac{R^2}{4} - \frac{R^2}{2}\ln R\right) - \frac{R^2}{2}\frac{dp}{dz}$$

$$\tag{3-10}$$

$$B = -\frac{1}{4}\frac{dp}{dz} \tag{3-11}$$

$$C = 0 \tag{3-12}$$

$$D = \frac{dp}{dz}\frac{\dfrac{1}{\alpha_{//}^2} - \dfrac{1}{4} + \dfrac{R^2}{4} - \dfrac{R^2}{2}\ln R}{K_0(\alpha_{//}^2 R) + \alpha_{//}RK_1(\alpha_{//}R)\ln R} \tag{3-13}$$

In the equations above, K_1 is the modified Bessel function of the second kind of the 1st

order.

The drag force acting on the cylinder, $F_{D//}$, can then be calculated as follows

$$\frac{F_{D//}}{Z} = 2\pi\frac{du_z}{dr}\bigg|_{r=1} = 2\pi\left(\frac{1}{2}\frac{dp}{dz} + A\right) \tag{3-14}$$

Simple force balance gives the relationship between the drag and pressure gradient as the

following:

$$-\frac{dp}{dl} = \frac{1-\varepsilon}{\pi}\frac{F_{D//}}{Z} \tag{3-15}$$

In the above equations, the length coordinate for each cylinder is denoted by z,

while Z is the total length of the cylinders. The depth coordinate for a porous medium

bed is denoted by l, while L is the depth of the bed. Substituting equations (3-10) and (3-14) into equation (3-15) yields the following transcendental equation for determination of $\alpha_{//}$.

$$\frac{1}{2}\left(1+\frac{1}{1-\varepsilon}\right) = \left(\frac{1}{\alpha_{//}^2}-\frac{1}{4}+\frac{R^2}{4}-\frac{R^2}{2}\ln R\right)\frac{\alpha_{//}RK_1(\alpha_{//}R)}{K_0(\alpha_{//}R)+\alpha_{//}RK_1(\alpha_{//}R)\ln R}+\frac{R^2}{2}$$

$$(3-16)$$

The dimensionless permeability $K_{//}$, which is only a function of the porosity ε, is then obtained once $\alpha_{//}$ is solved from (3-16):

$$K_{//} = \frac{1}{\alpha_{//}^2} \qquad\qquad (3-17)$$

Table 3-1 Permeability equations by different models for randomly packed uniform circular cylinders parallel to mean flow

Model (author)	$\alpha_{//}^2 = \dfrac{a^2}{k_{//}}$
Cell Model (Happel,1959)	$\alpha_{//}^2 = \dfrac{8(1-\varepsilon)}{1-4\varepsilon-2\ln(1-\varepsilon)-4(1-\varepsilon)^2}$
Brinkman (Spielman & Goren, 1968)	$\dfrac{1}{1-\varepsilon} = \dfrac{2K_1(\alpha_{//})}{\alpha_{//}K_0(\alpha_{//})}$
EMA Model (present)	$\dfrac{1}{2}\left(1+\dfrac{1}{1-\varepsilon}\right) = \left(\dfrac{1}{\alpha_{//}^2}-\dfrac{1}{4}+\dfrac{R^2}{4}-\dfrac{R^2}{2}\ln R\right)\dfrac{\alpha_{//}RK_1(\alpha_{//}R)}{K_0(\alpha_{//}R)+\alpha_{//}RK_1(\alpha_{//}R)\ln R}+\dfrac{R^2}{2}$
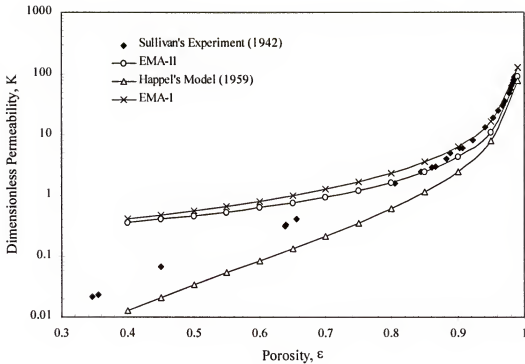
Figure 3-4 Permeability comparison between experimental data and model predictions for packing of uniform circular cylinders parallel to mean flow

Table 3-1 is a summary of the permeability equations for Happel's model, Brinkman's model and the EMA model obtained currently.

Figure 3-3 shows the comparison between the permeability predictions by EMA and Happel's models and the experimental data by Sullivan (1942). Sullivan's measurement were carried out by flowing conditioned air parallel through bundles of straightened goat wool, Chinese hair, glass wool, blond hair and copper wires. The tabulated measurement parameters were converted to the relations between K and ε by the author. Considering the fact that it is difficult to align the thin fibers perfectly in parallel to the flow direction at low porosities and the experiments tend to underestimate

the permeability, the EMA models with both choices of the size of the liquid envelope (EMA I and EMA II) agree with the experimental data reasonably well.

3-4 Packing of Uniform Circular Cylinders Perpendicular to Mean Flow

The solutions to the dimensionless equations (3-4) and (3-5) for fluid flow through a packing of uniform circular cylinders perpendicular to the superficial velocity are readily obtained by the use of stream functions:

$$u_r = -\frac{1}{r}\frac{\partial \psi}{\partial \theta} \tag{3-18}$$

$$u_\theta = \frac{\partial \psi}{\partial r} \tag{3-19}$$

Using ψ, equation (3-4) and (3-5) are reduced to

$$\nabla^4 \psi = 0 \qquad 1 < r < R \tag{3-20}$$

$$\nabla^4 \psi = \alpha_\perp^2 \nabla^2 \psi \qquad r < R \tag{3-21}$$

The far field condition (i.e., $u \to U$ as $r \to \infty$) suggests that

$$\psi(r, \theta) = f(r)\sin\theta \tag{3-22}$$

Using the no-slip condition for (3-20) and the far field condition for (3-21), the solution to (3-20) and (3-21) are given as

$$\psi_1 = \left[\left(r^3 - 2r + \frac{1}{r} \right)C + \left(2r + r\ln r - \frac{r}{2} - \frac{r^3}{2} \right)D \right]\sin\theta \tag{3-23}$$

$$\psi_2 = \left[r - \frac{A}{r} + B\alpha_\perp K_1(\alpha_\perp r) \right]\sin\theta \tag{3-24}$$

Here K_1 is the modified Bessel function of the first order. The subscript 1 and 2 indicate the fluid envelope region and the effective medium region, respectively.

The integration constants A, B, C and D in equations (3-23) and (3-24) are determined using the continuity conditions at r=R (i.e., continuity of velocity, normal and shear stresses). A set of four linear algebraic equations for these constants are obtained as:

$$A - \frac{\alpha_\perp R}{2}\left[2K_1(R\alpha_\perp) + \alpha_\perp RK_0(R\alpha_\perp)\right]B + \left(1 - R^4\right)C + \left(R^4 - R^2\right)\frac{D}{2} = 0$$

$$(3\text{-}25)$$

$$B\alpha_\perp^2 RK_0(R\alpha_\perp) + 2\left(2R - R^3 + R\ln R\right)D + 4\left(R^3 - R\right)C = 2R \qquad (3\text{-}26)$$

$$A\left(\frac{\alpha_\perp^2}{R} + \frac{4}{R^3}\right) - B\left(\frac{2\alpha_\perp^2 K_0(R\alpha_\perp)}{R} + \frac{4\alpha_\perp K_1(R\alpha_\perp)}{R^2}\right) + 4\left(\frac{1}{R^3} + R\right)C - 4\left(\frac{1}{R} + \frac{R}{2}\right)D = -\alpha_\perp^2 R$$

$$(3\text{-}27)$$

$$A\frac{4}{R^3} - B\left(\alpha_\perp^3 K_1(R\alpha_\perp) + \frac{4\alpha_\perp K_1(R\alpha_\perp)}{R^2} + \frac{2\alpha_\perp^2 K_0(R\alpha_\perp)}{R}\right) + 4\left(R + \frac{1}{R^3}\right)C - 2RD = 0$$

$$(3\text{-}28)$$

Once the stream function is determined, the pressure field is obtained from the momentum equations (3-4) and (3-5) as

$$p_1 = \left[8rC - \left(4r + \frac{2}{r}\right)D\right]\cos\theta$$

$$(3\text{-}29)$$

$$p_2 = -\left[\alpha_\perp^2 r + A\frac{\alpha_\perp^2}{r}\right]\cos\theta$$

$$(3\text{-}30)$$

The tangential and normal stresses acting on the surface of cylindrical element are

$$\sigma_{r\theta|r=1} = -4(2C - \frac{D}{2})\sin\theta \tag{3-31}$$

$$\sigma_{rr|r=1} = 2(D - 2C)\cos\theta \tag{3-32}$$

Thus the drag force per unit length, which has been scaled by μU can be obtained as

$$F_{D\perp} = \int_{0}^{2\pi} [\sigma_{rr|r=1}\cos\theta - \sigma_{r\theta|r=1}\sin\theta] d\theta = 4\pi D \tag{3-33}$$

From equations (3-25)-(3-28), D is obtained as

$$D = \frac{\alpha_\perp R}{Q} \left\{ [-2\alpha_\perp^2 R^2 + 3R^4\alpha_\perp^2 + 16R^2 - \alpha_\perp^2]K_1(\alpha_\perp R) + 8R^3\alpha_\perp K_0(\alpha_\perp R) \right\} \tag{3-34}$$

where

$$Q = \left[-\alpha_\perp^3 + 2\alpha_\perp R^2 + \alpha_\perp^3 R^4 \ln R - \alpha_\perp^3 R^4 - \alpha_\perp^3 \ln R + 16R^2\alpha_\perp \ln R\right]$$
$$RK_1(\alpha_\perp R) + \left[4\alpha_\perp^2 R^4 \ln R + 4\alpha_\perp^2 R^2 - 3\alpha_\perp^2 R^4 - \alpha_\perp^2 + 16R^2\right]K_0(\alpha_\perp R) \tag{3-35}$$

The overall pressure drop in the direction of flow is obtained by multiplying the drag force per unit cylinder length by total length of cylinders per unit volume of the porous medium, $(1-\varepsilon)/\pi$:

$$-\frac{dp}{dl} = F_{D\perp} \frac{1-\varepsilon}{\pi} \tag{3-36}$$

Substituting equation (3-33) into (3-36) yields,

$$-\frac{dp}{dl} = 4D(1-\varepsilon) \tag{3-37}$$

This pressure gradient should equal to $\alpha_\perp^2$ as obtained from equation (3-5) with a uniform approaching (or superficial) velocity. Thus,

$$\alpha_\perp^2 = 4D(1-\varepsilon) \tag{3-38}$$

This equation along with equation (3-34) represents an implicit equation for $\alpha_\perp$. Once $\alpha_\perp$ is determined, the pressure drop (or gradient) is given by equation (3-37).

Table 3-2 Permeability expressions by different models for randomly packed circular cylinders of uniform size perpendicular to mean flow

Model (author)	$\alpha_\perp^2 = \dfrac{a^2}{k}$
Cell model (Happel,1959)	$\alpha_\perp^2 = \dfrac{4(1-\varepsilon)}{-\dfrac{1}{2} - \dfrac{1}{2}\ln(1-\varepsilon) + \dfrac{(1-\varepsilon)^2}{1+(1-\varepsilon)^2}}$
Cell model (Kuwabara,1959)	$\alpha_\perp^2 = \dfrac{4(1-\varepsilon)}{\dfrac{1}{4} - \dfrac{1}{2}\ln(1-\varepsilon) - \varepsilon - \dfrac{1}{4}(1-\varepsilon)^2}$
Brinkman's model (Spielman & Goren,1968)	$\alpha_\perp^2 = 4(1-\varepsilon)\left[\dfrac{1}{2}\alpha_\perp^2 + \dfrac{\alpha_\perp^2 K_1(\alpha_\perp^2)}{K_0(\alpha_\perp^2)}\right]$
EMA (present)	$\alpha_\perp^2 = 4(1-\varepsilon)\dfrac{\alpha_\perp R}{Q}\left\{\begin{array}{l}[-2\alpha_\perp^2 R^2 + 3R^4\alpha_\perp^2 + 16R^2 - \alpha_\perp^2]K_1(\alpha_\perp R) \\ +8R^3\alpha_\perp K_0(\alpha_\perp R)\end{array}\right\}$

Similar procedure described above can be applied to the cell models and Brinkman model to obtain the expression for permeability. In table 3-2, the results for these models are given for comparison. As mentioned previously, the Brinkman's model (which was worked out by Spielman and Goren(1968)) is a special case of the EMA model with R=1.
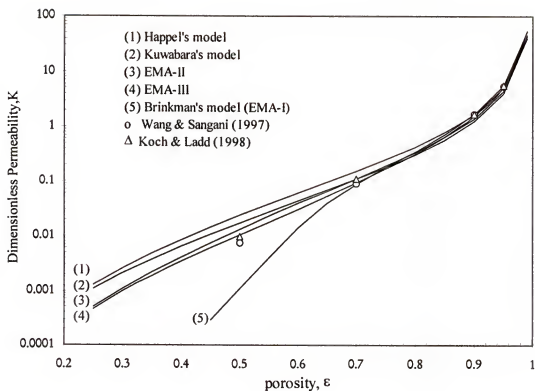
Figure 3-5 Comparison of theoretical predictions of the dimensionless permeability for fluid flow perpendicular to cylinder axes. (The lines are predictions by different theoretical models, the symbols are the results by numerical calculations)

Typical results for permeability are shown in Figure 3-4, where the dimensionless permeability $K=k/a^2$ is given as a function of porosity. Also plotted were the results of numerical calculations by Wang and Sangani (1997), and Koch and Ladd (1997), which have used different numerical techniques of recent development. Both of them are based numerical solution of the Stokes equation for the random array of cylinders. In the absence of experimental results, their numerical results may serve as the basis for comparison between various models. At high porosities, all models agree well with the numerical results. As the porosity is decreased, the predictions of each model start to

show some differences. The EMA-III shows the best agreement with the numerical results followed by EMA-II and the cell models in order. EMA-I , on the other hand, shows significant underestimation when the porosity is smaller than about 0.7. When porosity is smaller than about 0.45, the EMA-I does not even have a solution for permeability. This significant under prediction may be a consequence of not having the fluid envelope which exists in the other models. Considering the simplicity of these models, the permeability predictions appear to be quite reasonable in comparison with numerical and experimental results.

3-5 Planar Packing of Uniform Circular Cylinders with Mean Flow Parallel to Packing Planes

This case is corresponding to Flow-III as shown in Figure 3-2 (d). If ϑ is the angle between a cylinder axis and the direction of the superficial velocity, then the drag in the direction of flow is

$$F_D = F_{D\perp} \sin \vartheta + F_{D//} \cos \vartheta \qquad (3\text{-}39)$$

where $F_{D\perp}$ and $F_{D//}$ represent the drags contributed by the flow components normal to and parallel to the cylinder axis, respectively.

In a two dimensional planar random packing of uniform cylinders, i.e., the case in which the cylinder axis all lay randomly in a series of planes parallel to each other and the fluid flows parallel to the planes, the probability of finding a cylinder lying at any angle is the same. The probability density $P_a(\vartheta)$ of finding a cylinder lying at an angle ϑ can be found through the following normalization condition:

$$\int_0^{\pi/2} P_\vartheta(\vartheta) d\vartheta = 1 \tag{3-40}$$

Here we need only to distinguish the cylinder angle in 0-90° range, because cylinders with angles of ϑ, $\vartheta+\pi/2$, $\vartheta+\pi$ and $\vartheta+3\pi/2$ have the same effect to flow in a completely random packing.
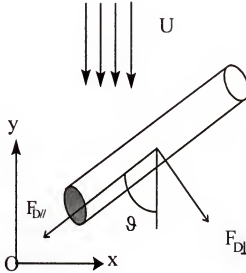
Figure 3-6 Drags acting on an oblique cylinder

In a two dimensional planar random packing, P_ϑ does not depend on ϑ. Therefore, we have

$$P_\theta = \frac{2}{\pi} \tag{3-41}$$

$$F_D = \int_0^{\pi/2} \left[F_{D\perp}(\vartheta) \sin\vartheta + F_{D//}(\vartheta) \cos\vartheta \right] P_\theta d\vartheta \tag{3-42}$$

From equation (3-36), we have

$$F_{D\perp}(\vartheta) = \frac{\pi\alpha_\perp^2}{1-\varepsilon}\sin\vartheta = \frac{\pi}{(1-\varepsilon)K_\perp}\sin\vartheta \tag{3-43}$$

where $\sin\vartheta$ term reflects the fact that the only the perpendicular component of the superficial velocity should be used to calculate the perpendicular drag, which is scaled by the μU. $F_{D//}$ is calculated from equation (3-15):

$$F_{D//}(\vartheta) = \frac{\pi\alpha_{//}^2}{1-\varepsilon}\cos\vartheta = \frac{\pi}{(1-\varepsilon)K_{//}}\cos\vartheta \tag{3-44}$$

Substituting equations (3-43) and (3-44) into equation (3-42) and carrying out the integration gives:

$$F_D = \frac{\pi}{2(1-\varepsilon)}\left(\frac{1}{K_\perp} + \frac{1}{K_{//}}\right) \tag{3-45}$$

Because

$$-\frac{dp}{dl} = \frac{1-\varepsilon}{\pi}F_D \tag{3-46}$$

where l is in the direction of the superficial velocity. Therefore

$$\frac{1}{K} = \frac{1}{2}\left(\frac{1}{K_\perp} + \frac{1}{K_{//}}\right) \tag{3-47}$$

or

$$\alpha^2 = \frac{1}{2}(\alpha_\perp^2 + \alpha_{//}^2) \tag{3-48}$$

The α^2 values turns out to be in a very simple relations with $\alpha_{//}^2$ and $\alpha_\perp^2$, mathematical average of the two.

3-6 Completely Randomly Packed Uniform Circular Cylinders

In the case of a completely random packing, i.e., the case in which cylinder axes are orientated in all possible directions, the probability of finding the number of cylinders which lay in a certain solid angle (see Appendix A, "Introduction to Solid Angle") is proportional to the steradian of the solid angle. If we denote P_ω as the probability density of finding a cylinder lying in solid angle ω, then the normalization condition gives,

$$\int_0^{2\pi} P_\omega \, d\omega = 1 \tag{3-49}$$

For an isotropic three dimensional packing, P_ω does not change with ω, therefore one obtains

$$P_\omega = \frac{1}{2\pi} \tag{3-50}$$

If the flow direction is in the negative z direction as shown in Figure A, the angle ϕ where the cylinder axis lies does not have any effect on the drag acting on the cylinder, so we need only to find the probability density of finding a cylinder whose cone angle is ϑ, $P_\vartheta(\vartheta)$. The normalization condition gives,

$$\int_{\vartheta=0}^{\pi/2} P_\vartheta(\vartheta) \, d\vartheta = 1 \tag{3-51}$$

Considering $d\omega = \sin\vartheta \, d\vartheta \, d\phi$, comparing equations (3-49) and (3-51) yields

$$P_\vartheta(\vartheta) = \sin\vartheta \tag{3-52}$$

Equation (3-52) shows that the spatial cylinder axis distribution in terms of the cone angle θ is not uniform in a 3-D random packing.

The drag force in the direction of the fluid flow is then obtained similarly by averaging equation (3-39) with the weighting function $P_\vartheta(\vartheta)$:

$$F_D = \int_0^{\pi/2}\left[F_{D\perp}(\vartheta)\sin\vartheta + F_{D//}(\vartheta)\cos\vartheta\right]P_\vartheta(\vartheta)d\vartheta \tag{3-53}$$
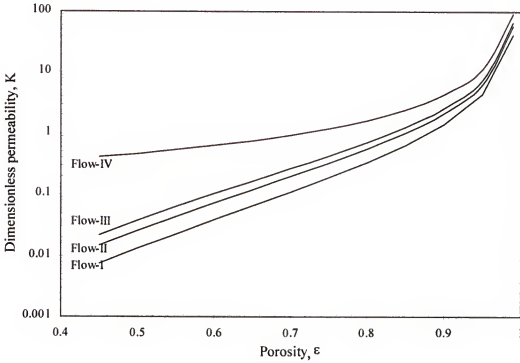
Figure 3-7 Comparison of permeability for different hydrodynamic cases of flow though fibrous media

From equations (3-36) and (3-15), we have:

$$F_{D\perp}(\vartheta) = \frac{\alpha_\perp^2\pi}{1-\varepsilon}\sin\vartheta \tag{3-54}$$

$$F_{D//}(\vartheta) = \frac{\alpha_{//}^2\pi}{1-\varepsilon}\cos\vartheta \tag{3-55}$$

Substituting equations (3-54) and (3-55) into equation (3-53), we get

$$F_D = \int_0^{\pi/2} \frac{\pi}{1-\varepsilon}\left(\alpha_\perp^2 \sin^2 \vartheta + \alpha_{//}^2 \cos^2 \vartheta\right)\sin\vartheta d\vartheta$$

$$= \frac{\pi}{1-\varepsilon}\left(\frac{2}{3}\alpha_\perp^2 + \frac{1}{3}\alpha_{//}^2\right) \tag{3-56}$$

Therefore, the α and K are obtained for the current flow problem as

$$\alpha^2 = \frac{2}{3}\alpha_\perp^2 + \frac{1}{3}\alpha_{//}^2 \tag{3-57}$$

$$\frac{1}{K} = \frac{2}{3K_\perp} + \frac{1}{3K_{//}} \tag{3-58}$$

Figure 3-6 shows the comparison of permeabilities for the four hydrodynamic cases. At the same porosity, the case with flow normal to the cylinders results the highest pressure drop while the case with flow parallel to all the cylinders gives the lowest. The permeability predictions by EMA for various flow cases through fibrous media are shown in Figure 3-7 along with the available experimental data. Jackson and James (1986) provided a very good collection of experimental data for permeability through fibrous media. The earliest work was that by Carman (1938). In the following year, Wiggins et al. (1939) determined the permeability of a wide variety of fibrous media: glass rods, glass fiber, copper wire and Celanese yarn. Each medium was a random packing of fibers in a tube, and several test liquids were used. Sullivan (1942) measured permeability of various wools and hairs. The most important detail of his work is that the fibers were packed in a tube such that they were somehow aligned with the flow. Brown's measurement (1950) was for flow of dry air through banks of heat exchanger tubes oriented normal to the flow. Davis (1952) presented a lot of experimental data for the permeability of flow through packings of glass wool, glass rods, cotton wool, camel hair,

kapok, merino wool, rayon, down, and a mixture of glass wool and copper wire. A few years later, Chen (1955) gathered data from various experiments on filter mats, in which the fibers were randomly oriented in planes normal to the flow. Some further data on filter mats were provided by Wheat (1963) and Labrecque (1968). Ingmanson et al. (1959) measured the flow of air through glass, nylon and paper fibers which were compressed as the pressure drop across the medium increased. White (1960) obtained the permeability of distilled water through various concentrations of cross linked acrylamide polymer gels which can be considered as fibrous media composed of polymer chains. Kirsch and Fuchs (1966) tested different arrangement of regular arrays of parallel fibers normal to the flow. Collagen is a protein which forms fibrous structures found throughout the human body. The earliest measurements of collagen permeability with sufficient information to determine the porosity were reported by Stenzel et al. (1971), older data are available but the porosity information was not available. Visvanadham et al. (1978) reported the similar tests. Kostornov and Shevchuck (1977) measured permeability of water and alcohol through discs of compressed 20%Cr-80%Ni alloy fibers, 50 μm in diameter and 3 mm long. Jackson and James (1982) studied the permeability of entangled hyaluronic acid polymer chains in solution. The most recent experiments were reported by Rahli et al. (1996), who measured permeability of random packing of metal wires of different aspect ratios (length/diameter). Their permeability data were lower than most other experimental results, which was believed to be caused by the end effect of the short fibers. Generally, the comparison made in Figure 3-7 shows that the EMA model agrees with most of the experimental data very well.

Figure 3-8 is a comparison of permeability predictions of EMA and the widely used Happel's model. In view of the comparisons made in Figure 3-7 with the big quantity of experimental data, the EMA model proves to be a better one than the Happel's, which under-estimates the differences in flow patterns.

3-7 Randomly Packed Non-uniform Circular Cylinders

In the case of a porous medium composed of poly-disperse elements, we can apply the analysis as we did in Sections 3-3 to 3-6 to each of the elements. If we scale the length parameters by the size of the corresponding element each time, we can easily see that we would get the same solutions for all the elements, i.e., the same six integral constants which are only functions of the porosity and element size. The dimensional drag for each of the elements can then be obtained and the pressure drop calculated.

From Section 3-4, we know that the drag acting on a cylinder of radius a sitting in a fibrous medium of porosity ε in the case of mean flow perpendicular to the cylinder axes is given by

$$F_D = 4\pi\mu D(R, \frac{a}{\sqrt{k}})UZ \qquad (3-59)$$

when a fluid flows through the medium with a superficial velocity of U, where Z is the length of the cylinder and $D(R, \frac{a}{\sqrt{k}})$ is given by equation (3-34) .
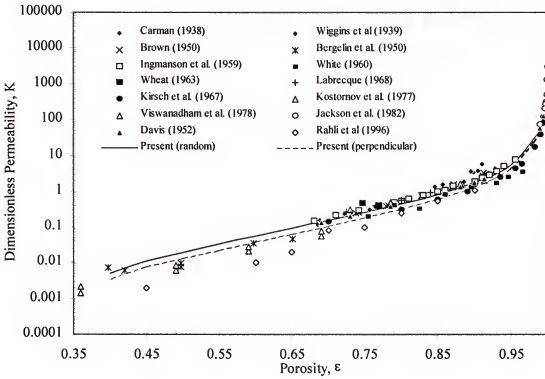
Figure 3-8 Comparison of EMA predictions of permeability of fibrous media with available experimental data

For a packing of polydisperse cylinders with a size-length distribution density of $P_a(a, Z)$, the number of cylinders with size in the range between a and a+da and length between Z and Z+dZ is then given by

$$dn(a) = NP_a(a, Z)dadZ \qquad (3-60)$$

where N is the total number of cylinders in the medium of volume V. The total volume of these cylinders is

$$V_s = \int_0^N \pi a^2 Z dn(a) = \pi N \int_0^\infty \int_0^\infty P_a(a, Z) Z a^2 dadZ \qquad (3-61)$$
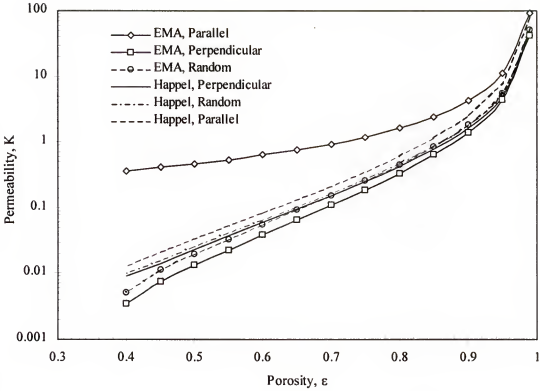
Figure 3-9 Comparison of predictions of permeability by EMA and Happel's models

Because there are N cylinders contained in the porous medium of volume V,

$$1 - \varepsilon = \frac{V_s}{V} = \pi\left(\frac{N}{V}\right)\int_0^\infty \int_0^\infty Za^2 P_a(a, Z)dadZ \tag{3-62}$$

or

$$\frac{N}{V} = \frac{(1 - \varepsilon)}{\pi}\left[\int_0^\infty \int_0^\infty Za^2 P_a(a, Z)da\right]^{-1} \tag{3-63}$$

If the lengths of the cylinders are much bigger than their diameters, the drag experienced on the ends of each of the cylinders can then be neglected. The total drag acting on all the cylinders in volume V is then obtained from equation (3-59),

$$F_t = 4\pi\mu UN \int_0^\infty \int_0^\infty ZD(R, \frac{a}{\sqrt{k}})P_a(a, Z)dadZ \tag{3-64}$$

The drag force is balanced by the pressure drop in a column of porous medium of length L and cross sectional area of A

$$-\frac{\Delta p}{L} = \frac{F_t}{LA} = 4\pi\mu U \frac{N}{V} \int_0^\infty \int_0^\infty ZD(R, \frac{a}{\sqrt{k}})P_a(a, Z)dadZ \tag{3-65}$$

Substituting equation (3-63) into equation (3.65), we get the following expression for the pressure drop in a porous medium composed of polydisperse cylinders perpendicular to the mean flow:

$$-\frac{\Delta p}{L} = 4\mu U(1-\epsilon)\frac{\int_0^\infty \int_0^\infty ZD\left(R, \frac{a}{\sqrt{k}}\right)P_a(a, Z)dadZ}{\int_0^\infty \int_0^\infty Za^2 P_a(a, Z)dadZ} \tag{3-66}$$

For the special case of uniform cylinders, equation (3-66) is reduced to equation (3-37) discussed in Section 3-4. Therefore, the equation for k is then

$$\frac{1}{k} = 4(1-\epsilon)\frac{\int_0^\infty \int_0^\infty ZD\left(R, \frac{a}{\sqrt{k}}\right)P_a(a, Z)dadZ}{\int_0^\infty \int_0^\infty Za^2 P_a(a, Z)dadZ} \tag{3-67}$$

This equation is the generalized permeability equation which can be used to calculate permeability of a polydisperse packing of cylinders perpendicular to the superficial velocity. In a polydisperse packing, the thickness of the clear liquid region around each solid element may be considered the same. The thickness δ can be estimated through the overall packing porosity.

$$1 - \varepsilon = \frac{\int\limits_0^\infty \int\limits_0^\infty a^3 P_a(a, Z) da dZ}{\int\limits_0^\infty \int\limits_0^\infty (a + \delta)^3 P_a(a, Z) da dZ} \tag{3-68}$$

R in the permeability equation is then obtained by $R = (a + \delta)/a$. If the size distribution is not very broad, equation (3-67) may be approximated by

$$\frac{1}{k} \approx 4(1 - \varepsilon) \frac{D\left(R(a_m), \dfrac{a_m}{\sqrt{k}}\right) \int_0^\infty \int_0^\infty Z P_a(a, Z) da dZ}{\int_0^\infty \int_0^\infty Z a^2 P_a(a, Z) da dZ} \tag{3-69}$$

where the cylinder size a in function $D[R, a / \sqrt{k}]$ has been replaced by a middle value a_m. Equation (3-69)) can also be written as

$$\frac{a_e^2}{k} \approx 4(1 - \varepsilon) D\left(R(a_m), \frac{a_m}{\sqrt{k}}\right) \tag{3-70}$$

where

$$a_e = \left(\frac{\int_0^\infty \int_0^\infty Z a^2 P_a(a, Z) da dZ}{\int_0^\infty \int_0^\infty Z P_a(a, Z) da dZ}\right)^{1/2} \tag{3-71}$$

is an average size, which may be a good estimate for a_m, i.e.,

$$a_m \approx a_e \tag{3-72}$$

Therefore, equation (3-69) is then reduced to the following

$$\frac{a_e^2}{k} \approx 4(1 - \varepsilon) D\left(R(a_e), \frac{a_e}{\sqrt{k}}\right) \tag{3-73}$$

which has the same form as equation (3-38). This implies that equation (3-71) is the definition of an "equivalent radius" of a polydisperse packing, the physical meaning of which can be understood as the radius of the uniform cylinders packed to give the same

permeability as the medium composed of polydisperse cylinders of the same porosity. It is also noted that $R(a_e)=1/(1-\varepsilon)^{1/3}$, it is only a function of the porosity. It can also be easily shown that extending the results for other types of packing described in Sections 3-3 to 3-6 to the corresponding polydisperse cases gives similar conclusion. The significance of equation (3-71) is that *all the equations derived before for the cases of uniform cylinders are also valid for polydisperse cylinders if we replace the radius of the cylinders with a_e.*

3-8 Summary

The Effective medium approximation, which assumes a model system in which a packing element (a single fiber in the fibrous medium and a single sphere in the granular medium) is surrounded by a fluid envelope and an effective-medium beyond the envelope, is applied to flow through fibrous media to predict the permeability of four different flow cases: Flow-I, the mean velocity is perpendicular to the axes of all fibers; Flow-II, the mean flow is parallel to the packing planes in which all fibers are randomly oriented; Flow-III, flow through completely randomly packed fibers and Flow-IV in which the superficial velocity is parallel to the axes of all the fibers. The new model integrated the important features of both the cell models and Brinkman's model. The analytical expressions for the permeability of flow through fibrous media are obtained. Comparisons with the experiment and the strictly numerical calculated results showed that the EMA based on the porosity matching and structure factor are better flow models

than the mostly used cell and Brinkman's models. The EMA analysis is also extended to the fibrous media with polydisperse elements.

The criteria for the derived equations to be valid may include the following. The aspect ratio (length/diameter) of the fibers should be sufficiently large so that the effect of the fiber ends could be neglected. The Reynolds number of the flow should be small enough in order to have the Stokes equation to hold. It is generally accepted that a Reynolds number of 1 is a critical one below which the flow is considered to be creeping flow. But engineering practice shows that this critical number could be extended to 10. Another criterion is that the Knudsen number (length of the mean free path / fiber diameter) should be less than 0.01 if the fluid is gas, because the no-slip condition has been used at the fiber surfaces.

CHAPTER 4

EFFECTIVE MEDIUM APPROXIMATION FOR GRANULAR MEDIA

4-1 Packing of Uniform Spheres

As pointed out previously, the important feature of the EMA model is that it reflects the physical situation for the flow around the representative element more realistically than the cell models which solve only equation (3-1). The flow field around each of the solid elements which constitute the packed medium collectively is affected by the neighboring elements which are represented by an effective medium in the current model. While each solid element is surrounded by an effective medium which has the same permeability as the entire porous medium, it contributes to that property at the same time. Thus, the permeability of the porous medium and the local flow field around each solid element are coupled together. The EMA model accounts for this coupling, whereas the cell models do not. This more realistic feature of the EMA model, however, results in a somewhat more complicated solution procedure although an analytic solution is still obtained.

The simple geometry of the model system allows analytic solution to these equations by the use of stream function:

$$u_r = -\frac{1}{r^2 \sin\theta}\frac{\partial\psi}{\partial\theta} = -\frac{2\,f(r)}{r^2}\cos\theta \tag{4-1}$$

$$u_\theta = \frac{1}{r\sin\theta}\frac{\partial\psi}{\partial r} = \frac{1}{r}\frac{df(r)}{dr}\sin\theta \qquad (4\text{-}2)$$

where

$$\psi = f(r)\sin^2\theta \qquad (4\text{-}3)$$

and u has been scaled to dimensionless by U, the superficial velocity of the fluid in the packed bed. All the length parameters have been scaled by the radius of the spheres, a.

Far away from the particle, the velocity field approaches the uniform superficial velocity. Thus, in the effective-medium region (r > R), the radial dependence of the stream function f(r) is given as

$$f_1(r) = -\frac{1}{\alpha^2 r}A + \left(\alpha + \frac{1}{r}\right)e^{-\alpha r}B - \frac{r^2}{2} \qquad (4\text{-}4)$$

Here α^2 is a^2/k which is the inverse of dimensionless permeability. In the fluid envelope region (1 < r < R), on the other hand, the no-slip condition at the particle surface gives the function f(r) as

$$f_2(r) = \left(-\frac{r^4}{20} + \frac{r^2}{12} - \frac{1}{30r}\right)C + \left(\frac{r^2}{3} - \frac{r}{2} + \frac{1}{6r}\right)D \qquad (4\text{-}5)$$

The subscripts 1 and 2 in Equations (4-4) and (4-5) represent the effective-medium region and the fluid envelope region, respectively.

The four constants A, B, C, and D appearing in Equations (4-4) and (4-5) are determined by the matching conditions at the surface of the fluid envelope (i.e., at r = R), which represent the continuity of velocity and stresses. These matching conditions provide a set of four linear equations which gives an analytic expression for A, B, C, and D in terms of α and R. The four linear equations are:

$$-\frac{1}{\alpha^2 R}A + \left(\alpha + \frac{1}{R}\right)e^{-\alpha R}B + \left(\frac{R^4}{20} - \frac{R^2}{12} + \frac{1}{30R}\right)C$$

$$-\left(\frac{R^2}{3} - \frac{R}{2} + \frac{1}{6R}\right)D = \frac{R^2}{2} \tag{4-6}$$

$$\frac{1}{\alpha^2 R^2}A - \left(\alpha^2 + \frac{\alpha}{R} + \frac{1}{R^2}\right)e^{-\alpha R}B$$

$$+\left(\frac{R^3}{5} - \frac{R}{6} - \frac{1}{30R^2}\right)C - \left(\frac{2R}{3} - \frac{1}{2} - \frac{1}{6R^2}\right)D = R \tag{4-7}$$

$$\left(-\frac{1}{R^2} + \frac{12}{\alpha^2 R^4}\right)A - \left(\frac{4\alpha^2}{R^2} + \frac{12\alpha}{R^3} + \frac{12}{R^4}\right)e^{-\alpha R}B$$

$$+\left(\frac{7R}{5} - \frac{2}{5R^4}\right)C + \left(\frac{-1}{R^2} + \frac{2}{R^4}\right)D = -\alpha^2 R \tag{4-8}$$

$$-\frac{6}{\alpha^2 R^4}A + \left(\frac{\alpha^3}{R} + \frac{3\alpha^2}{R^2} + \frac{6\alpha}{R^3} + \frac{6}{R^4}\right)e^{-\alpha R}B$$

$$+\left(\frac{3R}{10} + \frac{1}{5R^4}\right)C - \frac{1}{R^4}D = 0 \tag{4-9}$$

Using the velocity described above (i.e., Equations (4-1) and (4-2) along with (4-4) and (4-5)), the pressure field (scaled by $\mu U/a$) in each region is determined from the momentum equations (3-1) and (3-2) as follows:

$$p_1 = \left(-\alpha^2 r + \frac{1}{r^2}A\right)\cos\theta \tag{4-10}$$

$$p_2 = \left(rC + \frac{1}{r^2}D\right)\cos\theta \tag{4-11}$$

Since the velocity and the pressure fields are now known, the drag force (scaled by μUa) on individual particle can be determined as

$$F_D = \int_0^\pi 2\pi \left(\sigma_{r\theta}\big|_{r=a} \sin\theta - \sigma_{rr}\big|_{r=a} \cos\theta \right) \sin\theta \, d\theta \tag{4-12}$$

where the normal and shear stresses (scaled by $\mu U/a$ at the particle surface are given as

$$\sigma_{rr}\big|_{r=a} = (C + D)\cos\theta \tag{4-13}$$

$$\sigma_{r\theta}\big|_{r=a} = \left(\frac{1}{2}C - D \right)\sin\theta \tag{4-14}$$

Thus, the drag force on a single spherical particle is

$$F_D = -4\pi D \tag{4-15}$$

Assuming that the particles are uniformly distributed in the packed bed, the pressure drop over a unit distance in the flow direction is a multiple of F_D and the number density of the particle $3(1-\varepsilon)/4\pi$. Therefore, the pressure gradient in the flow direction l is given as

$$\frac{dp}{dl} = -\frac{3(1-\varepsilon)}{4\pi}F_D = 3(1-\varepsilon)D \tag{4-16}$$

From the Darcy's law (or Equation (3-2)), the pressure gradient for a uniform flow is − $1/K$. Therefore, the expression for K is obtained as

$$\alpha^2 = \frac{1}{K} = -3(1-\varepsilon)D \tag{4-17}$$

The solution of the Equations (4-6)-(4-9) gives the following expression for D.

$$D = -6 \frac{1}{Q} \begin{bmatrix} 6R^6\alpha^3 + 21\alpha^2 R^5 - 5R^4\alpha^3 + 45\alpha R^4 \\ -5R^3\alpha^2 + 45R^3 - \alpha^3 R - \alpha^2 \end{bmatrix} \tag{4-18}$$

where

$$\begin{aligned} Q = {}& 180R^3 + 24R^5\alpha^2 - 45R^4\alpha^2 - 9\alpha^2 + 4\alpha^3 + 180\alpha R^4 + 4R^6\alpha^3 \\ & + 10(\alpha R)^3 - 9R\alpha^3 - 9\alpha^3 R^5 + 30(\alpha R)^2 - 180R^3\alpha \end{aligned} \tag{4-19}$$

Equation (15) and (16) uniquely determine the value of the permeability K once the porosity ε (hence R) is specified.

4-2 Packing of Non-uniform Spheres

In this section, we consider the case of a porous medium composed of polydisperse spheres with a size distribution density of $P(a)$. For the convenience of presentation, all the variables in this section are dimensional. The number of particles with their radii in the range of a and $a + da$ is then given as

$$dn(a) = NP(a)da \tag{4-20}$$

Here N is the total number of particles in the porous medium of volume V. The total volume of these N particles is

$$V_s = \int_0^\infty \frac{4}{3}\pi a^3 dn(a) = \frac{4\pi}{3}NM_3 \tag{4-21}$$

where

$$M_3 = \int_0^\infty a^3 P(a)da \tag{4-22}$$

is the third moment of the particle size distribution. Since V_s/V represents the volume fraction occupied by the solid particles, the porosity of the packed bed is then given as

$$1 - \varepsilon = \frac{V_s}{V} = \frac{4\pi}{3}\left(\frac{N}{V}\right)M_3 \tag{4-23}$$

Therefore the particle number density of the porous medium is

$$\frac{N}{V} = \frac{3(1-\varepsilon)}{4\pi M_3} \tag{4-24}$$

Since the drag force on an individual particle of radius a sitting in a porous medium of porosity ε is given as Equation (13), the total drag force on all the particles in a unit volume is obtained as

$$F_t = -4\pi\mu U \frac{N}{V} \int_0^\infty aD(R,\alpha)P(a)da \qquad (4\text{-}25)$$

Since this total drag is equivalent to the pressure gradient in the porous medium, the following expression for the permeability of a porous medium composed of polydisperse spheres is obtained as

$$\frac{1}{k} = \frac{3(1-\varepsilon)}{M_3} \int_0^\infty aD(R,\alpha)P(a)da \qquad (4\text{-}26)$$

The thickness of the clear liquid envelope, δ, is estimated form the overall porosity of the packing.

$$1 - \varepsilon = \frac{\int\limits_0^\infty a^3 P_a(a)da}{\int\limits_0^\infty (a+\delta)^3 P_a(a)da} \qquad (4\text{-}27)$$

R in the permeability equation (4-26) is then obtained by R=1.028(a+δ)/a. The factor 1.028 will be discussed in the next section. For the special case of a bidisperse packing, equation (4-27) is reduced to:

$$\left(1 + \frac{\delta}{a_1}\right)^3 x_1 + \left(1 + \frac{\delta}{a_2}\right)^3 x_2 = \frac{1}{1-\varepsilon} \qquad (4\text{-}28)$$

where x_i is the volume fraction of particle size a_i.

For the special case of uniform spheres of size a, P(a) = δ(a), here δ(a) is the delta function. Thus $M_3 = a^3$ from Equation (4-22), and Equation (4-26) is reduced to Equation

(4-17) described in the last section. Thus, the permeability k of a packed bed filled with polydisperse spherical particles is represented by an implicit equation (4-26) along with Equation (4-18). Although this equation is complicated algebraically, the permeability k is rather easily determined by a simple numerical scheme once the particle size distribution P(a) and the porosity ε are specified.
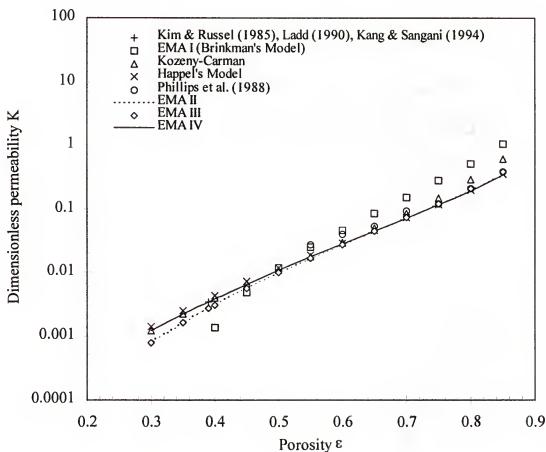
Figure 4-1 Comparisons of permeability predictions for packing of uniform spheres

4-3 Comparison of Permeability Predictions

In this section, the permeability predicted by the present model is compared with those obtained through pure numerical simulations and predicted by other models including the Kozeny-Carman correlation for a random packing of uniform spheres and non-uniform spheres. The numerical results for packing of uniform spheres by Ladd (1990), Kang and Sangani (1994) and Kim and Russel (1985) are almost identical. Essentially all these investigators calculated the permeability from a multipole-moment expansion of force density on the surface of solid particles. The porosity range reported by Phillips et al. (1988) and Kim and Russel (1985) is >0.5, Ladd (1990) is >0.55, and Kang and Sangani (1994) is > 0.39. The Kozeny-Carman correlation is represented by the following equation:

$$\frac{a^2}{k} = -45\frac{(1-\varepsilon)^2}{\varepsilon^3}$$

(4-29)

This equation was initially developed by Kozeny based on the capillary tube model, and later, Carman adjusted the numerical constant empirically from 16 to 45 to provide better agreement with experimental results (Carman, 1956; Tien, 1989). Thus, Equation (4-29) is a semi-empirical correlation. This Kozeny-Carman equation has been found to provide good agreement with numerous experimental observations for the porosity range of 0.26 to 0.8 which is achieved in packed beds and sedimentation experiments (Happel and Brenner, 1965). Carman (1956) also found that Equation (4-29) could be applied to

mixtures of various particle sizes if the hydraulic radius was used in place of the particle radius.
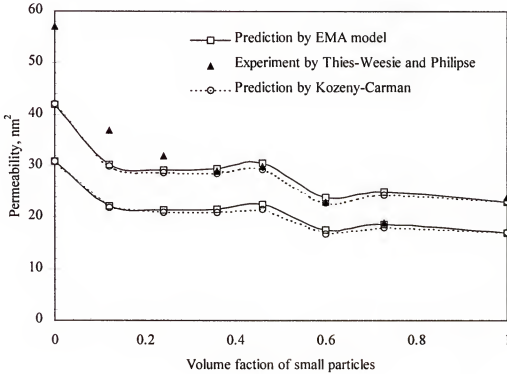
Figure 4-2 Comparison of permeability prediction by EMA model and experimental data for a bidisperse particle system. (The radii of the big and small particles are 147 nm and 103 nm, respectively)

For the simplicity of presentation, the EMA models with choices of R=1, R=1/(1-ε)$^{1/3}$ and R=[(1-S(0))/(1-ε)]$^{1/3}$ are denoted as EMA I, EMA II and EMA III, respectively. S(0) is the zero wavenumber structure factor of the sphere packing. The zero wavenumber structure factor S(0) is defined by

$$S(0) = \int [P(\mathbf{r}|\mathbf{0}) - n] d\mathbf{r} \qquad (4\text{-}30)$$

where $P(\mathbf{r}|\mathbf{0})$ is the probability for finding a particle with its center in the vicinity of $\mathbf{r}$ given a test particle at origin, and n is the number density of particles. $S(0)$ for randomly distributed spheres is given by the well-known Carnahan-Starling formula

$$S(0) = \frac{\varepsilon^4}{1 + 4(1-\varepsilon) + 4(1-\varepsilon)^2 - 4(1-\varepsilon)^3 + (1-\varepsilon)^4} \tag{4-31}$$
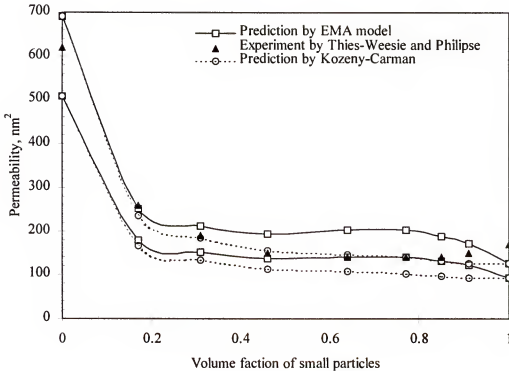
Figure 4-3 Comparison of permeability prediction by EMA model and experimental data for a bidisperse particle system (The radii of the big and small particles are 605 nm and 230 nm, respectively).

Figure 4-1 indicates that the cell model of Happel shows a very good agreement with the numerical simulation results. Considering its simplicity, the Happel's cell model appears to be an excellent model for the prediction of the permeability of packed beds filled with uniform spheres. We may also note that the Brinkman's model is poorer than

either model. When the porosity is smaller than about 0.4, this model cannot even provide a permeability prediction as the solution becomes singular. EMA II and EMA III agree with the numerical results very well for porosities higher than about 0.5, while EMA III is a little better than EMA II.
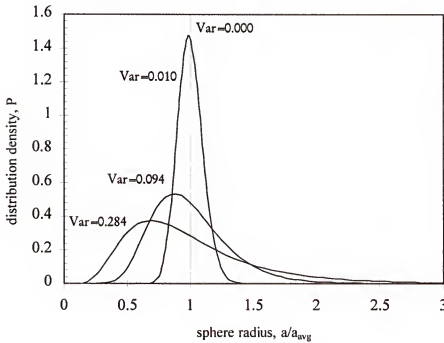
Figure 4-4 Logarithmic normal distributions of packing spheres

The permeability of a packed bed is directly associated the drag force on the packing particles (or the energy dissipation at the surface of the particles). When the porosity is high, the physical contacts between packing particles may be sparse, and the simplifying assumption that a spherical fluid envelope encapsulates the particle may not introduce a serious error since the drag force is mostly determined by the flow field in the immediate vicinity of the particles. With decreasing porosity, however, the number of

physical contacts between packing particles increases. Consequently, the assumption which redistributes the fluid uniformly around the particles may become more unrealistic and is likely to introduce a more significant error. This argument may explain the small discrepancy observed with the EMA model at a low porosity in comparison with the Kozeny-Carman correlation and numerical results.
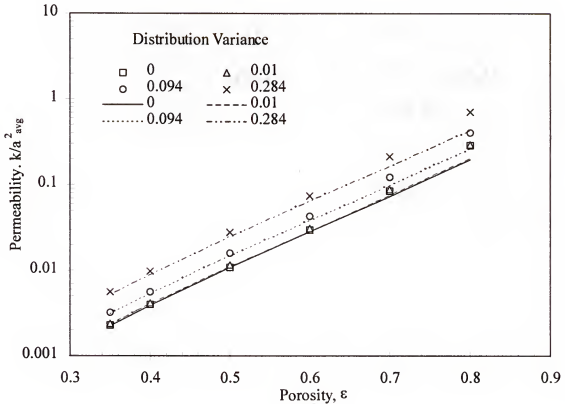
Figure 4-5 Permeability predictions by EMA and Kozeny-Carman correlation for polydisperse packing (Lines: EMA predictions (Eqn. 4-26); Symbols: Kozeny-Carman correlation)

Although it is a pure empiricism, a minor adjustment of increasing the radius of liquid envelope R by a mere 2.8 percent from $1/(1-\varepsilon)^{1/3}$ to $1.028/(1-\varepsilon)^{1/3}$ is found to improve the agreement with the numerical results providing an excellent match for the

whole porosity range. The Kozeny-Carman correlation clearly overestimates the permeability when the porosity is higher than about 0.6.

The major contribution of the present work may be the extension of the EMA model to the case of polydisperse packings. As far as we know, the present approach described in Section 3 is the first attempt which fully incorporates the particle size distribution for the permeability prediction. The permeability of a packed bed with polydisperse particles has been usually estimated using the Kozeny-Carman equation with the reciprocal mean particle size. The reciprocal mean particle size is the average size which corresponds to the same total specific surface area of packing particles. This approach has been known to provide a good prediction for the permeability of spherical as well as non-spherical packings if their particle size distribution is not very broad (Brenner, 1961; Standish and McGregor,1978; Perry, 1984).

In Figure 4-2 and Figure 4-3, comparisons are made between the permeability predictions of the EMA model using the adjusted R (i.e., R=1.028/(1-ε)$^{1/3}$), we will call it EMA IV, and the experimental data by Thies-Weesie and Philipse (1994), who investigated flow of cyclohexane through bidisperse silica spheres for various mixing ratios. The radii of the big and small particles are 103nm and 147nm in Figure 4-2, and 605 nm and 230 nm in Figure 4-3, respectively. In the calculation the measured porosity data as measured by the same authors were used. The measured porosity data have error bars, so we have two predicted curves for each case. Also shown in the same figures are the prediction of Kozeny-Carman correlation. It is shown that both the EMA IV model and the Kozeny-Carman correlation give very good predictions.

In Figure 4-5, a comparison is made between the predictions of the EMA model using the adjusted R and the Kozeny-Carman equation for the particle size distributions given in Figure 4-4. Although the logarithmic normal distribution has been used in the present study because of its wide use in particle sizing, any type of particle size distribution can be used. The size distributions shown in Figure 4 have the average size (number averaged) of 1 with an increasing variance from 0.00, corresponding to uniform spheres, to 0.284 which represents a very broad distribution. The agreement between the two predictions is reasonably good at low porosities, and the Kozeny-Carman correlation overestimates the permeability at higher porosities as is the case in monodisperse packings.

In the sense of predicting the permeability, the EMA model is more complicated than the Kozeny-Carman correlation. The advantage of EMA model over the Kozeny-Carman correlation is that it gives a flow field around each of the solid elements, which is very important for many heat and mass transfer processes in packed beds.

4-4 Summary

The permeability of packed beds filled with polydisperse spheres has been studied using the Effective Medium Approximation (EMA). The EMA assumes a model system in which a packing element (or particle) is surrounded by a fluid envelope and an effective-medium beyond the envelope. Since the local flow field around each packing element which is influenced by the neighboring elements contributes collectively to the permeability of the packed bed, the local flow and the permeability are coupled together.

The EMA model reflects this physical situation of coupling more realistically than other existing models. Furthermore, unlike other models, this model is capable of fully incorporating the packing size distribution in predicting the permeability of packed beds. Although the coupling between the local flow field around an individual packing element and the permeability of the collective medium (i.e., packed bed) makes the solution procedure complicated, the simple geometry of the model unit enables us to obtain an analytic expression for the permeability of the packed bed as a function of the packing size distribution and the porosity. The prediction of the present model shows a good agreement with the numerical results in the whole range of porosity and the Kozeny-Carman correlation at low porosities.

In modeling the effective heat or mass transfer coefficient in porous media (or packed beds), a representative flow field for a model system is needed. While the Kozeny-Carman correlation provides an excellent prediction for the permeability of a porous medium at low porosities, a representative flow field is not given for these purposes. The cell models and the EMA model, on the other hand, provide a representative flow field for the prediction of the effective transfer coefficients. Despite the simplicity of these models, the permeability prediction by them appears to be good probably due to the fact that the flow field in the immediate vicinity of the packing element is most important in determining the drag force on the packing elements (hence the permeability).

When the convection is dominant over diffusion, only the flow field in the immediate vicinity of the packing elements is important. Thus, the cell models or the EMA model are expected to provide a reasonable prediction for the effective transfer

coefficients. Application of the EMA model for that purpose is our major objective, and the present chapter is a part of that effort. Since the EMA model portrays the flow situation in a packed bed more realistically than the cell models, we expect that the prediction of effective heat or mass transfer coefficient by the EMA model will be better that those by other models, and the results will be presented in Chapter 6.

CHAPTER 5
PARTICLE DEPOSITION IN FIBROUS AND GRANULAR MEDIA

5-1 Particle Deposition on Circular Cylinders Parallel to Mean Flow

In Sections 1-3 and 1-4, it has been shown that under widely applicable conditions, particle deposition on solid surfaces in the presence of van der Waals, electric double layer, and hydrodynamic interactions can be treated by assuming convective mass transfer in the fluid and a first order reaction at the collector surface. In order to solve the convective diffusion equation, a representative flow field should be available. In the current case, i.e., liquid flows parallel to a cylinder surface, the mass transfer boundary layer develops in the flow direction. In a laminar flow outside a circular cylinder, the mass transfer boundary layer in the down stream can be quite thick and is limited by the presence of neighboring cylinders. We have shown in the foregoing chapters that only a flow field close to the cylinder surface is predictable by using the effective medium approximation. Therefore we can only solve the convective mass transfer equation in the end region, where mass transfer boundary layer has not fully developed. Fortunately, this limitation in analysis does not really pose a serious problem, because the deposition rate in the down stream is usually a few magnitude lower than the end region as shown later in this section. That is to say, particle deposition occurs mostly at the very end region, to which the remaining part of this section will be dedicated.

If the Peclet number $aU/\mathcal{D}$ has a value much higher than unity, the diffusion boundary layer will be sufficiently thin in the end region, so that the curvature effect and the tangential diffusion are negligible. Under these conditions, the convective diffusion equation assumes the following form:

$$u_z \frac{\partial c}{\partial z} = \mathcal{D} \frac{\partial^2 c}{\partial r^2} \tag{5-1}$$

The dimensionless form of equation (5-1) is

$$\hat{u}_z \frac{\partial \hat{c}}{\partial \hat{z}} = \frac{1}{Pe} \frac{\partial^2 \hat{c}}{\partial \hat{r}^2} \tag{5-2}$$

where $\hat{u}_z = u_z / U, \hat{r} = r / a, \hat{c} = c / c_0$, c_0 is the bulk particle concentration. For brevity, the carets indicating dimensionless variables are dropped in the following.

The above problem is the so-called extended Graetz problem, for which an infinite series solution can be obtained (Bowen et al. 1976). When the Peclet number is large, a simpler approximate solution which is asymptotically correct for the entrance region can be found. In the entrance region, the particle concentration boundary layer is still developing. The simplest approximate form is obtained when this boundary layer lies entirely within the region near the collector surface where the velocity profile can be replaced by its tangent line at the surface. Thus the problem is reduced to the one of particle deposition on a surface in an infinite medium undergoing a simple shear flow. Equation (5-2) is then reduced to

$$\tau_w y \frac{\partial c}{\partial z} = \frac{1}{Pe} \frac{\partial^2 c}{\partial y^2} \tag{5-3}$$

where y=r-1. Let $\tau_w y = 2Y$, and $X = (2/9z)^{1/3} Y$, equation (5-3) is transformed to the following ordinary differential equation

$$\frac{d^2c}{dX^2} + 3X^2 \frac{dc}{dX} = 0 \tag{5-4}$$

The corresponding boundary conditions are

$$c(X \to \infty) = 1 \tag{5-5}$$

$$c(X=0) - \left(\frac{\mathcal{D}_\infty}{aK_\Phi}\right)\left(\frac{2}{9z}\right)^{1/3}\left(\frac{dc}{dX}\right)_{X=0} = 0 \tag{5-6}$$

The solution of equation (5-4) satisfying the boundary conditions (5-5) and (5-6) is

$$c(X) = \frac{\left(\frac{\mathcal{D}_\infty}{aK_\Phi}\right)\left(\frac{2}{9z}\right)^{1/3} + \int_0^X e^{-\zeta^3} d\zeta}{\left(\frac{\mathcal{D}_\infty}{aK_\Phi}\right)\left(\frac{2}{9z}\right)^{1/3} + \Gamma\left(\frac{4}{3}\right)} \tag{5-7}$$

or
$$c(z,Y) = \frac{\left(\frac{\mathcal{D}_\infty}{aK_\Phi}\right)\left(\frac{2}{9z}\right)^{1/3} + \int_0^{(2/9z)^{1/3}Y} e^{-\zeta^3} d\zeta}{\left(\frac{\mathcal{D}_\infty}{aK_\Phi}\right)\left(\frac{2}{9z}\right)^{1/3} + \Gamma\left(\frac{4}{3}\right)} \tag{5-8}$$

The particle deposition flux is then readily obtained from equation (5-8)

$$Sh = \frac{Ja}{\mathcal{D}c_0} = \frac{\left(\frac{2a}{9z}\right)^{1/3}\left(\frac{a\tau_w}{2\mu U}\right)}{\left(\frac{\mathcal{D}}{aK_\Phi}\right)\left(\frac{2a}{9z}\right)^{1/3} + \Gamma\left(\frac{4}{3}\right)} \tag{5-9}$$

All the variables except Sh in equation (5-9) are dimensional. The shear stress term can be calculated from equation (3-8) to be
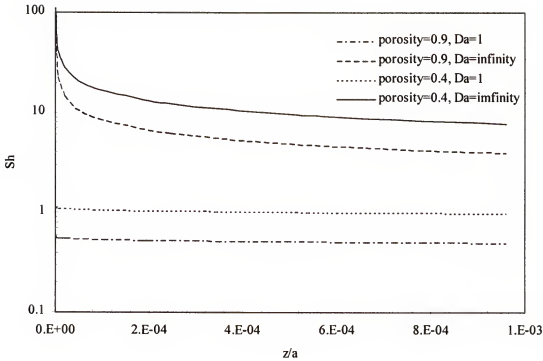
Figure 5-1. Mass transfer coefficient as a function of the distance from the ends of a bundle of parallel cylinders when fluid flows parallel to them

$$\frac{a\tau_w}{\mu U} = \frac{\alpha^2}{2} - \frac{R\alpha^3 K_1(\alpha R)}{K_0(\alpha R) + \alpha R K_1(\alpha R)\ln R}\left(\frac{1}{\alpha^2} - \frac{1}{4} + \frac{R^2}{4} - \frac{R^2}{2}\ln R\right) - \frac{R^2}{2}\alpha^2$$

(5-10)

Shown in figure 5-1 is the Sh as a function of dimensionless distance from the end of the cylinders. The packing with a lower porosity gives a little higher particle deposition rate. Particle deposition is significant only in the very entrance region where the diffusion boundary layer is still developing. Even at a position z/a=0.001 and Da=∞ (the surface reaction is instantaneous), the Sh is extremely small compared to the case of flow perpendicular to the cylinders where the Sh is usually in the order of 10^2 for most particle deposition processes (see Section 5-2). This treatment does not consider the

particle deposition on the end surfaces of the fibers, which may be neglected if the fiber aspect ratio (length/diameter) is big.

Table 5-1 The flow field parameter A_c for various models

Model (author)	A_c
Cell model (Happel, 1959)	$A_c = \dfrac{1}{2}\left(-\dfrac{1}{2} - \dfrac{1}{2}\ln(1-\varepsilon) + \dfrac{(1-\varepsilon)^2}{1+(1-\varepsilon)^2}\right)^{-1}$
Cell model (Kuwabara, 1959)	$A_c = \dfrac{1}{2}\left(\dfrac{1}{4} - \dfrac{1}{2}\ln(1-\varepsilon) - \varepsilon - \dfrac{1}{4}(1-\varepsilon)^2\right)^{-1}$
Brinkman's model (Spielman & Goren,1968)	$A_c = \dfrac{\alpha K_1(\alpha)}{2K_0(\alpha)}$, where $\dfrac{\alpha^2}{1-\varepsilon} = 2\alpha^2 + 4\alpha\dfrac{K_1(\alpha)}{K_0(\alpha)}$
EMA model (present)	$A_c = \dfrac{\alpha R}{2Q}\left\{ \begin{array}{l} \left[-4\alpha^2 R^2(1+\ln R) + 3R^4\alpha^2 + 16R^2 + \alpha^2\right]K_1(\alpha R) \\ + 8\alpha R\left[R^2 - 1\right]K_0(\alpha R) \end{array}\right\}$ where $Q = \left[-\alpha^3 + 2\alpha R^2 + \alpha^3 R^4 \ln R - \alpha^3 R^4 - \alpha^3 \ln R + 16R^2\alpha \ln R\right]$ $RK_1(\alpha R) + \left[4\alpha^2 R^4 \ln R + 4\alpha^2 R^2 - 3\alpha^2 R^4 - \alpha^2 + 16R^2\right]K_0(\alpha R)$

5-2 Particle Deposition on Circular Cylinders Perpendicular to Mean Flow

As discussed in Section 1-3, a linearized form of the flow field **u** is sufficient for the calculation of concentration distribution since the convective diffusion equation is applied within the diffusion boundary layer. For the case in which the flow direction is

perpendicular to the axes of the cylindrical collectors, the linearized velocity field is represented by the following stream function:

$$\psi = -2A_c(r-1)^2 \sin\theta \tag{5-11}$$

Here A_c is the flow field parameter which is unique to each of the porous medium models. For the EMA model, A_c can be obtained from the analysis shown in Section 3-4 to be:

$$A_c = \frac{\alpha R}{2Q}\left\{\left[-4\alpha^2 R^2(1+\ln R)+3R^4\alpha^2+16R^2+\alpha^2\right]K_1(\alpha R)+8\alpha R\left[R^2-1\right]K_0(\alpha R)\right\}$$

$$\tag{5-12}$$

Where Q is given by equation (3-35). The flow field parameter A_c for other models is summarized for comparison in Table 5-1.

Using the IFBL approximation, Spielman and Friedlander (1974) obtained the dimensionless particle deposition rate as:

$$Sh = 0.731A_c^{1/3}Pe^{1/3}\gamma_c(\beta_c) \tag{1-38}$$

In Figure 5-2, the mass transfer coefficients predicted by the EMA and the cell models are presented as a function of the packing porosity. Also plotted here are the recent numerical results of Wang and Sangani (1997). Wang and Sangani's work is not for a particle deposition process but for a heat transfer problem in which the overall heat transfer coefficient has been calculated numerically for a flow through an array of randomly positioned cylinders which are held at constant temperature. Since Wang and Sangani's results do not involve any assumptions other than a high Peclet number, they may serve as a basis to evaluate the effectiveness of various models. Figure 5-2 indicates that the EMA model provides very good predictions for the mass transfer coefficient for a

broad range of porosity. The cell models, on the other hand, appear to overestimate the Sh by about 20%.
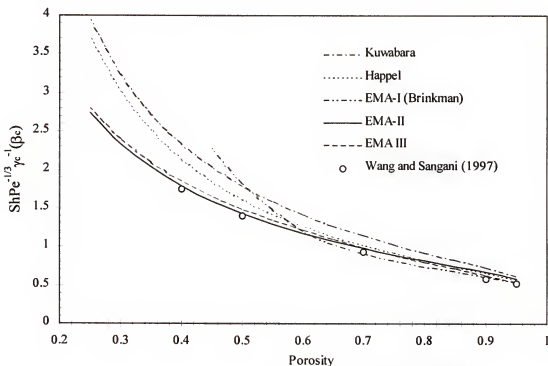
Figure 5-2. Sh predicted by various models for packing of fibers perpendicular to superficial velocity

5-3 Particle Deposition on Planar and Completely Randomly Packed Circular Cylinders

The particle deposition in the cases of Flow-III and Flow-IV is treated in this section based on the results from Sections 5-1 and 5-2. The fluid flow relative to each of the fibers can always be considered to be the vector summation of a perpendicular component and a parallel component relative to the fiber axis section wise due to the

linearity of the Stokes equation and the convective diffusion equation. As discussed in Section 5-1 and 5-2, the contribution of the parallel component to the total particle deposition is significant only in the very end region, where the diffusion boundary layer still undergoes development. The fiber aspect ratio is rather high in most applications. The particle deposition on the ends of the fibers and the particle deposition due to the parallel component of the fluid flow may be neglected.

If we denote the angle between the axis of a section of fiber and the superficial velocity by ϑ, then the perpendicular component of the superficial velocity contribution is

$$U_\perp = U \sin \vartheta \tag{5-13}$$

The Sh for this section of fiber can then be calculated by (from equation 1-38)

$$Sh(\vartheta) = 0.731 A_c^{1/3} Pe^{1/3} \gamma_c (\beta_c) \sin^{1/3} \vartheta \tag{5-14}$$

The overall Sh is then obtained as a probability average

$$Sh = 0.731 A_c^{1/3} Pe^{1/3} \gamma_c (\beta_c) \int_0^{\pi/2} P_\vartheta (\vartheta) \sin^{1/3} \vartheta d\vartheta \tag{5-14}$$

where $P_\vartheta (\vartheta)$ is the probability density of finding a fiber laying at an angle relative to the superficial velocity, which has been obtained for Flow-III and Flow-IV in Sections 3-5 and 3-6, respectively. Equation (5-14) may also be written in the following form:

$$Sh = 0.731 A_c^{1/3} Pe^{1/3} \gamma_c (\beta_c) \chi \tag{5-15}$$

where $\chi = \int_0^{\pi/2} P_\vartheta (\vartheta) \sin^{1/3} \vartheta d\vartheta$, which can be considered as a correction factor for the packing structure. For a Two-dimensional planar random packing,

$$\chi = \frac{2}{\pi} \int_0^{\pi/2} \sin^{1/3} \vartheta d\vartheta = \frac{2\Gamma\left(\frac{2}{3}\right)\Gamma\left(\frac{1}{2}\right)}{\pi\Gamma\left(\frac{7}{6}\right)} = 0.8235 \tag{5-16}$$

and in the case of completely randomly packed fibers,

$$\chi = \int_0^{\pi/2} \sin^{4/3}\vartheta\, d\vartheta = \frac{\Gamma\left(\frac{7}{6}\right)\Gamma\left(\frac{1}{2}\right)}{2\Gamma\left(\frac{10}{6}\right)} = 0.9107 \tag{5-17}$$

Table 5-2 The flow field parameter A_s for various models

Model (author)	A_s
Happel's cell model (Spielman & FitzPatik, 1973)	$A_s = \dfrac{2\left[1 - (1-\varepsilon)^{5/3}\right]}{2 - 3(1-\varepsilon)^{1/3} + 3(1-\varepsilon)^{5/3} - 2(1-\varepsilon)^2}$
Brinkman's model (Present)	$A_s = 1 + \alpha$
EMA model (Present)	$A_s = \dfrac{2}{Q}\left[\begin{array}{l} -30R^4\alpha^3 - 30R^3\alpha^2 + 90R^3 + 90\alpha R^4 + 42\alpha^2 R^5 \\ -15\alpha^4 R^2 + 12R^6\alpha^3 + 15\alpha^3 R^3 + 3\alpha^2 + 3\alpha^3 R \end{array}\right]$ where $Q = 180R^3 + 24R^5\alpha^2 - 45R^4\alpha^2 - 9\alpha^2 + 4\alpha^3 + 180\alpha R^3 + 4R^6\alpha^3$ $\quad + 10(\alpha R)^3 - 9R\alpha^3 - 9\alpha^3 R^5 + 30(\alpha R)^2 - 180R^3\alpha$

5-4 Particle Deposition on Randomly Packed Non-uniform Circular Cylinders

The particle deposition on randomly packed non-uniform cylinders can be treated readily based on the results of Sections 5-2 and 5-3 if the size distribution $P_s(a)$ and the surface area fraction available for each size, $P_A(a)$, or the length fraction for each size are known. The surface averaged flux can then be calculated by

$$J = 0.731\chi c_0 U^{1/3} \mathcal{D}^{2/3} \int_0^\infty A_c^{1/3}\left(\varepsilon, \frac{a}{\sqrt{k}}\right) a^{-2/3} \gamma_c(\varepsilon, a) P_a(a) P_A(a)\, da \tag{5-18}$$

here, the packing structure correction factor χ has been assumed to be independent of the cylinder size. The integral in equation (5-18) can only be calculated through numerical procedures due to the complicated functions $A_c(a)$ and $\gamma_c(a)$. This case will not be discussed further because there are no experimental data available yet in the literature to compare with.
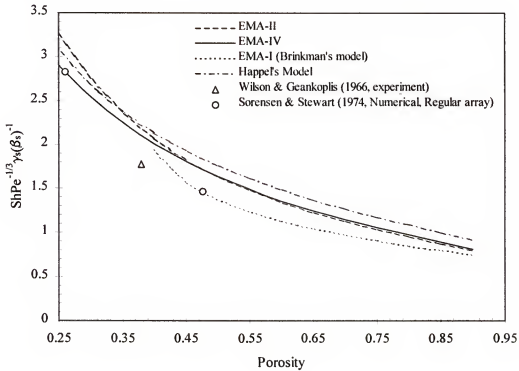

Figure 5-3. Sh predicted by various models for granular media

5-5 Particle Deposition on Randomly Packed Uniform Spheres

A representative linearized velocity field for flow passing through granular media is represented by the following stream function:

$$\psi = -\tfrac{3}{4} A_s (r-1)^2 \sin^2\theta \tag{5-19}$$

Here A_s is the flow field parameter which is unique to each of the porous medium models. For the EMA model, A_s can be obtained from the analysis shown in Section 4-1 to be:

$$A_s = \frac{2}{Q} \begin{bmatrix} -30R^4\alpha^3 - 30R^3\alpha^2 + 90R^3 + 90\alpha R^4 + 42\alpha^2 R^5 \\ -15\alpha^2 R^2 + 12R^6\alpha^3 + 15\alpha^3 R^3 + 3\alpha^2 + 3\alpha^3 R \end{bmatrix} \tag{5-20}$$

where Q is given by equation (4-19). The flow field parameter A_s for other models is summarized for comparison in Table 5-2.

Using the IFBL approximation, Spielman and Friedlander (1974) obtained the dimensionless particle deposition rate as:

$$Sh = 0.653 A_s^{1/3} Pe^{1/3} \gamma_s(\beta_s) \tag{1-38}$$

In Figure 5-3, the mass transfer coefficients predicted by the EMA and the cell models are presented as a function of the packing porosity. Also plotted here are the recent numerical results of Sorensen and Stewart (1994a, 1974b). Sorensen and Stewart's determined the heat and mass transfer coefficients for simple cubic and face-centered cubic arrays at their closest packing porosities of $\varepsilon=0.4764$ and 0.2595, respectively. The modified EMA-II model, i.e., the EMA model where the size of the liquid envelope has been modified to accommodate the matching of the permeability predictions with the experimental results, $R=1.028/(1-\varepsilon)^{1/3}$, gives exact prediction for the face-centered array, although it overestimates the mass transfer rate for simple cubic array by about 12%. As mentioned before, the EMA model is essentially developed for random arrays. It can neither distinguish the exact packing structure nor the flow direction relative to the

structure. Also shown in the same plot is the experimental results by Wilson and Geankoplis (1966). The experimental data appeared to be lower than the EMA prediction by about 12%. It is still too early to conclude which model gives better prediction at this stage. This requires well conditioned experiments or numerical algorithms for randomly packed spheres.

5-6 Particle Deposition on Randomly Packed Non-uniform Spheres

The particle deposition on randomly packed non-uniform spheres can be analyzed based on the results of Section 5-5 if the size distribution $P_a(a)$ is known. The surface averaged flux is

$$J = 0.635 c_0 U^{1/3} \mathcal{D}^{2/3} \int_0^\infty A_c^{1/3} \left(\varepsilon, \frac{a}{\sqrt{k}} \right) a^{-2/3} \gamma_c(\varepsilon, a) P_a(a) P_A(a) da \qquad (5\text{-}21)$$

where $P_A(a)$ is the fraction of surface area available for collector size a, which can be obtained from the size distribution density, $P_a(a)$.

$$P_A(a) = \frac{a^2 P_a(a)}{\int_0^\infty a^2 P_a(a) da} \qquad (5\text{-}22)$$

5-7 Summary

Effective medium approximation is applied to predict particle deposition rate in fibrous and granular media. The analytical solutions for the particle deposition are obtained. Comparison with available experimental data shows that the EMA model for fibrous media is superior to the other existing models. Well conditioned experiments are

needed for checking the validity of the EMA model for granular media. The EMA model is also extended to treat particle deposition in polydisperse fibrous and granular media.

The treatment here is not limited to the deposition of colloidal particles. It can be applied to other heat and mass transfer processes in laminar flow through fibrous and granular media.

CHAPTER 6
INFLUENCES OF VARIOUS SYSTEM PROPERTIES AND OPERATING
CONDITIONS ON PARTICLE DEPOSITION RATE

6-1 Influence of System Properties

Representative model predictions for various physical, chemical properties and the operating condition on the rate of deposition of colloidal particles will be presented in this section. This will be carried out for deposition onto cylindrical collectors perpendicular to the superficial velocity based on the effective medium approximation. It should be emphasized that the general dependence of the particle deposition rate on various parameters for other media is similar to the one discussed here.

Figure 6-1 shows the effects of Da and Pe on Sh. For the case where the Damkohler number (Da=$K_\phi a/D_\infty$) >> 1, the particle deposition is convective diffusion limited and the filter coefficient is independent of K_ϕ. This is equivalent to assuming that a perfect particle sink exists on the collector surface. When Da<<1, the particle deposition is then surface interaction limited. In most cases the particle deposition is almost impossible in this instance. The Figure 6-1 can be considered as a master plot which correlates the mass transfer coefficient with all the affecting parameters. The effects of these individual parameters will be discussed below.
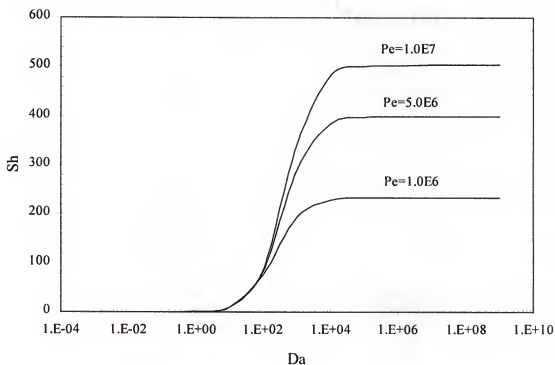
Figure 6-1 Influence of Da and Pe on Sh

6-1-1 Surface Potentials

Figure 6-2 illustrates the effect of particle and collector surface potentials on the mass transfer coefficient at various superficial velocities. The surface potentials affect the magnitude of the double layer interaction. From the expressions of the double layer interaction, it is noticed that it is the product of the surface potentials of the collector and particle that comes into effect. As observed, the mass transfer coefficient at a given superficial velocity decreases dramatically as the product of the surface potentials increases above a certain value. Also plotted in Figure 6-2 is the corresponding height

of the repulsive energy barrier. The energy barrier is very sensitive to the surface potentials, and it markedly increases as the product of the surface potentials increases above a critical value. The height of the energy barrier corresponding to this critical value is about 5 $k_B T$. As the height of the energy barrier increases, the mass transfer coefficient decreases rapidly and beyond an energy barrier of about 20 $k_B T$, the particle deposition becomes virtually impossible. It is also found from our numerous simulations that the particle deposition behavior interpreted in terms of height of energy barrier is almost independent of the system, i.e., the critical energy barriers of 5 $k_B T$ and 20 $k_B T$ are not dependent on the system parameters such as particle size, Hamaker constant and electrolyte concentration. A critical height of repulsive energy barrier of about 20 $k_B T$ has long been observed by many studies on particle aggregation (Elemelech et al. 1995). When the repulsive energy barrier is higher than 20 $k_B T$ a colloidal suspension is usually very stable. In fact particle deposition and aggregation are essentially the same physical phenomenon governed by the same natural law. Particle deposition can be considered to be a special case of particle aggregation in which small colloidal particles aggregate with relatively huge particles—collectors.

6-1-2 Ionic Concentration

Ionic concentration affects the mass transfer coefficient through the double layer interaction. The effect is shown in Figure 6-3. It is observed that the mass transfer coefficient increases as the electrolyte concentration increases. This is caused by the decrease of the range and magnitude of the repulsive double layer interaction, which is

usually called the compression of the electrical diffusion double layer. The results shown in Figure 6-3 also demonstrate that the effect of electrolyte concentration is much more profound for bigger particles than for smaller particles.
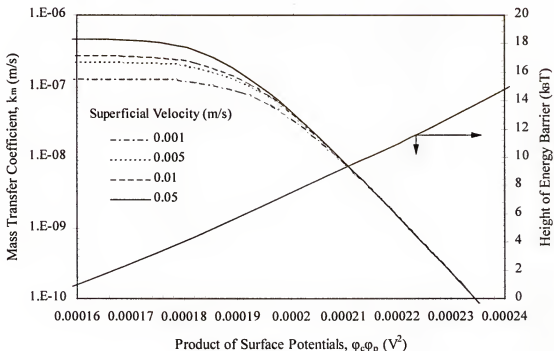
Figure 6-2 Influence of particle and collector surface potentials on mass transfer coefficient (Particle diameter=0.5 μm, electrolyte concentration=0.01M, Hamaker constant=8.5x10^{-21}J, 1-1 electrolyte, temperature = 298 K)

Shown in Figure 6-4 is the effect of particle size on the relative magnitudes of the van der Waals and double layer interactions. For particles much bigger than the van der Waals interaction range (e.g., 10 nm), both the double layer and van der Waals interaction energies are approximately proportional to the size of the particle. If the particle size is in the van der Waals interaction range, the van der Waals interaction energy becomes relatively independent of the particle size while the double layer interaction energy still

decreases as the particle size is reduced. Therefore the van der Waals force usually dominates over the double layer force for extremely small particles. In this instance the mass transfer coefficient becomes relatively insensitive to the changes in surface potentials and electrolyte concentration.
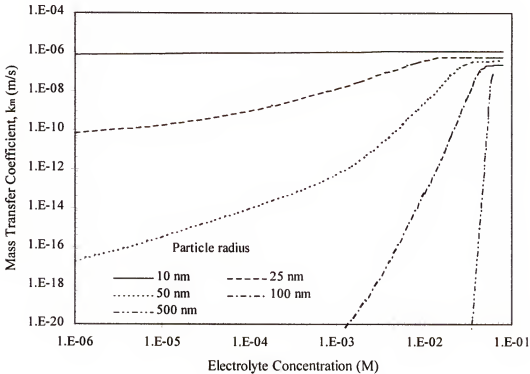
Figure 6-3 Influence of electrolyte concentration on mass transfer coefficient (Superficial velocity=1×10^{-3} m/s; surface potentials $\varphi_c = \varphi_p = 0.02$V, Hamaker constant $= 8.5 \times 10^{-21}$ J; 1-1 electrolyte; temperature = 298 K)

6-1-3 Particle Size

The results shown in Figure 6-3 also demonstrate the effect of particle size on the mass transfer coefficient. Particle size comes into the picture through the particle diffusion coefficient and the size effect on interaction energies. Decreasing the particle

size results in a higher particle diffusivity and a lower repulsive energy barrier, and therefore a higher particle deposition rate.

The current research focuses only on deposition of colloidal particles, in which the diffusion and convection are the main mechanisms for particles to be transported toward the collector surfaces. For deposition of bigger particles, other mechanisms such as particle inertia, interception may play major roles. It has been recognized that particles of sizes around 1μm are the most difficult to be captured. For particles bigger than 1μm, the deposition rate may increase as the their size is increased.
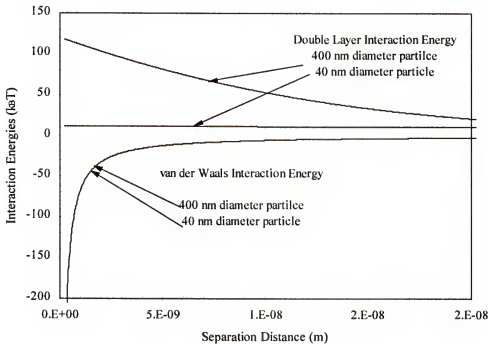
Figure 6-4 Influence of particle size on double layer and van der Waals interactions (Electrolyte concentration = 0.001M, 1-1 electrolyte; Hamaker constant=8.5x10-21 J; surface potentials $\varphi_c = \varphi_p = 0.02V$; temperature = 298 K)

6-1-4 Hamaker Constant

The van der Waals interaction energy is proportional to the Hamaker constant of the system. As the Hamaker constant is increased, the mass transfer coefficient increases due to the stronger attractive force. This is shown in Figure 6-5. Once the van der Waals force becomes strong enough, corresponding to an energy barrier of about 5 k_BT, the particle deposition is limited by the convection and diffusion of particles in the fluid medium and the mass transfer coefficient becomes independent of the Hamaker constant.
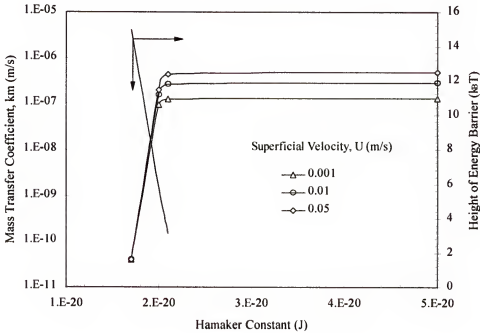
Figure 6-5 Influence of Hamaker constant on mass transfer coefficient (Particle diameter =0.5μm; electrolyte concentration = 0.01 M, 1-1 electrolyte; surface potentials $\varphi_c = \varphi_p = 0.02V$; temperature = 298 K)
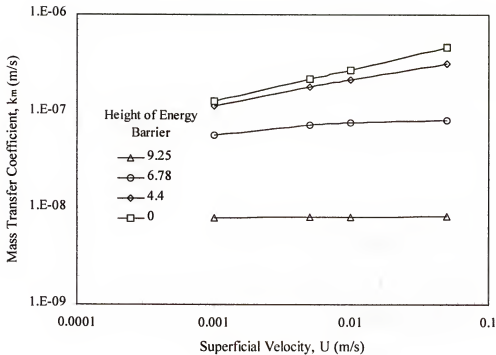
Figure 6-6 Influence of superficial velocity on mass transfer coefficient

6-2 Influence of Operating Conditions

The operating conditions may include the superficial velocity and suspension pH because these two parameters are often adjusted in the process to achieve optimum operation. The suspension pH affects the particle deposition rate by changing the surface potentials of the particle and collector and the electrolyte concentration. The correlation of surface potentials as a function of pH are usually obtained through experiments for different materials and tabulated in literature. The ionic concentration can be calculated readily from the value of pH and concentrations of other ions. Therefore the pH comes

into the picture through physical properties of the system, which has been discussed in Section 6-1. The effect of superficial velocity is discussed below.

The superficial velocity is a measure of the degree of convection. Figure 6-6 illustrates the effect of superficial velocity on mass transfer coefficient. When the particle deposition is convective diffusion limited (the height of repulsive energy barrier is lower than about 5 $k_B T$), the mass transfer coefficient is proportional to 1/3 power of the superficial velocity. As the role of surface repulsive force becomes more important, the contribution of convection decreases gradually. Although the particle deposition rate per unit area of the filter surface increases with superficial velocity, the filter coefficient, which is a measure of the speed of concentration decay decreases with increasing superficial velocity because the residence time of the particles in the filter is reduced.

6-3 Effect of Hydrodynamic Interaction

As a particle approaches very close to the surface, it becomes increasingly difficult for the liquid between them to drain out of the gap and this tends to contribute a repulsive force to the total interactions between the particle and the surface. This effect is usually termed as the hydrodynamic interaction.

One approach to incorporate the contribution of the hydrodynamic interaction into the particle deposition mechanism is to lump the effect to an effective diffusion coefficient, $\mathcal{D}_e$ (Ruckenstein and Prieve 1974). The particle mobility, m, defined as the velocity produced by applying a unit force on it, and the effective diffusion coefficient, $\mathcal{D}_e$, are related by the Nernst-Einstein equation:

$$\mathcal{D}_e = {}_mkT \tag{6-1}$$

The mobility of Brownian particles suspended in liquids can be determined by the well known Stokes equation:

$$m = \frac{1}{6\pi\mu a} \tag{6-2}$$

where μ is the viscosity of the liquid and a is the particle radius. The Stokes equation provides good agreement with experimental results obtained at small Reynolds numbers, i.e. Re <1. Some of the theoretical treatments of this subject has grown out of the early work of Stokes. An extension to account for the inertial effect has been made by Oseen (1910).

$$m = \frac{1}{6\pi\mu a\left(1 + \dfrac{3}{8}\dfrac{aU\rho}{\mu}\right)} \tag{6-3}$$

in witch U is the velocity of the particle relative to the liquid, ρ the density of the liquid. which has been shown to be valid for Re=$2aU\rho/\mu$ <5 (Schlichting, 1960).

When the particle is very near to the solid surface, the mobility is decreased as a result of friction between the surface and fluid which increases the force required to push the liquid out of the path of the approaching particle. By convention, the Stokes equation is modified by a dimensionless factor $g(h)$, so that:

$$m = \frac{1}{6g(h)\pi\mu a} \tag{6-4}$$

The hydrodynamic factor, $g(h)$, is a function of the separation distance, h . Some analytical expressions corresponding to the translational motion of single particles normal to the surface are give in Table 6-1. The rotational motion of particles is often considered

to have negligible effects on particle transport leading to deposition. In the range of separation distances when hydrodynamic effect needs to be considered ($h \ll a$), the motion of Brownian particles normal to the surface is dominant because of the strong van der Waals and Double layer interactions, and the negligible fluid velocity relative to the surface. So the hydrodynamic factors corresponding to the motion of particles parallel to the surface are not listed in Table 6-1.

Table 6-1 Hydrodynamic correction factors

Correction factor g(h)	Validity	Source
$1 + \dfrac{9}{8}\left(\dfrac{a}{h+a}\right)$	$a/(a+h) \ll 1$	Lorentz (1907)
$\dfrac{4}{3}\sinh\alpha\displaystyle\sum_{n=1}^{\infty}\dfrac{n(n+1)}{(2n-1)(2n+3)}$ $\times\left[\dfrac{2\sinh(2n+1)\alpha + (2n+1)\sinh 2\alpha}{4\sinh^2(n+\frac{1}{2})\alpha - (2n+1)^2\sinh^2\alpha} - 1\right]$ where $\alpha = \cosh^{-1}(1+h/a)$		Brenner (1961)
$\dfrac{a}{h} - 0.21\ln\left(\dfrac{h}{a}\right) + 0.97$	$h/a < 0.1$	Cox & Brenner (1967)

Fig. 6-7 shows the hydrodynamic correction factor as a function of the separation distance. Since $1 \geq 1/g(h) \geq 0$, the effective diffusion coefficient is always smaller in the region near the surface than in the bulk and it vanishes when the particle touches the surface.

After considering the hydrodynamic effect, the equation for determining the virtual chemical reaction constant K now becomes:

$$K_\Phi = \mathcal{D}_\infty \left\{ \int_0^\infty \left[g(h) e^{\Phi/kT} - 1 \right] dh \right\}^{-1} \tag{1-35}$$

The influence of hydrodynamic effect on the virtual chemical reaction constant is plotted in Figure6-8. It can be seen that the hydrodynamic effect can decrease the reaction constant by a factor of 100. Figure 6-9 shows the influence of the hydrodynamic effect mass transfer coefficient. The hydrodynamic effect is limited in a very narrow region close to the surface, it can be considered to be a kind of surface "force". So, it does not have effect on particle deposition if the process is convective diffusion limited.
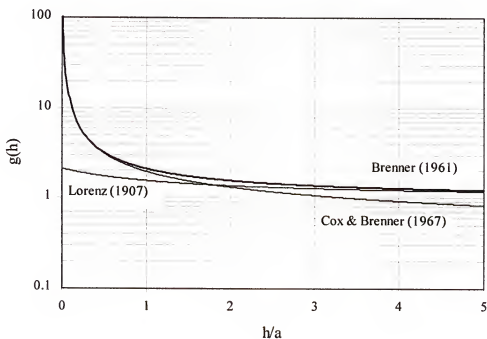
Figure6-7 Hydrodynamic retardation factor as a function of separation distance
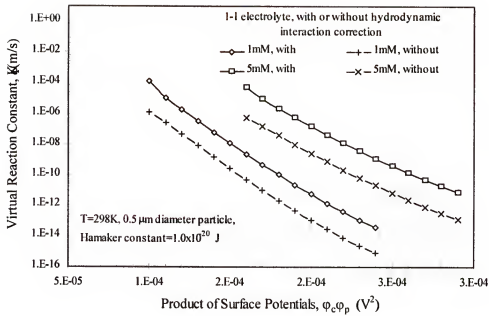
Figure 6-8 Influence of hydrodynamic effect on virtual reaction constant
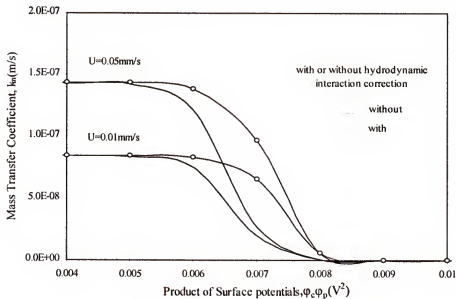

Figure 6-9 Influence of hydrodynamic effect on mass transfer coefficient (Particle diameter = 0.25μm; granular medium with collector diameter of 1mm; porosity = 0.6; Hamaker constant = 8.5×10^{-21} J, temperature = 298K; electrolyte concentration = 0.01M, 1-1 electrolyte)

6-4 Summary

Effects of various system properties and operating conditions on deposition of colloidal particles have been discussed. The physical or chemical conditions include the properties which affect the magnitude of double layer interaction, the electrolyte concentration and surface potentials, and the property which affects the van der Waals interaction, the Hamaker constant. Increasing the ionic concentration and decreasing the product of the surface potentials can enhance the particle deposition rate by reducing the magnitude of the repulsive double layer interaction. The attractive van der Waals interaction is proportional to the Hamaker constant, which depends on the properties of the particle and collector and also the suspending medium. As the Hamaker constant increases, the particle deposition usually is enhanced. It should be noted that the effects of the above properties is much more significant when the surface interactions play more important roles in the particle deposition, or when the height of the total interaction energy barrier is higher than 5 kBT. If the deposition is convective diffusion limited, these properties will not have any obvious effect at all. Particle deposition becomes virtually impossible when the height of the repulsive energy barrier increases beyond 20 k_BT. The effect of the hydrodynamic interaction can be considered as a kind of repulsive "surface" interaction. It exists whenever particles move close to the collector surface.

Decreasing particle size increases particle diffusivity and lowers the surface interaction energy barrier, therefore favors deposition of colloidal particles.

The effect of the operating superficial velocity is more significant when the particle deposition is convective diffusion limited. The particle deposition rate increases as the superficial velocity is increased.

CHAPTER 7
CONCLUSIONS AND SUGGESTIONS FOR FUTURE WORK

7-1 Conclusions

In this research, the Finite Element Method (FEM) and Effective Medium Approximation (EMA) have been used to determine the fluid flow permeability and particle capture efficiency of regular array and random arrays of cylindrical and spherical collectors. The FEM takes into account of the detailed layout of the packing but it can not handle randomly packed collectors yet at the current stage, while the EMA gives an averaged estimation of all the flow parameters but is not able to provide a resolution to distinguish the detailed structure differences and orientations. The EMA assumes a model system in which a packing element (a single fiber in the fibrous medium and a single sphere in the granular medium) is surrounded by a fluid envelope and an effective-medium beyond the envelope. It integrates the important features of both the cell models and Brinkman's model. The Stokes equation and Brinkman's equation are solved for the fluid envelope and effective medium regions, respectively, to obtain the permeability and close-to-surface velocity field around the collectors. The convective diffusion equation is then solved to determine the particle deposition rate. The analytical expressions for the permeability and particle deposition rate are derived for all possible cases of random packing of uniform and non-uniform cylinders and spheres.

The following major novel conclusions may be drawn from the current work:

1. The numerical simulation using the finite element method shows that not only the porosity but also the detailed packing structure relative to the flow has significant effect on particle deposition rate in a fibrous medium. The more tortuous the flow streamline is, the higher the particle deposition rate.

2. The following flow permeability equations were derived based on the effective medium approximation:

$$k = \frac{a^2}{\alpha^2}$$

   (1) For packing of uniform circular cylinders parallel to mean flow,

$$\frac{1}{2}\left(1 + \frac{1}{1-\varepsilon}\right) = \left(\frac{1}{\alpha_{//}^2} - \frac{1}{4} + \frac{R^2}{4} - \frac{R^2}{2}\ln R\right)\frac{\alpha_{//}RK_1(\alpha_{//}R)}{K_0(\alpha_{//}R) + \alpha_{//}RK_1(\alpha_{//}R)\ln R} + \frac{R^2}{2}$$

$$(3\text{-}16)$$

   (2) For packing of uniform circular cylinders perpendicular to mean flow,

$$\alpha_{\perp}^2 = 4(1-\varepsilon)\frac{\alpha_{\perp}R}{Q}\left\{\begin{array}{l}\left[-2\alpha_{\perp}^2R^2 + 3R^4\alpha_{\perp}^2 + 16R^2 - \alpha_{\perp}^2\right]K_1(\alpha_{\perp}R) \\ + 8R^3\alpha_{\perp}K_0(\alpha_{\perp}R)\end{array}\right\} \quad (3\text{-}38)$$

   where

$$Q = \left[-\alpha_{\perp}^3 + 2\alpha_{\perp}R^2 + \alpha_{\perp}^3R^4\ln R - \alpha_{\perp}^3R^4 - \alpha_{\perp}^3\ln R + 16R^2\alpha_{\perp}\ln R\right]$$
$$RK_1(\alpha_{\perp}R) + \left[4\alpha_{\perp}^2R^4\ln R + 4\alpha_{\perp}^2R^2 - 3\alpha_{\perp}^2R^4 - \alpha_{\perp}^2 + 16R^2\right]K_0(\alpha_{\perp}R)$$

$$(3\text{-}35)$$

   (3) For plenary packing of uniform circular cylinders with mean flow parallel to packing planes,

$$\alpha^2 = \frac{1}{2}(\alpha_\perp^2 + \alpha_{//}^2) \tag{3-48}$$

(4) For completely randomly packed uniform circular cylinders,

$$\alpha^2 = \frac{2}{3}\alpha_\perp^2 + \frac{1}{3}\alpha_{//}^2 \tag{3-57}$$

(5) For randomly packed non-uniform circular cylinders,

$$\frac{1}{k} = 4(1-\varepsilon)\frac{\int_0^\infty \int_0^\infty ZD\left(R, \frac{a}{\sqrt{k}}\right)P_a(a,Z)dadZ}{\int_0^\infty \int_0^\infty Za^2 P_a(a,Z)dadZ} \tag{3-67}$$

If the size distribution is not very broad, the following equivalent radius is defined:

$$a_e = \left(\frac{\int_0^\infty \int_0^\infty Za^2 P_a(a,Z)dadZ}{\int_0^\infty \int_0^\infty Z P_a(a,Z)dadZ}\right)^{1/2} \tag{3-71}$$

All the equations for the cases of uniform cylinders are valid for polydisperse cylinders if we replace the radius of the cylinders with the a_e defined above..

(6) For random packing of uniform spheres,

$$\alpha^2 = \frac{18(1-\varepsilon)}{Q}\left[\begin{array}{l} 6R^6\alpha^3 + 21\alpha^2 R^5 - 5R^4\alpha^3 + 45\alpha R^4 \\ -5R^3\alpha^2 + 45R^3 - \alpha^3 R - \alpha^2 \end{array}\right] \tag{4-17}$$

and

$$Q = 180R^3 + 24R^5\alpha^2 - 45R^4\alpha^2 - 9\alpha^2 + 4\alpha^3 + 180\alpha R^4 + 4R^6\alpha^3$$
$$+ 10(\alpha R)^3 - 9R\alpha^3 - 9\alpha^3 R^5 + 30(\alpha R)^2 - 180R^3\alpha \tag{4-19}$$

(7) For random packing of non-uniform spheres,

$$\frac{1}{k} = \frac{3(1-\varepsilon)}{\int_0^\infty a^3 P(a)da} \int_0^\infty aD(R,\alpha)P(a)da \tag{4-26}$$

The thickness of the clear liquid envelope, δ, is estimated form the overall porosity of the pack:

$$1 - \varepsilon = \frac{\int\limits_0^\infty a^3 P_a(a)da}{\int\limits_0^\infty (a+\delta)^3 P_a(a)da} \tag{4-27}$$

R in equation (4-26) is obtained by $R=(a+\delta)/a$.

3. The following particle deposition rate equations were derived based on the Interaction Force Boundary Layer Approximation (IFBLA) for surface interactions and Effective Medium Approximation (EMA) for the flow fields:

(1) For the entrance region of a random packing of circular cylinders parallel to mean flow,

$$Sh = \frac{Ja}{\mathcal{D}c_0} = \frac{\left(\dfrac{2a}{9z}\right)^{1/3}\left(\dfrac{a\tau_w}{2\mu U}\right)}{\left(\dfrac{\mathcal{D}}{aK_\phi}\right)\left(\dfrac{2a}{9z}\right)^{1/3} + \Gamma\left(\dfrac{4}{3}\right)} \tag{5-9}$$

(2) For random packing of circular cylinders perpendicular to mean flow,

$$Sh = 0.731 A_c^{1/3} Pe^{1/3} \gamma_c(\beta_c) \tag{1-38}$$

where

$$A_c = \frac{\alpha R}{2Q} \left\{ \begin{array}{l} \left[-4\alpha^2 R^2(1+\ln R) + 3R^4\alpha^2 + 16R^2 + \alpha^2\right]K_1(\alpha R) \\ + 8\alpha R\left[R^2 - 1\right]K_0(\alpha R) \end{array} \right\} \quad (5\text{-}12)$$

(3) For plenary and completely randomly packed circular cylinders,

$$Sh = 0.731 A_c^{1/3} Pe^{1/3} \gamma_c(\beta_c)\chi \quad (5\text{-}15)$$

where x=0.8235 for a plenary random packing and 0.9107 for a completely random packing.

(4) For randomly packed non-uniform circular cylinders,

$$J = 0.731\chi c_0 U^{1/3} \mathcal{D}^{2/3} \int_0^\infty A_c^{1/3}\left(\varepsilon, \frac{a}{\sqrt{k}}\right) a^{-2/3}\gamma_c(\varepsilon, a)P_a(a)P_A(a)da$$

$$(5\text{-}18)$$

(5) For randomly packed uniform spheres,

$$Sh = 0.653 A_s^{1/3} Pe^{1/3} \gamma_s(\beta_s) \quad (1\text{-}38)$$

where

$$A_s = \frac{2}{Q}\left[\begin{array}{l} -30R^4\alpha^3 - 30R^3\alpha^2 + 90R^3 + 90\alpha R^4 + 42\alpha^2 R^5 \\ -15\alpha^2 R^2 + 12R^6\alpha^3 + 15\alpha^3 R^3 + 3\alpha^2 + 3\alpha^3 R \end{array} \right] \quad (5\text{-}20)$$

(6) For randomly packed non-uniform spheres,

$$J = 0.635 c_0 U^{1/3} \mathcal{D}^{2/3} \int_0^\infty A_c^{1/3}\left(\varepsilon, \frac{a}{\sqrt{k}}\right) a^{4/3}\gamma_c(\varepsilon, a)\frac{P_a^2(a)}{\int_0^\infty a^2 P_a(a)da}da$$

$$(5\text{-}21)$$

4. In a random packing of circular cylinders, the fluid flow relative to each of the cylinders can be considered to be the vector summation of a perpendicular component and a parallel component relative to the cylinder axis. It has been

shown that the contribution of the parallel component to the overall particle deposition can be neglected compared with the perpendicular component.

5. It has been shown that if the height of the repulsive energy barrier in the overall surface interaction is lower than 5 k_BT, the particle deposition can be considered to be convective diffusion limited and once its height increases above 20 k_BT, the particle deposition becomes virtually impossible.

7-2 Suggestions for Future Work

7-2-1 Fluid flow through fibrous and granular media

Packing of circular cylinders of small aspect ratio

In a resent work, Rahli et al. (1996) found that the flow permeability through a random packing of uniform circular cylinders of small aspect ratios (e.g., short fibers, length / diameter < 20) can be 20% lower than that of a packing of long circular cylinders. It is believed that this is due to the effect of the fiber ends, which have been neglected in the case of long fibers. If the total surface area of the ends is comparable with the total surface area of the fiber sides, theses ends will have a significant contribution to the overall particle deposition rate. Theoretical analysis of the end effect on flow permeability and mass transfer could be very interesting.

Packing of non-spherical collectors

Granules of various shapes have been widely used in industry as packing materials for catalysis, absorption, adsorption as well as filtration processes. There have been large amount of flow permeability and mass transfer data available for packing of these granules (Standish and McGregor, 1978). The theoretical analysis for these systems has not been found in literature.

7-2-2 Non-DLVO interactions and colloidal interactions for non-ideal particles/collectors

Fundamental equations for non-DLVO interactions

Until now, only the fundamental theories for van der Waals and double layer interactions are well established. Researches on the other surface forces such as hydration, polymer bridging, steric interaction and hydrophobic interaction have been very active in the recent years. The ultimate goals of these researches are to obtain the fundamental equations for calculating these forces.

Colloidal interactions for non-spherical particles

The deposition of biological particles on solid surfaces has been a very hot research topic for many years due to its importance in health related applications (Dickinson, 1997). The interactions between these non-regular biological particles and solid surfaces ultimately determines whether they will be collected on the surfaces.

Surface interactions for rough surfaces and surfaces with non-uniform charges

It has been mentioned in Section 1-2-5 that the surface roughness and non-uniformity of charges on the particle and / or collector surfaces may have significant effect on the particle deposition rate. Although there has been some work done on this topic, all of the them are based on certain assumed patterns of roughness and charge distribution. Research is needed on experimental characterization of the surface roughness and charge distribution of the actual surfaces.

Particle-collector interactions for non-fresh collectors

As particle deposition proceeds, the surface characteristics of the collectors such as the surface roughness and surface potential changes. The effect of these deposited particles on the surface characteristics and the fluid flow is the key to dynamic modeling of the particle deposition process.

APPENDIX
INTRODUCTION TO SOLID ANGLE

A line is generated by sweeping a point linearly through space, an area is generated by sweeping a line through space, and an angle is generated by sweeping a line through an arc. A solid angle is generated by sweeping two "orthogonal"' angles (ϑ and ϕ) through arcs, as shown in Figure A.

A solid angle is two-dimensional by virtue of having no radial position, i.e., the solid angle remains fixed independent of radius. This provides the key to the mathematical formulation for a solid angle. A differential angle is defined as follows:

$$d\vartheta = \frac{ds}{r} \tag{A1}$$

where s is the differential arc length and r is the radius. A differential solid angle dω is defined by scaling up the differential arc length to a differential area and dividing by r^2 to make the solid angle independent of radial position (distance from the origin) as follows

$$d\omega = \frac{dA}{r^2} = \frac{|BD||BC|}{r^2} = \frac{(rd\vartheta)(r\sin\vartheta d\phi)}{r^2} = \sin\vartheta d\vartheta d\phi \tag{A2}$$

Referring to Figure A, note that length |BC| is generated by sweeping line |AB|= r sinϑ (not r), through angle dϕ, i.e. the revolution is of a line normal to the vertical axis |AB|, about the vertical axis |OA|. Contrariwise, line |BD| is generated by sweeping |OB|= r, through angle dϑ about the origin O.
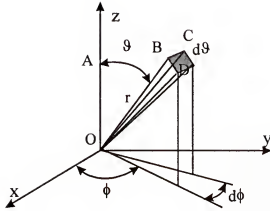
Figure A Solid angle

In Figure A, ϑ is the "cone" angle and ϕ is the "azimuthal" angle. While angles are measured in radians, solid angles are measured in steradians. A hemisphere contains 2π steradians, as follows:

$$\Delta\omega = \int_{\vartheta=0}^{\pi/2} \int_{\phi=0}^{2\pi} \sin\vartheta d\vartheta d\phi = 2\pi \tag{A3}$$

LIST OF REFERENCES

Adamczyk, Z. and van de Ven, T. G. M., 1981, "Deposition of particles under external forces in laminar flow through parallel-plate and cylindrical channels," *J. Colloid Interface Sci.,* **80**, 340

Adamczyk, Z., Czamecki, J., Dabros, T. and van de Ven, T. G. M., 1983, "Particle transfer to solid surfaces," *Adv. Colloid Interface Sci.,* **19**, 183

Adamczyk, Z., Zembala, M., Siwek, B. and Czanecki, J., 1986, "Kinetics of latex deposition from flowing suspensions," *J. Colloid Interface Sci.,* **110**, 188

Bear, J., 1988, Dynamics of Fluids in Porous Media, Dover Publications, New York

Berglin, O. P., Brown, G. A., Hull, H. L. and Sullivan, F. W., 1950, "Heat transfer and fluid friction during viscous flow across banks of tubes-III: a study of tube spacing and tube size," *Tans. ASME,* August, 881

Bird, R. B., Stewart, W. E. and Lightfoot, E. N., 1960, Transport Phenomena, John Wiley & Sons, New York

Bowen, B. D. and Epstein, N., 1979, "Fine particle deposition in smooth parallel-plate channels," *J. Colloid Interface Sci.,* **72**, 81

Bowen, B. D., Levine, S. and Epstein, N., 1976, "Fine particle deposition in laminar flow through parallel plate and cylindrical channels," *J. Colloid Interface Sci.,* **54**, 375

Brenner, H., 1961, "The slow motion of a sphere through a viscous fluid towards a plane surface," *Chem. Eng. Sci.,* **16**, 242

Brinkman, H.C.,1947, "A calculation of the viscous force exerted by a flowing fluid on a dense swarm of particles," *Applied Sci. Res.,* **A1**, 27

Brown, J. C. Jr., 1950, "Determination of the exposed specific surface of pulp fibers from air permeability measurements," *TAPPI,* **33**, 130

Carman, P.C.,1938 "The determination of the specific surface of powders," *J. Soc. Chem Ind., London. (Trans.)* , **57**, 225

Carman, P.C., 1956, The flow of gases through porous media, Academic press, New York

Chea, D. G., Ree, F. H. and Ree, T., 1969, "Radial distribution functions and equation of state of the hard disk fluid," *J. Chem. Phys.*, **50**, 1581

Chari, K. and Rajagopalan, R., 1985a, "Deposition of colloidal particles in stagnation-point flow," *J. Chem. Soc., Faraday Trans. II*, **81**, 1354

Chari, K. and Rajagopalan, R., 1985b, "Transport of colloidal particles over energy barriers," *J. Colloid Interface Sci.*, **107**, 278

Chen, C. Y., 1955, "Filtration of aerosol by fibrous media," *Chem. Rev.*, **55**, 595

Cox, R. G., 1970, "The motion of long slender bodies in a viscous fluid, Part I. General theory," *J. Fluid Mech.*, **44**, 791

Czarnecki, J., 1979, "Van der Waals attraction energy between sphere and half space," *J. Colloid Interface Sci.*, **72**, 361

Dabros, T. and Adamczyk, Z. 1979, "Noninertial particle transfer to the rotating disc under an external force field (laminar flow)," *Chem. Eng. Sci.*, **14**, 1041

Dabros, T. and van de Ven, T. G. M., 1983, "A direct method for studying particle deposition onto solid surfaces," *Colloid & Polymer Sci.*, **261**, 694

Dabros, T. and van de Ven, T. G. M., 1987, "Deposition of latex particles on glass surfaces in an impinging jet," *Phys. Chem. Hydrodynamics*, **8**, 171

Dahneke, B., 1974, "Diffusional deposition of particles," *J. Colloid Interface Sci.*, **48**, 520

Davis, C. N., 1952, "The separation of airborne dust and particles," *Proc. Inst. Mech. Eng. (London)*, **B1**, 185

Derjaguin, B. V. And Landau, L. D., 1941, "Theory of the stability of strongly charged lyophobic sols and the adhesion of strongly charged particles in solutions of electrolyte," *Acta Physicochim. URSS*, **14**, 733

Dickinson, R. B., 1997, "A dynamic model for the attachment of a Brownian particle mediated by discrete macromolecular bonds," *J. Colloid Interface Sci.*, **190**, 142

Dodd, T. L., Hammer, D. A., Sangani, A. S. and Koch, D. L., 1995, "Numerical simulations of the effect of hydrodynamic interactions on diffusivities of integral membrane proteins," *J. Fluid Mech.*, **293**, 147

Drummond, J. E. and Tahir, M. I., 1984, "Laminar viscous flow through regular array of parallel solid cylinders," *Int. J. Multiphase Flow*, **10**, 515

Edwards, D. A., Shapiro, M. and Brenner, H., 1993, "Dispersion and reaction in the two dimensional model porous media," *Phys. Fluids A*, **5**, 837

Elimelech, M., 1991, "Kinetics of capture of colloidal particles in packed beds under attractive double layer interactions," *J. Colloid Interface Sci.*, **146**, 337

Elimelech, M., Gregory, J., Jia, X. and Williams, R., 1995, Particle deposition and Aggregation, Measurement, Modeling and Simulation, Butterworth Heinemann, Oxford

Elimelech, M. and O'Melia, C. R., 1990a, "Effect of particle size on collision efficiency in the deposition of Brownian particles with electrostatic energy barriers," *Langmuir*, **6**, 1153

Elimelech, M. and O'Melia, C. R., 1990b, "Kinetics of deposition of colloidal particles in porous media," *Environ. Sci. Technol.*, **246**, 1153

Elimelech, M. and Song, L., 1992a, "Theoretical investigation of colloid separation from dilute aqueous suspensions by oppositely charged granular media," *Separations Technol.*, **2**, 2

Elimelech, M. and Song, L., 1992b, "Deposition of Colloids in porous media: theory and numerical solution," in *Transport and Remediation of Substance Contaminants; Colloidal, Interfacial, and Surfactant Phenomena,* (ed. Sabatini, D. A. and Knox, R. C.) *American Chemical Aociety Symposium Series 491*, 26

Epstein, N., 1988, "Particulate fouling of heat transfer surfaces: mechanisms and models," Melo, L. F., Bott, T. R. and Bernardo, C. A., Eds., Kluwer Academic Publishers, Dordrecht, The Netherlands, 143

Goldman, A. J., Cox, R. G. and Brenner, H. , 1967a, "Slow viscous motion of a sphere parallel to a plane wall-I. Motion through a quiescent fluid," *Chem. Eng. Sci.*, **22**, 637

Goldman, A. J., Cox, R. G. and Brenner, H. , 1967b, "Slow viscous motion of a sphere parallel to a plane wall-II. Couette flow," *Chem. Eng. Sci.,* **22,** 653

Goren, S. L. and O'Neill, M. E., 1971, "On the hydrodynamic resistance to a particle of a dilute suspension when in the neighborhood of a large obstacle," *Chem. Eng. Sci.,* **26,** 325

Gregory, J., 1975, "Interaction of unequal double layers at constant charge," *J. Colloid Interface Sci.,* **61,** 44

Gregory, J., 1981, "Approximate expressions for the retarded van der Waals interaction," *J. Colloid Interface Sci.,* **83,** 138

Gregory, J., 1993, "The role of colloidal interactions in solid-liquid separation," *Wat. Sci. Tech.,* **27,** 1

Gregory, J. And Wishart, A. J., 1980, "Deposition of latex particles on alumna fibers," *Colloids Surfaces,* **1,** 313

Guzy, C. J. and Bonano, E. J. and Davis, E. J., 1983, "The analysis of flow and colloidal particle retention in fibrous porous media," *J. Colloid Interface Sci.,* **95,** 523

Hamaker, H. C., 1937, "The London-van der Waals attraction between spherical particles," *Physica,* **4,** 1058

Happel, J., 1949, "Pressure drop due to vapor flow through moving beds," *Ind. Eng. Chem.* **41,** 1161

Happel, J., 1958, "Viscous flow in multiparticle systems: slow motion of fluids relative to beds of spherical particles," *AIChE. J.* **4,** 197

Happel, J. and Brenner, H., 1965, Low Reynolds number hydrodynamics, Prentice-Hall, Englewood Cliffs, New Jersey

Ho, N. F. H. and Higuchi, W. I., 1968, "Preferential aggregation and coalescence in heterodispersed systems," *J. Pharm. Sci.,* **57,** 436

Hogg, R., Healy, T. W. and Fuerstenau, D. W., 1966, "Mutual coagulation of colloidal dispersions," *Trans. Faraday Soc.,* **66,** 1638

Hough, D. B. And White, L. R., 1980, "The calculation of Hamaker constants from Lifshitz theory with applications to wetting phenomena," *Adv. Colloid Interface Sci.*, **14**, 3

Hull, M. and Kitchener, J. A., 1969, "Interaction of spherical colloidal particles with planar surfaces," *Trans. Faraday Soc.*, **65**, 3093

Ingmanson, W. L., Andrews, B. D. and Johnson, R. C., 1959, "Internal pressure distribution in compressible mats under fluid stress," *TAPPI*, **42**, 840

Israelachivili, J. N., 1992, Intermolecular and Surface Forces, Academic Press, Orlando

Jackson, G. W. and James, D. F., 1982, "The hydrodynamic resistance of hyaluronic acid and its contribution to tissue permeability," *Biorheology*, **19**, 317

Jackson, G. W. and James, D. F., 1986, "The permeability of fibrous porous media," *Can. J. Chem. Eng.*, **64**, 364

Jaroniec, M. and Madey, R., 1988, Physical Adsorption on Heterogeneous Solids, Elsevier, Amsterdam.

Kang, S.-Y. and Sangani, A. S., 1994, "Electrokinetic properties of suspensions of colloidal particles with thin, polarized double layers," *J. Colloid Interface Sci.*, **165**, 195

Karabelas, A. J., Wegner, T. H. and Hanratty, T. J., 1971, "Use of asymptotic relations to correlate mass transfer data in packed bed," *Chem. Eng. Sci.*, **26**, 1581

Kihira, H., Ryde, N. and Matijevic, E., 1992, "Kinetics of heterocoagulation, Part 2-The effect of discreteness of surface charge," *J. Chem. Soc., Faraday Trans.*, **88**, 2379

Kim, S. and Russel, W. B., 1985, "Modeling of porous media by renormalization of the Stokes equations," *J. Fluid Mech.*, **154**, 269

Kirsch, A. A. amd Fuchs, N. A., 1967, "Studies on fibrous aerosol filters-II. Pressure drop in systems of parallel cylinders," *Ann. Occup. Hyg.*, **10**, 23

Kostornov, A. G. and Shevchuk, M. S., 1977, "Hydraulic characteristics and structure of porous metal fiber materials III. Laws of liquid permeability of materials," *Poroshkovaya Metallurgiya*, **9**, 50

Kuwabara, S., 1959, "The force experience by randomly distributed parallel circular cylinders or spheres in a viscous flow at small Reynolds numbers," *J. Physics Soc. Japan.* **14**, 527

Kyan, C. P., Wasan, D. T. and Kintner, R. C., 1970, "Flow of single-phase fluids through fibrous beds," *Ind. Eng. Chem. Fundam.,* **9**, 596

Labreque, R. P., 1968, "The effect of fiber cross sectional shape on the resistance to the flow of fluids through fiber mats," *TAPPI,* **51**, 8

Ladd, A. J. C., 1990,"Hydrodynamic transport coefficients of random dispersions of hard spheres," *J. Chem. Phys.*, **93**, 3484

Langmuir, I., 1942, "Reports of smokes and filters", Part IV of a report for the office of scientific research and development, OSRD, No. 865, Ser. No. 353, "Filtration of aerosols and development of filter materials," by Redebush, W. H, September 4

Lee, K. W. and Liu, B. Y. H., 1982, "Experimental study of aerosol filtration by fibrous filters," *Aerosol Sci. Tech.* **1**, 35 (1982)

Levique, A., 1928, "Law of heat transmission by convection," *Ann Mines*, **13**, 201

Levich, V. G., 1962, Physicochemical Hydrodynamics, Prentice-Hall, Englewood Cliffs, New Jersey

Li, Y. and Park, C.-W., 1997, "Deposition of Brownian particles on cylindrical collectors in a periodic array," *J. Colloid Interface Sci.*, **185**, 49

Li, Y. and Park, C.-W., 1998, "Permeability of packed beds filled with polydisperse spherical particles," *Indus. Eng. Chem. Research* (to be published)

Li, Y. and Park, C.-W., 1998, "A predictive model for the removal of colloidal particles in fibrous filter media," *Chem. Eng. Sci.* (to be published)

Liftshitz, E. M., 1956, "Theory of molecular attractive forces," *Soviet Physics JETP,* **2**, 73

Marshal, J. K. and Kitchener, J. A., 1966, "The deposition of colloidal particles on smooth solids," *J. Colloid Interface Sci.,* **22**, 342

Matijevic, E. and Kellay, N., 1983, "Kinetics of deposition of colloidal metal oxides particles on a steel surface," *Croatica Chem. Acta.,* **56**, 649

Mo, G. and Sangani, A. S., 1993, "A method for computing Stokes flow interactions among spherical objects and its application to suspensions of drops and porous particles," *Phys. Fluids,* **6**,1673

Neale, G. and Masliyah, J. H., 1975, "Flow perpendicular to mats of randomly arranged cylindrical fibers (Importance of cell models)," *AIChE J.*, **21**, 805

O'Melia, C. R. and Stumm, W., 1967, "Theory of water filtration," *J. Am. Water Works Assoc.*, 59, 1393

Orr, C., 1977, Filtration: Principles and Practices, Marcel Dekker, New York

Oseen, C. W., 1910, "Ueber die Stokes'sche formel und ueber die verwandte aufgabe in der hydrodynamik," *Arkiv. Mat. Astron Fys.*, **6**, 75

Payatakes, A. C., Rajagopalan, R. and Tien, C., 1974a, "On the use of Happel's model for filtration studies," *J. Colloidal Interface Sci.*, **49**, 321

Payatakes, A.C., Rajagopalan, R. and Tien, C., 1974b, "Application of porous media models to the study of deep bed filtration," *Can. J. Chem. Eng.* , **52**, 722

Perry, R. H. and Green, D. W., 1984, Perry's Chemical Engineers' Handbook, 6th Edition, McGraw-Hill, New York

Phillips, R. J., Braday, J. F., and Bossis, G., 1988, "Hydrodynamic transport properties of hard sphere dispersions, II. Porous media," *Phys. Fluids*, **31**, 3473

Pich, J., 1986, "Gas filtration theory", in Filtration Principles and Practices, Eds Matteson, M. J. And Orr, C., Marcel Dekker, New York

Prieve, D. C., and Lin, M. M., 1980, "Adsorption of Brownian hydrosols onto a rotating disc aided by a uniform applied force," *J. Colloid Interface Sci.*, **76**, 32

Prieve, D. C. and Ruckenstein, E., 1974, "Effect of London forces upon the rate of deposition of Brownian particles," *AIChE J.*, **20**, 1178

Prieve, D. C. and Ruckenstein, E., 1976, "Rate of deposition of Brownian particles calculated by lumping interaction force into boundary condition," *J. Colloid Interface Sci.*, **57**, 547

Prieve, D. C. and Russel, W. B., 1988, "Simplified predictions of Hamaker constants from Liftshitz theory," *J. Colloid Interface Sci.*, **125**, 1

Rahli, O., Tadrist, L, Santini, R. and Pantaloni, J., 1993, "Fluid flow and heat transfer analysis in fibrous porous media," *World Conf. on Exp. Fluid Mech. and Heat Transf.*, Honolulu, HI, Vol. 2, 1577

Rahli, O., Tadrist, L. and Miscevic, M., 1996, "Experimental Analysis of Fibrous Porous Media Permeability," *AIChE J.*, 42, 3547

Rajagopalan, R. and Kim, J. S., 1981, "Absorption of Brownian particles in the presence of potential barriers: effect of different modes of double layer interaction," *J. Colloid Interface Sci.*, **83**, 428

Rajagopalan, R. and Tien, C., 1976, "Trajectory analysis of deep bed filtration with the sphere-in-cell porous media model," *AIChE J.*, **22**, 523

Rajagopalan, R. and Tien, C., 1979, "The theory of deep bed filtration," in *Progress in Filtration and Separation* (Ed. Wakeman, R. J.) Vol. 1, Elsevier, Amsterdam, 179

Ruckenstein, E. and Prieve, D. C., 1973, "Rate of deposition of Brownian particles under the action of London and double layer forces," *J. Chem. Soc. Faraday Trans. II*, **69**, 1522

Russel, W. B., Saville, D. A. And Schowalter, W. R., 1989, Colloidal Dispersions, Cambridge University Press, Cambridge

Sahraoui, M. and Kaviany, M., 1992, "Slip and no-slip boundary condition at interface of porous, plain media," *Int. J. Heat Mass Transfer*, **35**, 927

Sangani, A. S. And Mo, G., 1997, "Elastic interactions in particlulate composites with perfect as well as imperfect interfaces," *J. Mech. Phys. Solids*, **45**, 2001

Sangani, A. S. and Acrivos, A., 1982, "Slow flow past periodic arrays of cylinders with application to heat transfer," *Int. J. Multiphase Flow*, **8**, 193

Sellars, J. R., Tribus, M. and Klein, J. S., 1954, "Heat transfer to laminar flow in a round tube or flat conduit-the Greatz problem extended," *Trans. ASME*, 441

Schenkel, J. H. and Kitchener, J. A., 1960, "A test of the Derjaguin Vervey-Overbeek theory with a colloidal suspension," *Trans. Faraday Soc.*, **56**, 161

Schlichting, H., 1960, *Boundary Layer theory*, 7th edn, English translated by Kestin, J, McGraw-Hill, New York

Shapiro, M. and Brenner, H., 1988, "Dispersion of a chemically reactive solute in a spatially periodic model of a porous medium," *Chem. Eng. Sci.*, **43**, 551

Shapiro, M., Brenner, H. and Guell, D. C., 1990, "Accumulation and transport of Brownian particles at solid surfaces: Aerosol and Hydrosol deposition processes," *J. Colloid Interface Sci.*, **136**, 552

Sjollema, J. and Busscher, H. J., 1989, "Deposition of polystyrene latex particles toward polymethymethacrylate in a parallel plate flow cell," *J. Colloid Interface Sci.*, **132**, 382

Sjollema, J. and Busscher, H. J., 1990, "Deposition fo polystyrene particles in a parallel plate flow cell, 1. The influence of collector surface properties on the experimental deposition rate," *Colloids Surfaces*, **47**, 323

Song, L., and Elimelech, M., 1992, "Deposition of Brownian particles in porous media: modified boundary conditions for the sphere-in-cell model," *J. Colloid Interface Sci.*, **153**, 294

Song, L., and Elimelech, M., 1993, "Calculation of particle deposition rate under unfavorable particle-surface interactions," *J. Chem. Soc. Faraday Trans.*, **89**, 3443

Song, L., Johnson, P. R. And Elimelech, M., 1994, "Kinetics of colloid deposition onto heterogeneously charged surfaces in porous media," *Environ. Sci. Technol.*, 28, 1164

Sorensen, J. P. and Stewart, W. E., 1974, "Computation of forced convection in slow flow through ducts and packed beds," *Chem. Eng. Sci.*, **29**, 827

Sparrow, E. M. and Loeffler, A. L. Jr. , 1959, "Longitudinal laminar flow between cylinders arranged in regular array," *AIChE J.*, **5**, 325

Spielman, L. A. , 1977, "Particle capture from low speed laminar flows," *Annu. Rev Fluid Mech.*, **9**, 297

Spielman, L. and Goren, S. L., 1968, "Model for predicting pressure drop and filtration efficiency in fibrous media," *Environ. Sci. Technol*, **2**, 279

Spielman, L. A. and FitzPatrick, J. A., 1973, "Theory for particle collection under London and gravity forces," *J. Colloid Interface Sci.,* **42**, 607

Spielman, L. A. and Friedlander, S., 1974, "Role of electrical double layer in particle deposition by convective diffusion," *J. Colloid Interface Sci.,* **46**, 22

Spielman, L.A. and Goren, L., 1968, "Model for predicting pressure drop and filtration efficiency in fibrous media," *Environ. Sci. Tech.,* **2**, 279

Spoito, G., 1984, The Surface Chemistry of Soils, Oxford University Press, New York

Standish, N. and McGregor, G., 1978, " The average shape of a mixture of particles in a packed bed," *Chem. Eng. Sci.* , **33**, 618

Stenzel, K. H., Rubin, A. L., Yamayoshi, W., Miyata, T., Suzucki, T., Sohde, T. and Nishizawa, N., 1971, "Optimization of collagen dialysis membranes," *Trans. Amer. Soc. Artif. Int. Organs*, **17**, 293

Sullivan, R. R., 1942, "Specific surface measurements on compact bundles of parallel fibers," *J. Appl. Phys.*, **13**, 725

Suresh, L. and Waltz, J., 1996, "Effect of surface roughness on the interaction energy between a colloidal sphere and a flat plate," *J. Colloid Interface Sci.,* **183**, 199

Thies-Weesie, D. M. E. and Philipse, A. P., 1994, "Liquid permeation of bidisperse colloidal hard sphere packings and the Kozeny-Carman scaling relation," *J. Colloid Interface Sci.*, **162**, 470

Tien, C., 1989, *Granular Filtration of Aerosols and Hydrosols*, Butterworth Publishers, Stoneham, Massachusetts

Usui, S., 1973, "Interaction of electrical double layers at constant surface charge," *J. Colloid Interface Sci.,* **44**, 107

Vaidyannthan, R. And Tien, C., 1991, "Hydrosol deposition in granular media under unfavorable surface conditions," *Chem. Eng. Sci.*, 46, 967

Vasak, F., Bowen, B. D., Chen, C. Y., Kastanek, F. and Epstein, N., 1995, "Fine particle deposition in laminar and turbulent flows," *Can. J. Chem. Eng.*, **73**, 785

Venkatesan, M. and Rajapolalan, R., 1980, "A hyperboloidal constricted tube model of porous media," *AIChE J.*, **26**, 694

Verwey, E. J. W. and Overbeek, J. Th. G., 1948, Theory of the Stability of Lyophobic Colloids, Elsevier, Amsterdam

Viswanadham, R., Agrawal, D. C. and Kramer, E. J., 1978, "Water transport through reconstructed collagen hollow fiber membranes," *J. Appl. Poly. Sci.*, **22**, 1655

Wang, W. and Sangani, A.S., 1997, "Nusselt number for flow perpendicular to arrays of cylinders in the limit of small Reynolds and large Peclet numbers," *Phys. Fluids*, **9**, 1529

Weiss, N. and Silberg, 1977, "Inhomogeneity of poly-acrylamide gel structure from permeability and viscoelasticity," *Brit. Polymer J.*, **9**, 144

Wheat, J. A., 1963, "The air flow resistance of glass fiber filter paper," *Can. J. Chem. Eng.*, **41**, 67

White, M. L., 1960, "The permeability of an acrylamide polymer gel," *J. Phys. Chem.*, **64**, 1563

Wiese, G. R. and Healy, T. W., 1970, "Effect of particle size on colloid stability," *Trans. Faraday Soc.*, **66**, 490

Wiggins, E. J., Campbell, W. B. and Maass, O., 1939, "Determination of the specific surface of fibrous materials," *Can. J. Research, Sec. B.*, **17**, 318

Wilson, E. J. and Geankoplis, C. J., 1966, "Liquid mass transfer at very low Reynolds number in packed beds," *Ind. Eng. Chem. Fund.*, **59**, 9

Yao, K. M., Habibian, M. T. and O'Melia, C. R., 1971, "Water and waste water filtration: concepts and applications," *Environ. Sci. Technol.*, **5**, 1105

Yoon, R.-H. and Ravishankar, S. A. , 1994, "Application of extended DLVO theory III. Effect of octanol on the long-range hydrophobic forces between dodecylamine-coated mica surfaces," *J. Colloid Interface Sci.*, **166**, 215

Yotsumoto, H. and Yoon, H.-R., 1992, "Application of extended DLVO theory I. Stability of rutile suspensions," *J. Colloid Interface Sci.*, **157**, 426

Yotsumoto, H. and Yoon, H.-R., 1993, "Application of extended DLVO theory II. Stability of silica suspensions," *J. Colloid Interface Sci.*, **157**, 434

BIOGRAPHICAL SKETCH

Yongcheng Li was born in the Inner Mongolian Autonomous Region, China, on November 8, 1964. He received his Bachelor of Technology and Master of Technology degrees both in Chemical Engineering from Dalian University of Technology, Dalian, China in 1985 and 1988, respectively. He then joined the faculty of the Department of Chemical Engineering at the Tianjin Institute of Technology, Tianjin, China. He entered the doctoral research program in the Department of Chemical Engineering at the University of Florida in August 1994.

I certify that I have read this study and that in my opinion it conforms to acceptable standards of scholarly presentation and is fully adequate, in scope and quality, as a dissertation for the degree of Doctor of Philosophy.

Chang-Won Park, Chair
Associate Professor of Chemical
    Engineering

I certify that I have read this study and that in my opinion it conforms to acceptable standards of scholarly presentation and is fully adequate, in scope and quality, as a dissertation for the degree of Doctor of Philosophy.

Tim Anderson, Cochair
Professor of Chemical Engineering

I certify that I have read this study and that in my opinion it conforms to acceptable standards of scholarly presentation and is fully adequate, in scope and quality, as a dissertation for the degree of Doctor of Philosophy.

Ben Koopman
Professor of Environmental Engineering
    Sciences

I certify that I have read this study and that in my opinion it conforms to acceptable standards of scholarly presentation and is fully adequate, in scope and quality, as a dissertation for the degree of Doctor of Philosophy.

Raj Rajagopalan
Professor of Chemical Engineering

I certify that I have read this study and that in my opinion it conforms to acceptable standards of scholarly presentation and is fully adequate, in scope and quality, as a dissertation for the degree of Doctor of Philosophy.

Dinesh O. Shah
Professor of Chemical Engineering

I certify that I have read this study and that in my opinion it conforms to acceptable standards of scholarly presentation and is fully adequate, in scope and quality, as a dissertation for the degree of Doctor of Philosophy.

Spyros A. Svoronos
Professor of Chemical Engineering

This dissertation was submitted to the Graduate Faculty of the College of Engineering and to the Graduate School and was accepted as partial fulfillment of the requirements for the degree of Doctor of Philosophy.

May, 1998

Winfred M. Phillips
Dean, College of Engineering

Karen A. Holbrook
Dean, Graduate School